UNIVERSITY OF Southampton

University of Southampton Research Repository

Copyright © and Moral Rights for this thesis and, where applicable, any accompanying data are retained by the author and/or other copyright owners. A copy can be downloaded for personal non-commercial research or study, without prior permission or charge. This thesis and the accompanying data cannot be reproduced or quoted extensively from without first obtaining permission in writing from the copyright holder/s. The content of the thesis and accompanying research data (where applicable) must not be changed in any way or sold commercially in any format or medium without the formal permission of the copyright holder/s.
When referring to this thesis and any accompanying data, full bibliographic details must be given, e.g.
Thesis: Author (Year of Submission) "Full thesis title", University of Southampton, name of the University Faculty or School or Department, PhD Thesis, pagination.
Data: Author (Year) Title. URI [dataset]

UNIVERSITY OF SOUTHAMPTON

FACULTY OF NATURAL AND ENVIRONMENTAL SCIENCES

Chemistry

Volume 1 of 1

Electrophoretic deposition of binder free electrodes for lithium ion batteries

by

Rebecca Ruth Mangham

Thesis for the degree of Master of Philosophy

September 2017

UNIVERSITY OF SOUTHAMPTON

ABSTRACT

FACULTY OF NATURAL AND ENVIRONMENTAL SCIENCES

Chemistry

Thesis for the degree of Master of Philosophy

Electrophoretic deposition of binder free electrodes for lithium ion batteries

Rebecca Ruth Mangham

Current batteries for soldier systems rely on many different standard power source sizes, shapes and weights. The integration of power sources into space-limited platforms and to fit to a soldier correctly is difficult. Conventional layer by layer manufacturing approaches are still relied on for battery production. 3D battery systems offer the potential to produce batteries that are bespoke to equipment size and shape whilst maintaining the advantages of the thin film battery manufacturing techniques. There are several techniques available to produce these 3D battery systems and this thesis will look at the application of on one such technique, electrophoretic deposition to lithium iron phosphate (LFP) battery positive electrode materials. Electrophoretic deposition is a technique where an electric field is used to deposit particles from a colloidal suspension onto a conducting surface.

This thesis will present the development of the electrophoresis technique for flat plate samples of the LFP through deposition from a suspension of LFP particles in iso propyl alcohol with a metal salt. The results of studies using cyclic voltammetry and impedance spectroscopy will then be presented and discussed in relation to deposition parameters and to gain a greater understanding of the resistances present between the LFP particles in the binder and carbon additive-free electrodes.

Table of Contents

List of Tables

List of Figures

Declaration of Authorship

I, Rebecca Ruth Mangham .....

declare that this thesis and the work presented in it are my own and has been generated by me as the result of my own original research.
Electrophoretic deposition of binder free electrodes for lithium ion batteries .....

.....

I confirm that:

1. This work was done wholly or mainly while in candidature for a research degree at this University;
2. Where any part of this thesis has previously been submitted for a degree or any other qualification at this University or any other institution, this has been clearly stated;
3. Where I have consulted the published work of others, this is always clearly attributed;
4. Where I have quoted from the work of others, the source is always given. With the exception of such quotations, this thesis is entirely my own work;
5. I have acknowledged all main sources of help;
6. Where the thesis is based on work done by myself jointly with others, I have made clear exactly what was done by others and what I have contributed myself;
7. None of this work has been published before submission

Signed: .....

Date: .....

Acknowledgements

I would like to give special thanks to my main supervisor Dr Nuria Garcia-Araez for her advice and guidance throughout this MPhil and to Professor John Owen for his support, in particular with the impedance spectroscopy.

Thanks also go to my fellow students on the 7th floor at Southampton and my colleagues at Dstl. Particularly to Darren Browning, the capability advisor for power sources. I am grateful for the support from my employer, Dstl, without which this work would not have been possible. I would also like to thank Alan Groves whose plan for early career scientists at Dstl led to this work and others in developing our research careers.

Thanks to my family for all they have done to get me to this point. Finally, thanks go to my husband, Oliver, for putting up with the lost weekends and evenings that it took to complete this MPhil and for his support throughout this, I wouldn't have got here without it.

List of Abbreviations

Abbreviation	*Explanation*
LFP	LiFePO4 cathode material
EPD	Electrophoretic Deposition
NMC	LiNixMnyCozO2 cathode material
NCA	LiNixCoyAlzO2 cathode material
HCP	Hexagonal Close Packed
EC	Ethylene Carbonate
PC	Propylene Carbonate
DMC	Dimethyl Carbonate
DEC	Diethyl Carbonate
EMC	Ethyl Methyl Carbonate
PEO	Polyethylene Oxide
PVDF	Polyvinylidene Fluoride
LISICON	Lithium Super Ionic Conductor,

Abbreviation	*Explanation*
NASICON	Sodium (Na) Super Ionic Conductor
CVD	Chemical Vapour Deposition
PVD	Physical Vapour Deposition
ALD	Atomic Layer Deposition
CV	Cyclic Voltammetry
CPE	Constant Phase Element
SEM	Scanning Electron Microscopy
EDS	Energy Dispersive Spectroscopy
IPA	Iso Propyl Alcohol
NMP	N Methyl 2 Pyrrolidone

List of Terms

Term	*Explanation*
ΔG	Gibbs free energy
n	Number of electrons
F	Faraday constant (96,485 C mol^{-1})
E^0_{CELL}	Equilibrium potential of the cell.
R	gas constant (8.314 J K^{-1} mol^{-1})
T	Temperature
a_O and a_R	Activities of the oxidised and reduced species respectively
E^0_e	Standard potential which is the equilibrium potential under standard conditions
c_O and c_R	Concentration of oxidised and reduced species respectively
E'^0	Formal potential which is the equilibrium potential when $c_O = c_R$
η	Overpotential
E	potential of cell

Term	*Explanation*
E_{eq}	potential at equilibrium
J	current density
j_0	exchange current density
α_a	electron transfer coefficients of the anode reaction
$-\alpha_c$	electron transfer coefficients of cathode reaction
k_s	Standard rate constant
D	Diffusion coefficient
c	Concentration
x	Distance from the electrode.
I_P	Peak current
v	Potential
θ	extent of adsorption as a fraction of the surface covered
ΔG^0_{ads}	the free energy of adsorption under standard conditions.

Term	*Explanation*
R_u	Uncompensated solution resistance
C_{dl}	double layer capacitance
ε	Permittivity
ε_0	vacuum permittivity
φ_0	standard potential, E-E_z,
E_z	potential of zero charge
F_e	electrophoretic force
q	charge carried by the body
E_f	electric field
F_f	friction forces
v_p	Particle velocity
f_r	frictional coefficient
μ_e	Coefficient of electrophoretic mobility
ζ	zeta potential

Term	*Explanation*
$f(\kappa a)$	Henry's function
η_s	viscosity of the suspension
m	mass
C_s	suspension concentration
S	deposition area
t	Time
f	Frequency
φ	Phase difference
ω	2 x π x f
I	current
Q	Charge
Z	Impedance
R	Resistance

Chapter 1: Introduction

1 Introduction

Throughout military and civilian applications, there is an increasing reliance on portable electronics. In the past 10 years portable electronic devices have not only seen a decrease in size but also an increase in the number of functions that devices such as mobile phones etc. are required to perform. This increase in performance requirements and decrease in size has led to a greater demand on the energy storage systems that power these devices.

In developing and selecting any electrical energy storage system the following key factors must be considered:

- Specific energy / Wh Kg^{-1} – The Energy in Wh (power multiplied by time) produced per Kg of a battery system
- Energy Density / Wh m^{-3} – The Energy in Wh produced per m^3 of a battery system
- Power density / W m^{-3} – The power in W produced per m^3 in a system
- Cycle life – The number of charging and discharge cycles a system can undergo before it drops below a critical energy density
- Safety

Energy storage system development is a careful balance of each factor to produce the best system for the specification requirements.

Current batteries for soldier systems rely on many different standard power source sizes, shapes and weights. The integration of power sources into space-limited platforms and to fit to a soldier correctly is difficult and still relies on the layer by layer manufacturing approaches used in conventional battery production. There is therefore a need to develop alternative methods of producing batteries that can enable small batches of power sources to be produced on demand to fit bespoke missions and systems. This thesis will focus on the application of alternative methods of producing lithium ion batteries to enable increased automation in coating techniques and the potential for manufacture of bespoke batteries in 3D formats based on military requirements.

2 A theoretical background to Lithium Ion Batteries

Batteries, including lithium ion batteries, are electrochemical systems which enable the conversion of the energy liberated in a chemical reaction into electricity.[1] The loss of an electron from a chemical substance is described as its oxidation, the gain of an electron is described as reduction. Reactions where electrons transfer between species are referred to as redox reactions. Most chemical substances are able to donate or accept electrons from other substances in a redox reaction leading to different oxidation states.

In reality any system that involves oxidation or reduction can be termed as electrochemical but the term is usually used to refer to the following systems:

- where an electrical current is applied to promote electron transfer leading to a chemical reaction e.g. electroplating
- where a chemical reaction involving electron transfer is used to produce an electrical current e.g. batteries

The first type of electrochemical system will be discussed later on in this thesis when electrophoresis, an electrodeposition technique, is introduced. However this introductory section will focus on the latter type, highlighting the 5 key concepts that are important in determining and describing the behaviour of a battery system.[2]

2.1 Cell potential

A battery is an electrochemical system where the electron transfer resulting from a chemical reaction is used to produce current. When considering the thermodynamics of an electrochemical cell reaction in a battery it is useful to begin by considering the system at equilibrium. At chemical equilibrium the rate of reaction in the forwards and reverse direction are the same so the system gives the appearance of having a static composition. The equilibrium potential is the potential difference at this point.

The standard equilibrium potential of a cell, E_e^0 is the potential when all the reactants and products in the electrochemical system are in their standard states. It is common in an electrochemical redox reaction to consider the

oxidation and reduction reactions separately with each electrode undergoing a half cell reaction with its own standard potential. For example, in a simple Daniel cell in which copper and zinc metal rods are suspended in an aqueous suspension, the overall reaction in the system is:

$$Cu^{2+}_{(aq)} + Zn_{(s)} \rightleftharpoons Cu_{(s)} + Zn^{2+}_{(aq)}$$

This can be considered as two half-cell reactions with the following reaction occurring at the zinc electrode:[2]

$$Zn^{2+}_{(aq)} + 2e^- \rightleftharpoons Zn_{(s)} \qquad E^0 = -0.76 \text{ V}$$

And the copper electrode undergoing the following reaction:[2]

$$Cu^{2+}_{(aq)} + 2e^- \rightleftharpoons Cu_{(s)} \qquad E^0 = +0.34 \text{ V}$$

The standard potential for the cell can then be calculated from the difference between the two electrode half-cell potentials:

$$E^0 = +0.34-(-0.76) = +1.10 \text{ V}$$

The cell electrode potential can be used to calculate the standard Gibbs free energy change of the electrochemical reaction using the equation:

$$\Delta G^0 = -nFE^0_{CELL}$$

Equation 1

Where:
ΔG = Gibbs free energy
n = number of electrons transferred
F = Faraday constant
E^0_{CELL} = equilibrium potential of the cell.

For the redox reaction:

$$Ox + ne^- \rightleftharpoons Red$$

The Gibbs free energy of the reaction can be found from the standard Gibbs free energy using the following equation:

$$\Delta G = \Delta G^0 + \frac{RT}{nF} \ln \frac{a_O}{a_R}$$

Equation 2

Where:
R = gas constant (8.314 J K^{-1} mol^{-1})
T = temperature
n = number of electrons transferred
F = Faraday constant (96,485 C mol^{-1})
a_O and a_R = activities of the oxidised and reduced species respectively

By substituting equation 1 into this equation, the equilibrium potential of the system can be found, giving the following equation:[3]

$$E = E^0 + \frac{RT}{nF} \ln \frac{a_O}{a_R}$$

Equation 3

Where:

a_O and a_R = activities of the oxidised and reduced species respectively
E_e^0 = standard potential which is the equilibrium potential under standard conditions

The activity is the effective concentration of the species in the mixture and accounts for non-ideality in the system. It is typical however, to only consider the concentrations of the species in an electrochemical system and apply the first equation to the system. For most electrochemical systems this is a good approximation as the excess of electrolyte used means that there are relatively low concentrations of Ox and Red in the solution. This means that the activity coefficients for Ox and Red are almost the same and the equation cancels to the Nernst equation:

$$E = E'^{0} + \frac{RT}{nF} \ln \frac{c_o}{c_R}$$

Equation 4

Where:
c_O and c_R = concentration of oxidised and reduced species respectively
E'^{0} = formal potential which is the equilibrium potential when $c_O = c_R$

2.2 Rate Capability

As well as the total energy stored by a battery and its voltage, the rate that it undergoes charge and discharge is important as it ultimately determines the current of the battery. Several factors are of importance in determining the rate capability of a battery. The first factor we will consider here is the effect of electron transfer during the electrochemical reaction.

Applying the equilibrium potential to a cell would not mean the reaction would proceed at a significant rate. Instead an overpotential, η must be applied to drive the electron transfer reaction in the battery. The overpotential is the difference between the experimental potential and the equilibrium potential of a cell. A positive overpotential will drive an oxidation reaction (positive current) and a negative overpotential will drive a reduction reaction (negative current).

The current density of the reaction generated by the overpotential can be described using the Butler-Volmer equation:

$$j = j_0 \left[\exp\left(\frac{\alpha_a nF}{RT}\eta\right) - \exp\left(\frac{-\alpha_c nF}{RT}\eta\right) \right]$$

Equation 5

Where:
j = current density
j_0 = exchange current density
α_a = electron transfer coefficients of the anode reaction
$-\alpha_c$ = electron transfer coefficients of cathode reaction
n = number of electrons.

The exchange current density can be found using the following equation:[2]

$$j_0 = nFk_s(c_O)^{\alpha_a}_{x=0}(c_R)^{\alpha_c}_{x=0}$$

Equation 6

Where:
k_s = Standard rate constant

The Butler-Volmer equation therefore means that the electron transfer current at a battery electrode is dependent on the following parameters:

- Electrode area, A
- Overpotential, η
- Kinetic parameters, j_0 and α
- Reactant concentration
- Temperature

However, this only takes into account the kinetics of electron transfer in a reaction. An electrochemical reaction is considered to proceed through three steps:

$$Ox_{bulk} \xrightarrow{\text{Mass transport}} Ox_{electrode}$$

$$Ox_{electrode} + e^- \xrightarrow{\text{Electron transfer}} Red_{electrode}$$

$$Red_{electrode} \xrightarrow{\text{Mass transport}} Red_{bulk}$$

This means that in addition to the kinetics of electron transfer we must also consider mass transport, the movement of electrons to and from the point of the electron transfer reaction. Mass transport is essential to the electrochemical reaction as it provides the reactants and removes the products of the reaction. There are three forms of mass transport:

- Migration - the movement of charged species due to a potential gradient. When a current is passed between the two electrodes an electric field is generated which is the gradient of electric potential across the solution. In many applications migration control can be avoided by using a highly conductive electrolyte, so migration is fast.

- Convection - the movement of species due to stirring or hydrodynamic control, it can generally be quite fast. Natural convection, the natural movement of samples due to equipment vibrations etc. can be particularly difficult to control.
- Diffusion - the movement of species in a concentration gradient. Species move from an area of solution with a higher concentration to a lower concentration. Diffusion can often be slow and so can have a significant impact on electrochemical reactions.

Many battery systems are diffusion limited, diffusion can be described by Fick's second law which states that for a reduction reaction:

$$\frac{\partial c_O}{\partial t} = D_O \frac{\partial^2 c_O}{\partial x^2} \quad \text{and} \quad \frac{\partial c_R}{\partial t} = D_R \frac{\partial^2 c_R}{\partial x^2}$$

Equation 7

Where:
D = diffusion coefficient
c = concentration
x = distance from the electrode.

Initially there is only oxidant present in the solution so that $D_O = D_R$. This can be used to determine the peak current, I_p using the following equation:

$$I_P = -(2.69 \times 10^5)\, n^{\frac{3}{2}}\, c_O^{\infty}\, D^{\frac{1}{2}}\, v^{\frac{1}{2}}$$

Equation 8

Where:
I_P = Peak current
v = potential

As this function is valid for reversible reactions, a quick test for reversibility can be obtained by plotting I_P against $v^{1/2}$. A straight line will suggest that the reaction is reversible. The gradient of this plot can be used to determine the diffusion constant for the system.[4]

2.3 Capacity of an electrochemical cell

The capacity is a measure of the amount of species reduced or oxidised within the cell. This can also be described as the total charge transferred during

charge or discharge of the cell. If a current, I flows for time, δ*t* then *I*δ*t* charge passes through the circuit. Considering the reaction:

$$M^{x+}_{(aq)} - ne \rightarrow M^{(x+n)+}_{(aq)}$$

Each M^{x+} ion gives up n electrons to the external circuit to form $M^{(x+n)+}$. The number of moles of reactant consumed by current, I, passing through the circuit is therefore given by:

$$N_M = \frac{1}{nF}\int_0^t i\mathrm{d}t$$

Equation 9

If N_M is a representation of all the moles available in the system we can calculate the total charge that can be applied to the circuit using the following equation:

$$Q_T = \int_0^t i\mathrm{d}t = nFN_M$$

Equation 10

When considering a two electrode cell the second electrode reaction must also be considered:

$$P^{y+}_{(aq)} + n'e \rightarrow P^{(y-n)+}_{(aq)}$$

By substituting n’ with n in the equation for N_M we get the equation for N_P. The total charge available in a cell, the maximum capacity, is determined by the lower of the two values, N_M or N_P.

By using the molar mass of the electrode compound of interest, the theoretical capacity in mAh/g can be determined. Theoretical capacity is a good determination of how a material will perform as an electrode material. Due to practical issues such as capacity fade, material properties and *IR* drop, there can be a substantial difference between theoretical capacity and the achievable capacity of a cell.[1]

2.4 Phase change and the Gibbs Phase Rule

This chapter has mainly discussed the kinetics of electron transfer but in lithium ion batteries electron transfer is performed through lithium intercalation and so there is a change in the material with the insertion or removal of lithium. When considering the thermodynamics of lithium intercalation it is useful to consider the Gibbs phase rule. The Gibbs phase rule is used to determine the number of degrees of freedom within a reaction which can be determined by the following relationship:

$$F = C + n - P$$

Equation 11

Where:
F = degrees of freedom
C = number of components
n = number of intensive variables (except component mole fractions) used to describe the system
P = number of phases present.

For electrochemical systems temperature and pressure are considered as the only intensive variables so $n = 2$. By assuming the temperature and pressure are constant during the reaction, the terms for the intensive variables cancel. The reaction at the cathode is considered binary so $C = 2$. This means the number of degrees of freedom can be calculated as: [5-7]

$$F = (2 + 2 - P) - 2 = 2 - P$$

Equation 12

Lithium insertion in lithium ion batteries can proceed in two main mechanisms depending on the level of interaction between the lithium ions in the electrode. Considering the $LiCoO_2$ electrode reaction:

$$LiCoO_2 \rightarrow Li_{1-x}CoO_2 + xLi^+ + xe^-$$

Lithium insertion proceeds through a solid solution model where interactions between lithium ions within the lattice are minimal. This means it is favourable for the lithium ion to locate anywhere within the lattice. This means any phase change is homogeneous and it can be considered as a single phase containing

Li_xCoO_2. Applying the Gibbs phase rule to this system we can see that the number of degrees of freedom for the single phase $LiCoO_2$ system is 1, so that as the amount of lithium (x) varies we observe a linear relationship shown in figure 3. [5-7]

The lithium iron phosphate (LFP) reaction:

$$LiFePO_4 \rightarrow Li_{1-x}FePO_4 + xLi^+ + xe^-$$

has attractive reactions occurring between the lithium ions as they intercalate. This means that the lithium ions will preferentially locate near to other lithium ions so the intercalation proceeds heterogeneously as shown in figure 1. The attractive interactions of lithium ions in $LiFePO_4$ means it has regions of $FePO_4$ and regions with $LiFePO_4$. It therefore exists as a two phase material.[8] For materials such as $LiFePO_4$ there are two phases present so the number of degrees of freedom are zero leading to a constant potential during lithium intercalation. [5-7]

Homogeneous phase change e.g. $LiCoO_2$

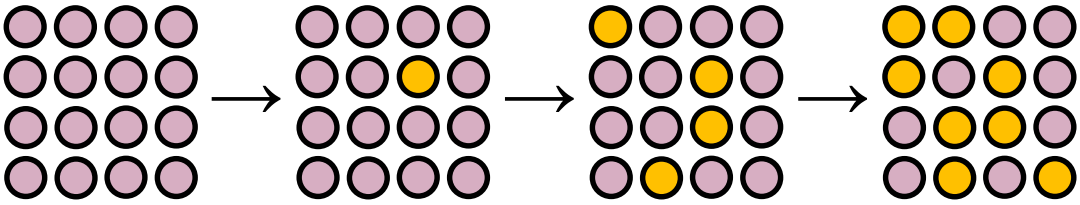

Heterogeneous phase change e.g. $LiFePO_4$

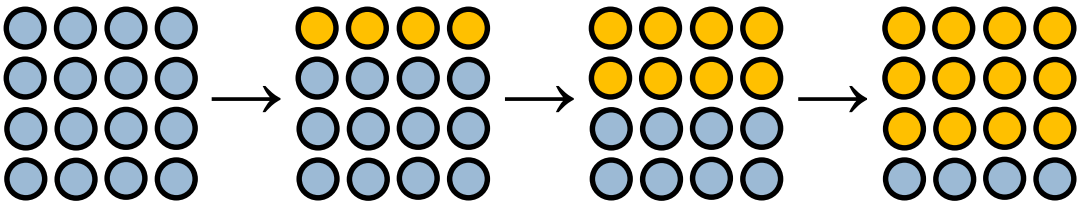

Figure 1. Diagram to show the differences between heterogeneous and homogeneous phase change materials

When considering the intercalation of lithium ions into a solid electrode as the potential changes, two features can be observed as part of the process. Firstly the lithium ions are occupying unoccupied sites within the host structure and as such there are a limited number of sites to be occupied. Secondly the lithium ions are able to move between sites within the structure as the battery is

charged/discharged. This definition of the intercalation led comparisons to be drawn with adsorption isotherms such as the Langmuir and Frumkin isotherms.[9]

The Langmuir isotherm assumes that different adsorbates have no lateral interactions and each adsorbate that approaches the surface is treated the same. This leads to following equation:

$$\frac{\theta}{1-\theta} = c \exp\left(\frac{-\Delta G^{0}_{ads}}{RT}\right)$$

Equation 13

Where:
θ = extent of adsorption as a fraction of the surface covered
c = a constant
ΔG^{0}_{ads} = the free energy of adsorption under standard conditions.

This can be applied to lithium ion intercalation through the Gibbs equation, giving:

$$\frac{x}{1-x} = Kc \exp\left(\frac{FE}{RT}\right)$$

Equation 14

Where:
x = extent of lithium intercalation into electrode material

This leads to the potential-composition relationship:

$$E = E_0 - \frac{RT}{F} \ln\left(\frac{x}{1-x}\right)$$

Equation 15

As figure 2 shows, this can then be used to plot a simulated cyclic voltammetry experiment. Figure 2 also demonstrates the concept of IR drop and its effect on the electrode potential. For example, in a non-ideal electrochemical cell there are resistances due to electrical contacts. The effect of these resistances is found through $V=IR$ and as such they are commonly referred to as the IR drop. This can be seen in figure 2 as an increasing separation of the peaks giving the distinctive shape of cyclic voltammetry measurements discussed later on in this thesis.

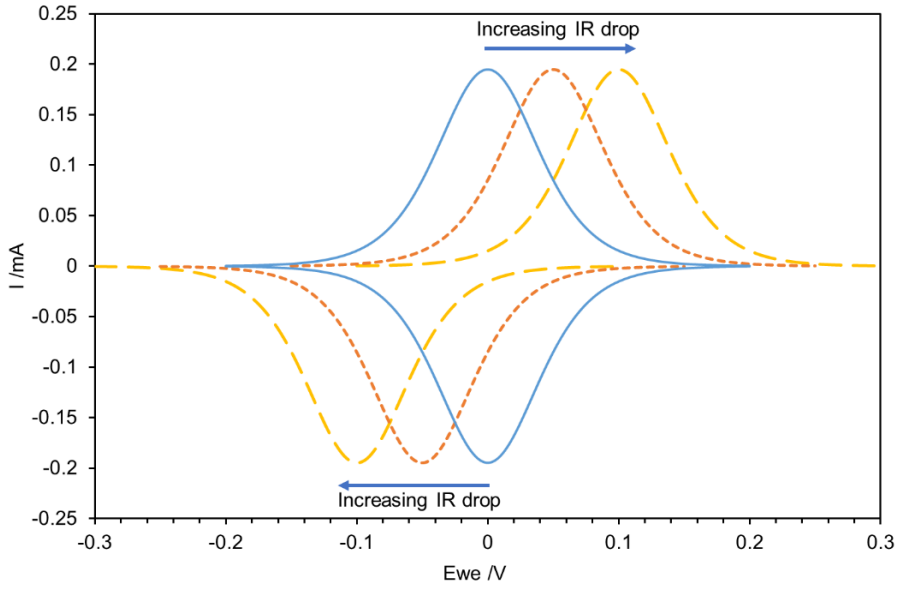

Figure 2. Graph showing a simulated Langmuir isotherm. The graph shows the effect of an increasing IR drop on the separation of the peaks.

The Frumkin isotherm is similar to the Langmuir isotherm but takes into account interactions between the adsorbed and adsorbing species. The Gibbs energy of adsorption is given a linear relationship with coverage of a monolayer:

$$\frac{\theta}{1-\theta} = c \exp\left(\frac{-\Delta G^{0}_{ads}}{RT}\right) \exp\left(\frac{-r\,\theta}{RT}\right)$$

Equation 16

For lithium intercalation the potential composition relationship becomes:

$$E = E^{0} - \frac{RT}{F} \ln\left(\frac{x}{1-x}\right) + kx$$

Equation 17

For lithium intercalation k corresponds to the level of attraction between adsorbing lithium ions and as figure 3 shows this leads to a change in shape of the plot. At high values of k, the plot corresponds to the two phase behaviour observed in $LiFePO_4$. At low values of k the plot corresponds to the single phase behaviour observed in $LiCoO_2$ and the lithium ion interactions are low.

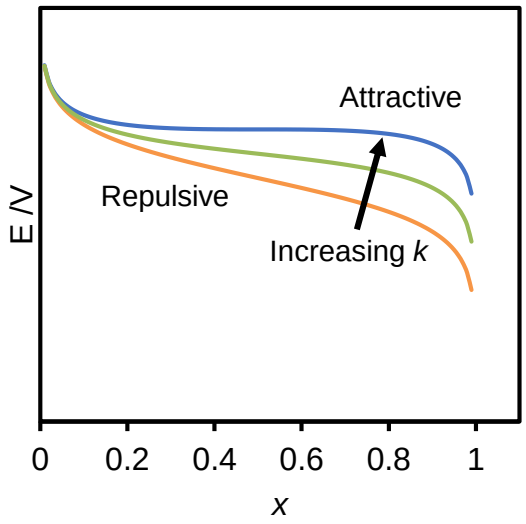

Figure 3. A plot of the composition-potential relationship of three species with different degrees of attraction.

2.5 The electric double layer

Most electrochemical systems consist of a solid electrode with a liquid electrolyte. When a potential is applied to an electrode a charge will build on the electrode surface based on the potential applied, the electrode material and the electrolyte composition. This in turn affects the charged ions and dipoles of molecules within the liquid electrolyte. The opposite charged particles will arrange on the surface creating an effect called the electrical double layer.

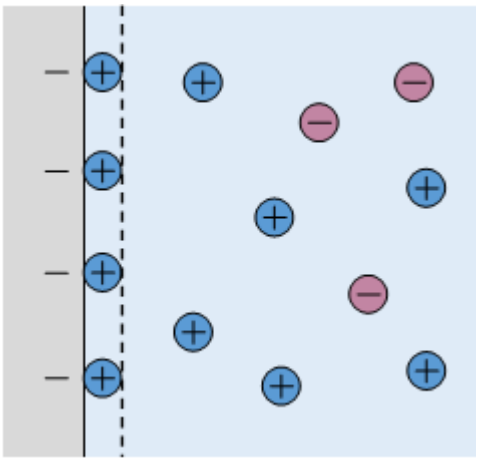

Figure 4. Diagram to demonstrate the electrical double layer on a negatively charged electrode

The electric double layer can be considered to behave as a capacitor. In the example in **Error! Reference source not found.** when the potential of the electrode is changed to be more negative, the negative charge on the surface

will increase and more positive ions will be attracted to balance the charges. A change in the electrode potential changes the amount of charge stored at the interface. There is therefore a charging current applied to charge the surface. The surface can be modelled using an equivalent circuit:

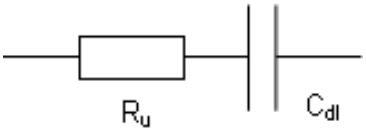

Where:
R_u = Uncompensated solution resistance
C_{dl} = double layer capacitance

This means that when a potential change is applied to the electrode the current must first flow through the equivalent circuit, above, before there is a change in potential at the electrode. The current can be quantified using the following equation:

$$I = \frac{\Delta E}{R_u} \exp\left(-\frac{t}{R_u C_{dl}}\right)$$

Equation 18

Four main models exist to describe the potential at the double layer. The Helmholtz model is the simplest model and assumes that all charge is balanced at the surface by ions of the opposite charge from the solution forming a layer. This means that the double layer is very thin and the capacitance of the double layer is independent of the electrode potential.[10]

The Gouy-Chapman model assumes ions are in random thermal motion and are on average more likely to be found at the electrode surface with the opposite charge to their own. This is referred to as an ion atmosphere near the electrode surface and its extent depends on the concentration of the electrolyte. In this case the capacitance will vary with potential and capacitance is given by:

11-13

$$C_{dl} = \left(\frac{2z^2e^2\varepsilon\varepsilon_0 c_\infty}{RT}\right)^{1/2} \cosh\left(\frac{ze\varphi_0}{2kT}\right)$$

Equation 19

Where:
ε = permittivity
ε_0 = vacuum permittivity
φ_0 = standard potential, E-E_z,
E_z = potential of zero charge

The Stern model is used to describe more concentrated solutions and takes both of the two models, assuming most charge is balanced by the compact Helmholtz layer and the rest of the charge is balanced by a more diffuse Gouy-Chapman layer with both their capacitances in series.[14]

The fourth model is the triple layer model which recognises that the adsorption of the opposite charged ions on the electrode surface (the inner Helmholtz plane) will be balanced by a third layer of the same charge as the electrode (outer Helmholtz plane), creating a triple layer model.[2, 15]

3 Lithium ion batteries

A simple electrochemical cell consists of two electrodes with a potential difference between them. A positive and a negative electrode are shown in figure 5. In all electrochemical cells positively charged ions dissolve into solution and move to the anode where they react, gaining electrons. If the anode and cathode are connected this creates a flow of electrons (a current). Two main types of batteries are used: primary and secondary batteries.

Primary batteries were the first to be developed and can be dated back to Volta in the 1800s. They are single use systems which are thrown away once the electrical energy has been depleted. In rechargeable secondary batteries, such as lithium ion batteries, the process can be reversed by applying a current to the battery, allowing the battery to be used again.[16]

Although several different rechargeable lithium metal batteries were proposed and developed, problems with their safe operation meant that they were not widely used. It was not until the development of Lithium ion batteries by Sony in 1991 that a safe way to harness the high energy densities of lithium intercalation compounds was achieved.[1, 17]

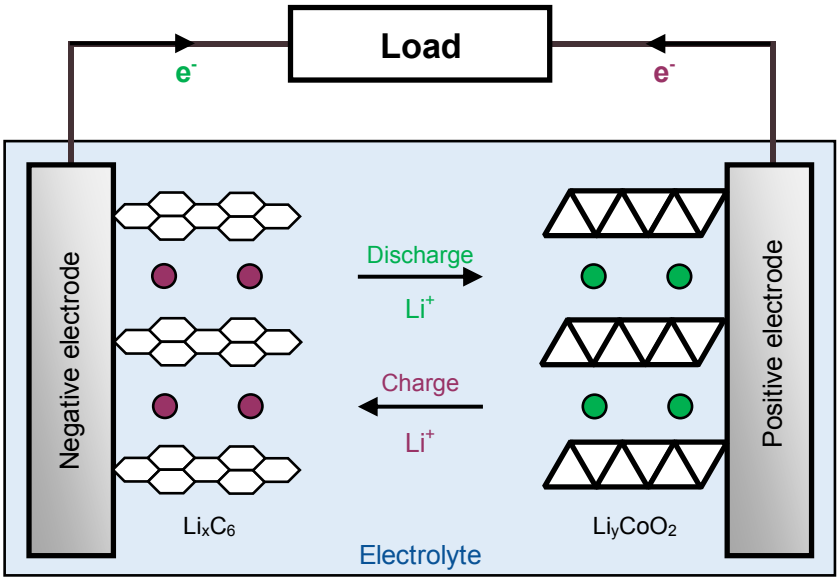

Figure 5. Diagram to demonstrate charging and discharging in a lithium ion battery.

All lithium ion batteries are based on the same principal as the first Sony battery, often called the “rocking chair” battery. The battery consists of two lithium insertion electrodes which act as the positive or negative electrode. The first lithium ion battery is demonstrated in figure 5 with layers of carbon (graphite) acting as the negative electrode and the layered intercalation compound $LiCoO_2$ acting as the positive electrode material. The cell reaction equation for this and subsequent lithium ion battery systems is shown below:[1, 17]

$$Li_xC_nD_m(s) + A_zB_y(s) \underset{\text{charge}}{\overset{\text{discharge}}{\rightleftharpoons}} C_nD_m(s) + Li_xA_zB_y(s)$$

Since the initial development of lithium ion batteries, scientists have sought to improve the materials for batteries and many different positive and negative electrodes have been produced.

In general, six strategies have been employed to enhance the performance of lithium ion batteries across a range of chemistries and cell designs:

- Reducing particle size
- Composite electrode formation
- Doping electrode materials with other elements
- Electrode morphology control
- Coating and encapsulation
- Electrolyte modification

Through research into these strategies, a huge number of different battery systems have been developed. This introduction will discuss the key materials by structure type used for positive and negative electrodes and some of the benefits and challenges of each material as well as discussing the role of the electrolyte in lithium ion batteries.[18]

3.1 The positive electrode

When developing or selecting a positive electrode material there are several criteria that a material must conform to. In their review article Whittingham et. al.

discuss the 8 key properties that must be considered when choosing a positive electrode material for a rechargeable lithium ion battery:[19]

1. The electrode material must contain an ion that is easy to reduce or oxidise.
2. The reaction of the electrode material with lithium must be reversible so that the battery can be charged and discharged without a significant reduction in capacity.
3. The reaction with lithium must have a high free energy of reaction, a high capacity and a high voltage, leading to a large amount of energy stored.
4. The reaction with lithium must proceed rapidly for both charging and discharging in order to give a high power density.
5. The electrode must also be a good electronic conductor to enable electrons to be added or removed easily.
6. The electrode material should be stable throughout charge and discharge.
7. The electrode material should not be prohibitively expensive.
8. The material should not be environmentally hazardous.

This extensive criteria list for positive electrodes has led to a large range of different positive electrodes available. This section will discuss the different types of positive electrode by structure type, highlighting the most commonly used materials and the challenges of developing lithium ion batteries using these materials.

3.1.1 Layered-type

Since the development of the Sony rocking chair battery using $LiCoO_2$ in 1991, the layered transition metal oxides have been the most successful positive electrode material for lithium ion batteries. Their popularity is mainly due to their relatively high voltage operation, up to 4 V and high theoretical capacities.

The structure of the different layered transition metal oxides is similar and is based on a rock-salt structure with lithium and transition metal cations

occupying alternate layers of octahedral sites in a distorted cubic close-packed octahedral lattice.[1, 20]

3.1.1.1 $LiCoO_2$

$LiCoO_2$ was the first lithium ion positive electrode material to be developed commercially. However, there are issues with the application of Li_xCoO_2. Despite offering the potential to reach capacities greater than 200 mAh/g, in practical cells Li_xCoO_2 is only known to reach a capacity of around 140 mAh/g. This is because only half of the lithium can be removed without changing the structure of the Li_xCoO_2. This irreversibility below x = 0.5 is thought to be due to a topotactic phase transition at lower values of x from a monoclinic structure to a hexagonal phase.[21-22] This phase change is thought to impact the electrochemistry of the electrode in two ways. The phase change, like any change in structure, can destabilise the electrode so it no longer functions as expected. Secondly, the lithium depleted phase is less conductive and has a slower reaction rate than at higher values of *x*.[19]

The increasing cost of cobalt in $LiCoO_2$ and concerns over safety and thermal stability led to the study of other transition metal oxides within the group and the materials can be considered as $LiMO_2$ where M=Ni, Co, Mn, Al. [22-23]

3.1.1.2 $LiNiO_2$ and $LiMnO_2$

Li_xNiO_2 was an early contender to replace Li_xCoO_2 since the cost of Ni was considerably lower than the expensive cobalt metal. Li_xNiO_2 also demonstrated a similar structure to Li_xCoO_2 and demonstrated a greater stability on lithium removal. [22, 24]

Extraction of lithium from Li_xNiO_2 follows four stages of structural change. Initially when $x > 0.75$ the Li_xNiO_2 has a rhombohedral structure. As more lithium is removed and $0.45 \leq x \leq 0.75$ there is a phase change to a monoclinic phase. When $0.25 \leq x \leq 0.45$ the structure returns to the rhombohedral phase again. When x is below 0.25 the Li_xNiO_2 interlayer distance increases to such a point that there is a significant capacity fade. In practical cells using Li_xNiO_2 lithium

discharge can occur when $0.25 \leq x \leq 1$ which still gives a greater practical capacity than Li_xCoO_2.

However, Li_xNiO_2 is not widely used because it is difficult to synthesise a phase-pure material. During synthesis the Nickel ions can migrate to a location in between the layers, replacing the lithium ions and adversely affecting the performance of the electrode material.[24-26]

$LiMnO_2$ also offers the potential to lower cost and has a lower toxicity, however, it is not generally used in commercial cells due to its more complex structure and poor rate capability. This is mainly due to the phase change to a spinel structure during cycling and around 25% of the Mn ions have been observed to migrate to the lithium occupied sites on cycling.[27-28]

3.1.2 $LiNi_xMn_yCo_zO_2$ (NMC)

As discussed, there were several issues with the $LiMO_2$ materials including phase change behaviour, thermal stability and cost. Some of these problems have been solved by intercalating elements within the structures leading to mixed transition metal oxide materials. This has been very successful in tweaking the properties of the materials to gain the best properties at the best cost. One of the most successful combinations was to use $LiNi_{1/3}Mn_{1/3}Co_{1/3}O_2$. The different transition metal cations have a different susceptibility to move to the Lithium ion site and form a spinel structure which leads to capacity fade. It is thought the high cycle life and structural stability of $LiNi_{1/3}Mn_{1/3}Co_{1/3}O_2$ is due to the change in structure as lithium is removed from the sample. When lithium is removed the unit cell expands in the *c* direction and contracts in the *a* dimension, keeping the unit cell volume the same. This is different to LCO electrode materials in which there is a change in the unit cell volume during discharge. In macroporous samples of $LiNi_{1/3}Mn_{1/3}Co_{1/3}O_2$ the capacity is as high as 234 mAh g^{-1}.[18, 22, 29-30]

3.1.3 $LiNi_xCo_yAl_zO_2$ (NCA)

Another commercially available material is $LiNi_xCo_yAl_zO_2$ (NCA). In these materials the Cobalt acts to stabilise the structure of the electrode and prevents

the Ni from moving to sites between the layers giving a high usable capacity (~200 mAh g^{-1}).[18] The aluminium is not redox active and is thought to prevent the complete removal of lithium from the structure. This prevents some of the phase changes discussed previously that can lead to poor cycling behaviour.[19, 31-32]

3.1.4 Spinel-type

Unlike the layered transition metal oxides in which the lithium ions are located between the layers, in the spinel structure the lithium ions and transition metal ions occupy different sites within a framework. $LiMn_2O_4$ has a cubic close-packed structure with manganese ions occupying half the octahedral sites and lithium occupying one eighth of the tetrahedral sites. This structure gives a three dimensional pathway for lithium diffusion through the structure. [1, 20, 33-35]

Two issues exist with the lithium insertion and de-insertion process for spinel electrodes. The first is that the charge discharge has two plateaus each corresponding to a two phase process. This is due to ordering of the lithium ions in the tetrahedral sites. A large activation energy is required to move the lithium from one site to another creating ordering in the material so that instead of forming a solid solution, where lithium ions can be anywhere, two phases of material exist with a lithium rich and lithium poor structure. Another issue is the Jahn-Teller distortion at low lithium ion compositions which leads to strain and rapid capacity loss. This means the spinel materials, like other lithium ion electrodes are not cycled to full lithium discharge, limiting the capacity to lower than the theoretical capacity. The manganese ions can also dissolve in the electrolyte reducing the structural stability and causing capacity fade in the electrode[33-35]

As with other materials for lithium ion positive electrodes, success has been achieved by doping the $LiMn_2O_4$ structure with other transition metal ions. The most successful of these compounds studied was $LiNi_{0.5}Mn_{1.5}O_4$ which demonstrates a high stability. It is thought the high stability is due to the nickel suppressing the dissolution of Mn into the electrolyte as well as reducing the

Jahn-Teller distortion by increasing the average oxidation state of manganese ions.[35-36]

3.1.5 Olivine-type electrodes

The relatively low cost and low toxicity of iron led to the proposition that positive electrodes made out of iron may offer a good alternative to the layered Cobalt and manganese containing materials. Initial studies looked at using $LiFeO_2$ but the relative stability of the FeO_2 layered structure and the instability of the Li_xFeO_2 meant these materials did not produce a satisfactory positive electrode material. In addition the Fe^{4+}/Fe^{3+} redox energy was too far below the Fermi energy of a lithium anode and the $Fe^{2+/}Fe^{3+}$ couple was too close to it. Other iron compounds were considered but Goodenough et. al. found that PO_4 and SO_4 stabilised the structure and lowered the energy of the $Fe^{2+/}Fe^{3+}$ redox reaction to a level that made the electrode practical. [20, 37-40]

Like the spinel materials, Olivine electrodes have a 3D structure. Lithium iron phosphate (LFP) has a slightly distorted hexagonal close-packed (HCP) oxygen array with lithium ions and iron (II) ions occupying octahedral sites and phosphorus occupying tetrahedral sites.[18, 41] The voltage of LFP as a positive electrode was found to be 3.4 V which is within the 3-4 V window required for high capacities without affecting electrolyte performance. The Olivine materials also offer a high theoretical capacity at 170 mAh/g.[37, 40]

Unfortunately, LFP suffered from a poor conductivity and low power densities. Padhi et. al. stated that this low conductivity is solely due to the separation of the FeO_6 octahedra by PO_4 polyanions, which reduces the conductivity, and they determined that lithium diffusion is fast.[40] This is not in agreement with later research which has found that the lithium diffusion rate is also low.[42]

Several methods have been used to improve the conductivity of LFP cathode materials focusing on the two aspects of the poor conductivity; the poor electronic conductivity and poor lithium diffusion through the material. Two common techniques are used to improve the rate capability of LFP. The first method used was to reduce the size of the particles. This in turn reduces the diffusion pathways within the sample and increases lithium ion diffusion.[43-44] In

addition to reducing their size, the main approach to improve electrical conductivity of LFP particles has been to coat them with carbon.[45-46] Electronic conductivity has also been improved by coating with other materials such as silver [47] but the relatively low cost has made carbon coating the preferred technique.[48] Kang et. al. found that coating the LFP particles with an amorphous LFP layer improved lithium ion diffusion through the material by aligning the entrance position of the iron phosphate lattice with the lithium ion direction of motion.[49]

As with the other positive electrode materials, doping has also been used to improve the properties of the material. Doping with supervalent cations such as Mg, Al, Ti, Nb or W has been shown to improve the electrical conductivity of the samples.[48] Meethong et. al. found that the addition of Niobium to the LFP compound reduced strain in the material, increasing the lithium diffusion rate and enhancing rate capability.[50]

LFP is a two phase material. As discussed earlier on in this chapter, this means that instead of lithium intercalation occurring in a random way, there are interactions between the lithium ions as they intercalate which leads to a two phase state with regions of $LiFePO_4$ and $FePO_4$. As shown in Figure 6 this leads to a flat discharge profile as lithium intercalates into the material. Figure 6 also demonstrates the core shell model for LFP discharge which proposes that the $LiFePO_4$ phase forms from the outside of the LFP particle into the centre, until the particle is a single phase of material.[42, 51]

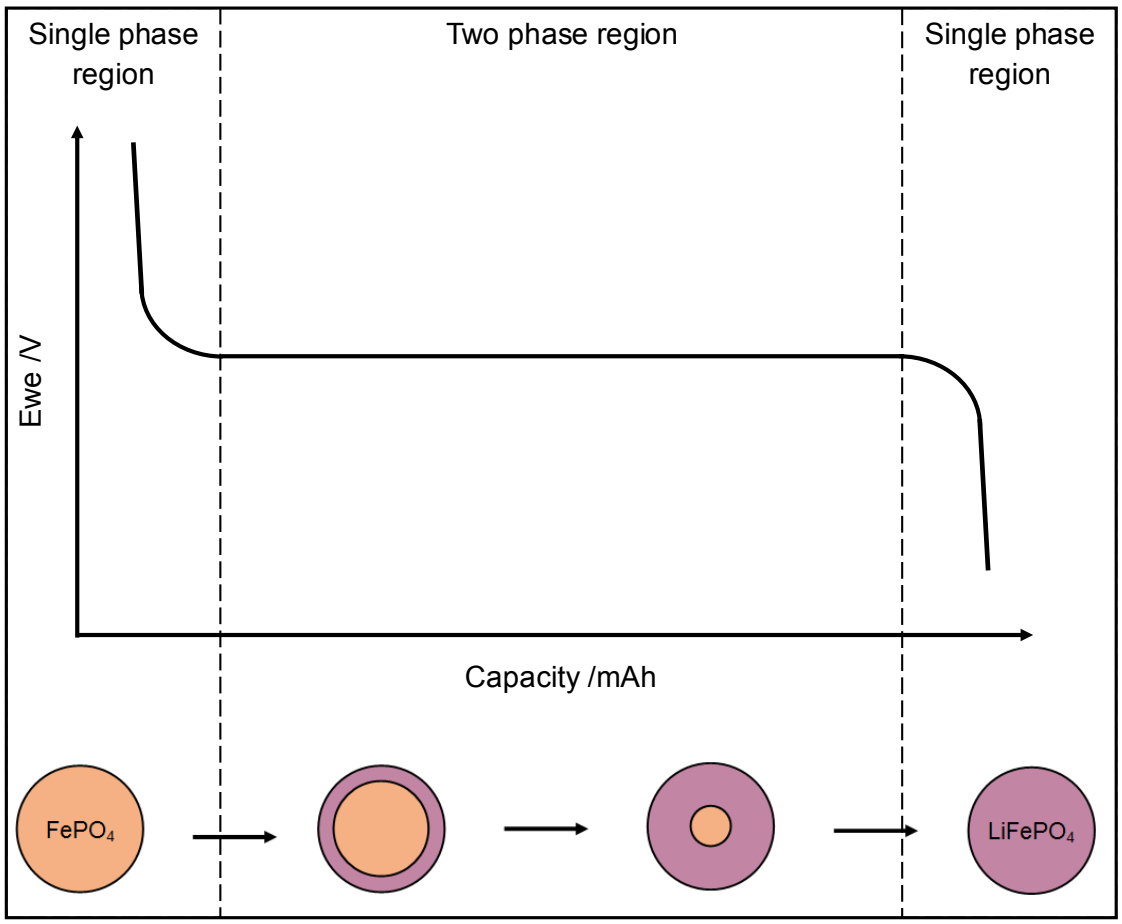

Figure 6. Galvanostatic discharge of LFP to demonstrate the two phase behaviour of LFP and the core-shell model for discharging.[42, 51]

3.1.6 Summary of lithium ion cathodes

Material	*Structure type*	*Specific capacity mAhg-1*	*Midpoint V vs. Li at C/20*	*Comments*
$LiCoO_2$	Layered	155	3.9	Co is expensive. Specific capacity is lower than theoretical to avoid phase transition.
LiNixMnx Co_yO_2 (NMC)	Layered	140-180	≈3.8	Safer and less expensive than LiCoO2.
$LiNi_xCo_yAl_zO_2$ (NCA)	Layered	200	3.73	About as safe as LiCoO2, high capacity.
$LiMn_2O_4$	Spinel	100-120	4.05	Inexpensive, safer than LiCoO2, poor high temperature stability.
$LiNi_{0.5}Mn_{1.5}O_4$	Spinel	130	4.6	Requires an electrolyte that is stable at the high voltage.
$LiFePO_4$	Olivine	170	3.45	Very safe. Low volumetric energy. Poor conductivity.

Figure 7 A summary of the properties of the main types of lithium ion positive electrodes.[52]

3.2 The negative electrode

Although lithium ion positive electrode materials are often tested against lithium as a negative electrode, safety concerns mean lithium metal is not routinely used in commercial lithium ion cells. Instead lithium intercalation compounds are used.[1] The requirements for a negative electrode material are similar to those for a positive electrode material: reversible capacity, good conductivity, high lithium diffusion rate whilst maintaining a low cost, low environmental impact and producing safe batteries.[53]

3.2.1 Carbon

Carbon-based materials are the most commonly used as negative electrodes. Within this group is graphite, which is used in the majority of commercial lithium ion batteries. Graphite, along with the other positive electrode materials, is a

lithium insertion/deinsertion material.[53] Graphite undergoes the following reaction during charging or discharging with the lithium ions intercalating between the layers within graphite:

$$Li^+ + e^- + C_6 \rightleftharpoons LiC_6$$

This means that each lithium ion is accommodated by 6 carbon atoms, limiting the capacity of graphite. The issues with the low capacity of graphite have led to the investigation of other forms of carbon as negative electrode materials including carbon nanotubes and graphene which have demonstrated much higher capacities due to a greater availability of sites for lithium ions to intercalate. Theoretically, single wall carbon nanotubes offer intercalation as LiC_2 which could potentially lead to a much higher capacity than graphite which is LiC_6.[54-57]

3.2.2 Lithium titanate

Lithium titanate ($Li_4Ti_5O_{12}$) is another intercalation material which has been studied as a negative electrode material for lithium ion batteries. The lithium titanate structure remains relatively stable during insertion/deinsertion of lithium ions, giving it a good cycle life and improving its safety. Lithium titanate does however have a relatively low capacity, limiting its practical application in lithium ion batteries.[18, 53, 58]

3.2.3 Silicon

Unlike the previous negative electrode materials, silicon does not react using a lithium intercalation reaction. Instead the lithium ions are electrochemically alloyed into the silicon structure, reacting with the silicon. This is different to the intercalation reactions because it involves the breaking of chemical bonds and the formation of new chemical bonds with the lithium. These alloying reactions are known for having a very high theoretical capacity (>4000 mAh/g for silicon) but they see very large expansion of the material (300-400%) on lithium insertion. As well as affecting the volumetric capacity of the material, this structural change can also cause the material particles to disintegrate and lose electrical contact. To mitigate this, the silicon is often used as a nanocomposite

with carbon and a binder. This provides the material with mechanical stability as well as the carbon enabling shorter lithium ion diffusion paths.[18, 53, 59]

3.3 Electrolytes

The electrolyte is an important part of a lithium ion battery, forming the basis for transport of lithium ions within the battery. In selecting an electrolyte for a lithium ion battery, a key factor is the rate of diffusion of the lithium ions between the electrode and the electrolyte. It is important that the electrolyte conductivity is ionic and not electronic to avoid shorting out the cell whilst allowing ions to diffuse through the structure.[1]

The second key factor is the stability of the electrolyte under the conditions of operation of the cell. In rechargeable systems the battery is expected to be stable under a wide range of voltages through charge and discharge. The electrolyte should also be stable under the full expected temperature range of the cell. Most electrolytes are designed for room temperature operation and high and low temperatures can cause the electrolyte to degrade or stop working. Sometimes additional safety features are added to the electrolyte including flame retardant materials and materials that limit the negative effects of electrolyte degredation.[1-2, 60]

An excess of electrolyte is often used in electrochemical systems and studies. The electrolyte is important in the development of the electrical double layer on the surface of the electrode. The formation of an interface between the solid and electrolyte is important to enable diffusion of ions and the size of the double layer has an enormous impact on the performance of the electrode. Too thick and it will limit diffusion, too thin and the electrode may degrade during cycling.[2, 61]

3.3.1 Solvent electrolytes

The most common electrolytes for lithium ion batteries are lithium salts dissolved in organic solvents. These salts are designed around the standard operating potential of a standard $LiCoO_2$ – graphite battery system, 4 V. Typically $LiPF_6$ salt is used as a compromise in properties since it is more

stable than other salts in the group. There are, however, still issues with $LiPF_6$ as it decomposes to form LiF and PF_5. PF_5 can then hydrolyse to form HF and PF_3O which react with both the negative and positive electrodes, degrading their performance. [60-62]

Solvents for electrolyte solutions are selected primarily on their stability at the required voltage and typically alkyl carbonates are used. Often solvents are a mix of these carbonates to achieve the desired properties. To enable lithium ion transport, the solvents used require a high dielectric constant and a low viscosity. Cyclic materials such as ethylene carbonate (EC) shown in figure 8 are used to stabilise the negative electrode through the formation of a passivation film on the electrode surface. They offer a high dielectric constant but a low viscosity. The linear carbonates such as dimethyl carbonates (DMC) are less viscous but offer a lower dielectric constant. This means solvents are typically a mixture of different types. A 1:1 ratio of EC:DMC is an example of such a solvent commonly used for lithium ion batteries. [60, 63]

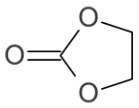

Ethylene carbonate (EC)

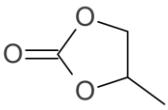

Propylene carbonate (PC)

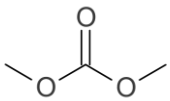

Dimethyl carbonate (DMC)

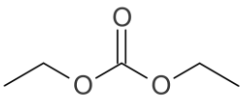

Diethyl carbonate (DEC)

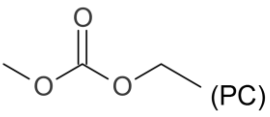

Ethyl methyl carbonate (EMC)

Figure 8. The structure of alkyl carbonate solvents for lithium ion batteries

3.3.2 Solid electrolytes

The practicalities and safety concerns of liquid electrolytes has led to the development of solid state electrolytes. These electrolytes, when combined with solid electrodes, give the potential to develop an all solid state battery system. Two types of solid state electrolytes are typically considered, the first is polymer electrolytes where polymers replace the solvents used with lithium ion salts. The polymer electrolytes can be further grouped into two types:

- Solid polymer electrolytes dissolve the lithium salt in a high molecular weight polymer host.
- Gel polymer electrolytes incorporate the solvents discussed in the previous section into a gelled polymer matrix.

The solid polymer electrolytes are typically lower conductivity than the gelled materials but offer a higher mechanical stability. Both types typically use polyethylene oxide (PEO) as a host material but PVDF can also be used.[64]

The second type of solid state electrolytes are inorganic intercalation-type inorganic solid state materials that use the properties of these solid state compounds to transport lithium ions between the electrodes. A range of materials and structures have been investigated to be used as electrolytes including LISICON and NASICON -type structures, spinels and garnets. [65]

4 Approaches to producing battery electrodes

In order to produce working electrodes for a lithium ion battery the materials for positive or negative electrodes are combined with conductive additives and binders as an ink and applied to a current collector material. The electrode is then typically rolled and assembled into a battery as shown in figure 9. In developing a battery system there is an increasing drive to maximise energy density and reduce cost. To get the greatest energy density in an ideal battery system the amount of active material (anode and cathode) should be maximised and the other aspects of the battery (separator, electrolyte, casing, binder etc.) would be minimised. The search for cheaper and lower cost batteries has led to several methods of manufacturing electrodes.

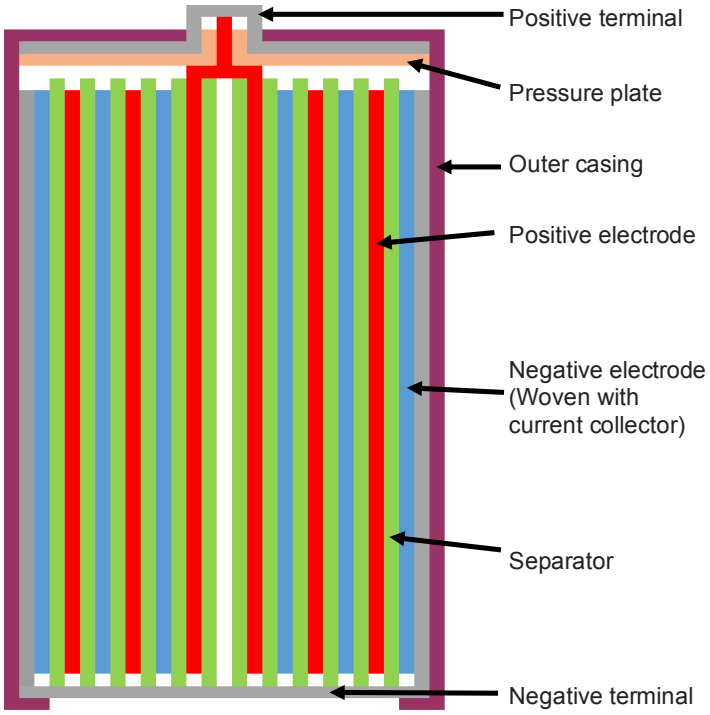

Figure 9. Diagram to demonstrate construction of a “jelly roll” type battery construction.[66]

Generally, commercial electrodes are manufactured using roll to roll processing and so are considered 2D. Even cylindrical battery forms are manufactured using this method before rolling up the thin films into a cylindrical shape. One way to maximise energy density would be to make the films of active material thicker, putting more material in each battery layer. In reality this is not practical as the thicker films suffer from poor diffusion through the electrode, poor

conductivity and poor mechanical stability. A solution to this issue is the potential of moving away from the electrode layered systems to develop 3D battery systems. 3D battery systems seek to use 3D structured current collectors to get the maximum capacity from a volume whilst maintaining the advantages of thin film processing techniques. Figure 10 shows a simple example of a pseudo-3D structure where the ink is patterned on a substrate and a 3D structure where the layers have been built up or applied to a 3D current collector to produce a 3D battery. More complex 3D structures have been investigated with metal foams and meshes used as current collectors before coating by the active material.[67]

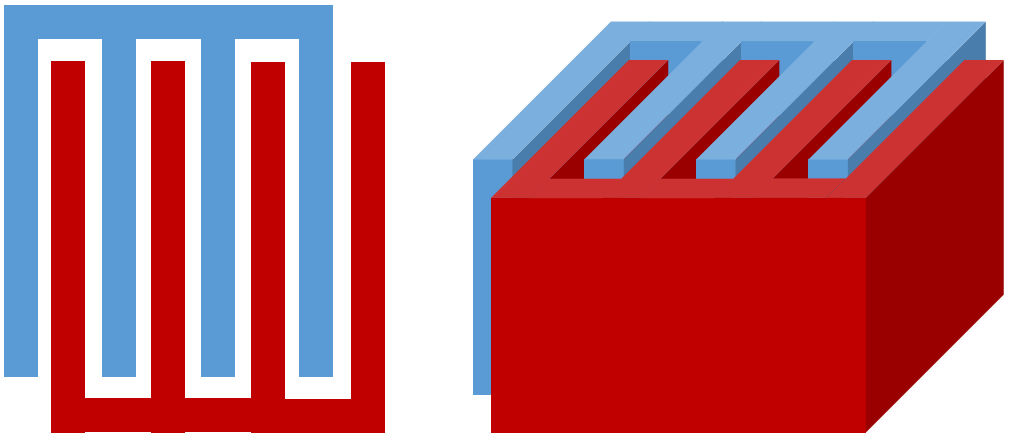

Figure 10. *Left* Pseudo – 3D battery structure. *Right* 3D structure[67]

This review will outline techniques to manufacture both positive and negative electrode materials. In developing a new method of battery manufacture other aspects of the battery would need to be considered including the electrolyte, separator and packaging. It is outside the scope of this thesis to consider these aspects so they will only be discussed in relation to their interface with the electrode rather than their manufacture.

4.1 Printing techniques

Printing techniques are the most common commercial methods used to produce battery electrodes. They start from an ink which is then applied to a surface and post-processed depending on the method of printing. Typically an ink used in a battery material is a mixture of the active electrode material, a conductive additive such as carbon black, a binder material and a solvent. For all inks, a

key element of their development is the dispersion and mixing of the solid powders in the printing media. It is important that the particles remain dispersed during the printing process and sometimes milling is required to reduce the particle size and aid with dispersion.

The main difference between the inks for the different printing techniques is their viscosity. Some techniques such as inkjet printing systems require inks with very low viscosities and other systems such as dispersion 3D printing systems accept inks with both low and high viscosities. How the dispersion flows, the rheology, is also important as it determines how the material will flow during the printing process which ultimately affects the quality of the deposit.

For this review the printing techniques can be split into different categories based on the level of dimensional control during printing. Techniques such as blade coating can only coat an entire surface so there is no control over the dimensions of the print. Screen printing and spray coating techniques enable some degree of control of the print in two dimensions. Digital techniques enable even greater control of the print in three dimensions.

4.1.1 Conventional printing techniques

The typical method of constructing electrodes both in the lab and on a commercial scale is to use a doctor blade. In this, a blade is passed over the current collector with the ink on it. The blade is at the same height as the layer required and enables an even layer of ink to be deposited on the electrode. In commercial systems this is carried out using reel to reel processing which spreads the material in an even coating on a continuous roll of current collector.[68-71]

4.1.2 Two dimensional printing systems

Several different two dimensional printing techniques exist. These enable a greater control over the material deposition in two dimensions than conventional techniques, giving the opportunity to produce pseudo-3D battery structures with interdigitated patterns shown in figure 10.

Stencil printing is the simplest form of two dimensional printing system used for batteries and is a modification of the blade coating process with a stencil to achieve the desired pattern. The blade is replaced by a squeegee which absorbs the ink and reduces bleeding of the ink into areas covered by the stencil. It has been used to produce Zn–MnO_2 batteries.[72] A key advantage of this printing technique is its use with a wide range of ink viscosities and its ability to produce thicker films required for batteries. It cannot however be used for reel to reel printing as the stencil must be rinsed in between uses. [72-73]

Screen printing is another technique that uses a stencil. In this, the ink is pushed through a mesh with a stencil blocking areas of pattern. The mesh is then placed onto the required surface transferring the pattern. Screen printing has been used widely to produce batteries with a range of materials and like the previous technique is capable of printing thicker films but with less definition than other techniques. [74-76]

Flexographic printing is another technique used to deposit materials onto a surface. This uses a patterned roll similar to a rubber stamp onto which the material to be printed is applied. The surface to be printed is then passed over the roll and the ink will be applied to the material. MnO_2 inks have been developed to deposit battery materials using this technique but the thin layers produced and narrow viscosity range have limited the practical application of this technique for lithium ion batteries. [77]

Spray painting techniques have also been used to apply battery materials to current collectors. Singh et. al. were able to produce full cells using the technique. Spray painting is quick drying which means electrodes can be quickly deposited in multiple layers. Spray painting does however offer low dimensional control which could limit its use for smaller battery systems. [78]

4.1.3 Three dimensional printing systems

The recent research interest into digital printing technologies and 3D printing has led to a large amount of interest in applying these techniques to develop 3D batteries. Two printing techniques have been used to produce 3D battery electrodes. Both 3D techniques can be used to deposit free standing electrodes

and so do not necessarily require a 3D current collector. The dispenser technique in its crudest form can be considered as a pipette which is controlled to drop material, when required, creating a pattern. The material is usually deposited as a continuous stream generating a layer of material. These layers of material can be built on top of each other to generate a 3D electrode. This has been successfully used to develop 3D interdigitated micro structures for batteries. An advantage of this technique over the inkjet method is that delivery systems can be developed bespoke to the ink to be deposited so a wide range of viscosities can be deposited.[79-81]

Inkjet printing is a technique that uses computer controlled deposition of inks to produce high detail deposits onto the surface. Inkjet printing deposits droplets of material that when combined together produce a film of material. Research has focussed on the development of inks for inkjet printing and a wide range of battery electrode materials have been considered. Although it can be considered a 2D process, by printing multiple layers of ink 3D structures can be produced. One of the main issues with the use of inkjet printing is the difficulty of producing inks for the process as the viscosity range is very low. There is also an issue with sedimentation of material during deposition which can block up the deposition head.[82-83]

4.2 Electroplating

Electrodeposition techniques use a potential difference and an applied electrical current to deposit materials onto a metallic substrate. Battery materials are well suited to be produced using electrodeposition techniques as they will usually require a conducting substrate which is also needed for electrodeposition. Electrodeposition techniques also enable material to be coated onto a wider range of structures than printing techniques as the material to be coated is suspended in solution and does not need to be accessed by a printer head or coater. This is particularly useful when considering deposition onto nanostructured surfaces and foams to make 3D and pseudo 3D battery systems.

There are two key types of electrodeposition techniques: electroplating and electrophoretic deposition. Electrophoretic deposition will be discussed later on in this chapter. Electroplating is an electrodeposition technique commonly used to deposit metals on a surface where metal ions are dissolved in a solution, moved using an applied current and then reduced or oxidised onto the surface to be plated onto. Several lithium ion battery materials have been produced using electroplating. Generally, plating has been applied to the low voltage positive electrodes such as V_2O_5,[84] MnO_2,[85] and MoS_2 [86] but the technique has also been used to produce anodes such as Cu_2Sb [87].

Electroplating offers a similar level of control of the coating as electrophoretic deposition but as the material to be deposited reacts as it is plated, it will only work for a small number of lithium ion battery materials. In particular, carbon coated materials such as LFP would not be able to be electroplated.

4.3 Vapour deposition techniques

The use of vapour deposition techniques such as chemical vapour deposition (CVD), physical vapour deposition (PVD) and atomic layer deposition (ALD) have also been suggested for producing lithium ion battery materials. Chemical vapour deposition uses different techniques to generate a vapour containing volatile chemicals and the material to be deposited. The material then reacts or decomposes at the electrode which is heated. Atomic layer deposition is a sub set of CVD in which sequential gases are added to the reaction chamber allowing a much greater control over the surface structure. Physical vapour deposition is similar to CVD but the atoms or ions are vaporised from the solid form without volatile compounds. PVD is performed in the vacuum and gives a high control over the structure of the film. The vapour deposition techniques have shown some promise in producing lithium ion battery materials with a high degree of control of the film deposited. The main barrier to their use in lithium ion batteries has been the cost of CVD and PVD systems and the speed of deposition which at the moment is not practical for commercial applications.[88-90]

5 An introduction to Electrophoretic deposition

Electrophoretic deposition (EPD) is an electrodeposition technique in which particles are deposited using Electrophoresis. Electrophoresis is defined as the movement of charged colloidal particles in a liquid under the influence of an external electric field.[91] EPD has long been used to deposit thin ceramic coatings onto metal surfaces and in more recent years has found further application in the deposition of nanoparticles.[92] In this section we will begin by discussing the theory of EPD before conducting a brief review on the application of EPD to lithium ion batteries.

5.1 The theory of electrophoretic deposition

Electrophoretic deposition is a complex technique with many different variables affecting the coating quality. Van der Biest et. al. refer to electrophoretic deposition as a two phase process consisting of firstly the movement of particles within the solution due to an applied potential and the charged particle surface. In the second step the particles collect at an electrode and form a high quality film on the surface of either the positive or negative electrode depending on the surface charge.[93]

In developing an appropriate synthesis method using this technique there are a large number of factors that can affect the quality of the coating. The factors can be split into two main groups: those factors that relate to the colloidal suspension and those factors that relate to the electrophoretic deposition process.[94]

Factors relating to the colloidal suspension:

- Particle size
- Concentration of particles in the suspension
- Dielectric constant of the liquid
- Conductivity of suspension
- Viscosity of suspension
- Zeta potential of the particles
- Stability of the suspension

Factors relating to the electrophoretic deposition process:

- Deposition time
- Applied voltage
- Concentration profile of the particles during deposition
- The nature of the Substrate (electrode)

Several attempts have been made to determine the kinetics of how these properties relate to the final quality of the coating. This section will discuss the theories behind the three main aspects of electrophoretic deposition of particles: surface charge development, migration and deposition.

5.1.1 The development of the surface charge

The relationship between the suspension and the particle is important in ensuring the migration and deposition of the particles on the required surface. A key factor of this relationship is the development of the charge onto the surface of the particles. Surface charge is usually measured by a suspensions zeta potential which is the potential at the point in the solvent where movement of the particle will not affect the solvent molecules and is discussed later on in this chapter. Four mechanisms have been identified in which the surface charge on the particle develops:[94]

1. **Selective adsorption of ions from the liquid onto the surface of the solid particle:** When ions in solution move near the particle, their charge repels or attracts electrons at the surface of the particle, depending on if the ion is negative or positive respectively. This creates either a deficit or an excess of electrons thus creating a positive or negative charge on the surface.

2. **Ions dissociating from a particle into the liquid:** If a particle contains soluble ions they can dissolve or dissociate into the solution. The ions are charged and so their removal leaves a residual charge on the particle. As ions are more likely to dissolve from the surface of the particle, this leaves a surface charge on the particle.

3. **Adsorption or orientation of dipolar molecules at the particle surface:** This is similar to the adsorption of ions but instead of a charged ion it is the negatively charged or positively charged part of a dipolar molecule that repels or attracts electrons at the surface of the particle respectively. This then also creates either a deficit or an excess of electrons thus creating a positive or negative charge on the surface.

4. **Electron transfer between the particle and the liquid:** If the particle and the liquid have different work functions it may be energetically favourable for an electron to transfer between them, creating a charge on the surface.

5.1.1.1 Surface charge modification

For most particles the surface charge developed by simply adding the particles to the suspension media is not enough to produce a stable suspension. It is therefore typical to include additives to the suspension to modify surface charge. In some cases these additives modify the surface charge to an extent that the deposit electrode can be changed from positive to negative.[95]

The main method of surface modification is through the first mechanism of surface charge development, which is through adsorption of ions onto the surface of the particle. Acidic, alkali and metal ions are introduced to the suspension and provide ions of the required charge to adsorb on the surface. Acids and alkalis provide hydrogen or hydroxide ions to the suspension that adsorb to the particle surface modifying its charge. Iodine and acetone suspensions have also been used, the iodine reacts with the acetone, producing protons.[94, 96] Metal ions are introduced in the suspension through addition of salts such as $Mg(NO_3)_2$, $La(NO_3)_3$, $Y(NO_3)_3$, $MgCl_2$, or $AlCl_3$. In addition to charging the surface of the particle, the metal ions can lead to the formation of hydroxides that can improve adhesion in the deposit.[93, 96]

Some organic solvents and acids such as carboxylic acid and acetone can also enhance surface charge through the third surface charge mechanism by orientating their dipole to produce a positive or negative charged surface. Large surfactant molecules such as ammonium polymethacrylate (Darvan-C) also use this mechanism to enhance surface charge by orientating their dipole to modify

surface charge on the powder particle.[96-97]Recent studies have sought to look at bio-inspired approaches to modifying surface charge for electrophoretic deposition with successful EPD deposits produced by the addition of biomolecules from catechol, salicylic acid, gallic acid and chromotropic acid families.[96]

5.1.2 Migration of particles between the electrodes

Descriptions of the migration of particles in EPD rely heavily on the concept of the electric double layer. As discussed previously, the electric double layer is derived from capacitor studies and is used to explain the distribution of charges within a system that consists of an electrode and an electrolyte or solvent. In this application the electrode is the particle which exhibits a surface charge. The electrolyte is the suspension solution. [93-94]

The force provided to move the particle comes from the applied electric field which can be quantified using the following equation:

$$F_e = q\,E_f$$

Equation 20

Where:
F_e = electrophoretic force
q = charge carried by the body
E_f = electric field

This is countered by the forces of friction acting against the particle

$$F_f = v_p\,f_r$$

Equation 21

Where:
F_f = friction forces
v_p = particle velocity
f_r = frictional coefficient.

If we assume that there is a net force of zero on the particle, the particle is not moving and the force due to friction is equal to the force provided by the electric field. At this point we get the following equation:

$$q\,E_f = v\,f_r$$

Equation 22

More frequently this is used to determine the coefficient of electrophoretic mobility, μ_e, which is a measure of the velocity of particle movement in a suspension in a given electric field strength. [91] Electrophoretic mobility can be found from the following equation:

$$\mu_e = \frac{v}{E_f} = \frac{q}{f_r}$$

Equation 23

However, this does not accurately consider the particle in suspension. The particle is modelled as a point and the double layer of ions around the particle are not considered. As figure 11 shows, in solution the solvent ions of the opposite charge are arranged close to the charged particle surface. This creates the electric double layer. At a certain distance from the electrode the effect of the charged particle becomes more diffuse leading to a diffusion zone where the solvent ions are less affected by the charged particle.

When the electric field is applied, the ions in the suspension and the particle should move in opposite directions. However, the double layer means that ions near the particle surface will move with the particle and ions in the bulk will move in the opposite direction. This means that the movement of the particle is not only due to the surface charge but the net charge enclosed in the sphere around the particle including the ions close to the surface. The potential at which the interface between these two occurs is the zeta potential and is shown in figure 11. [93-94]

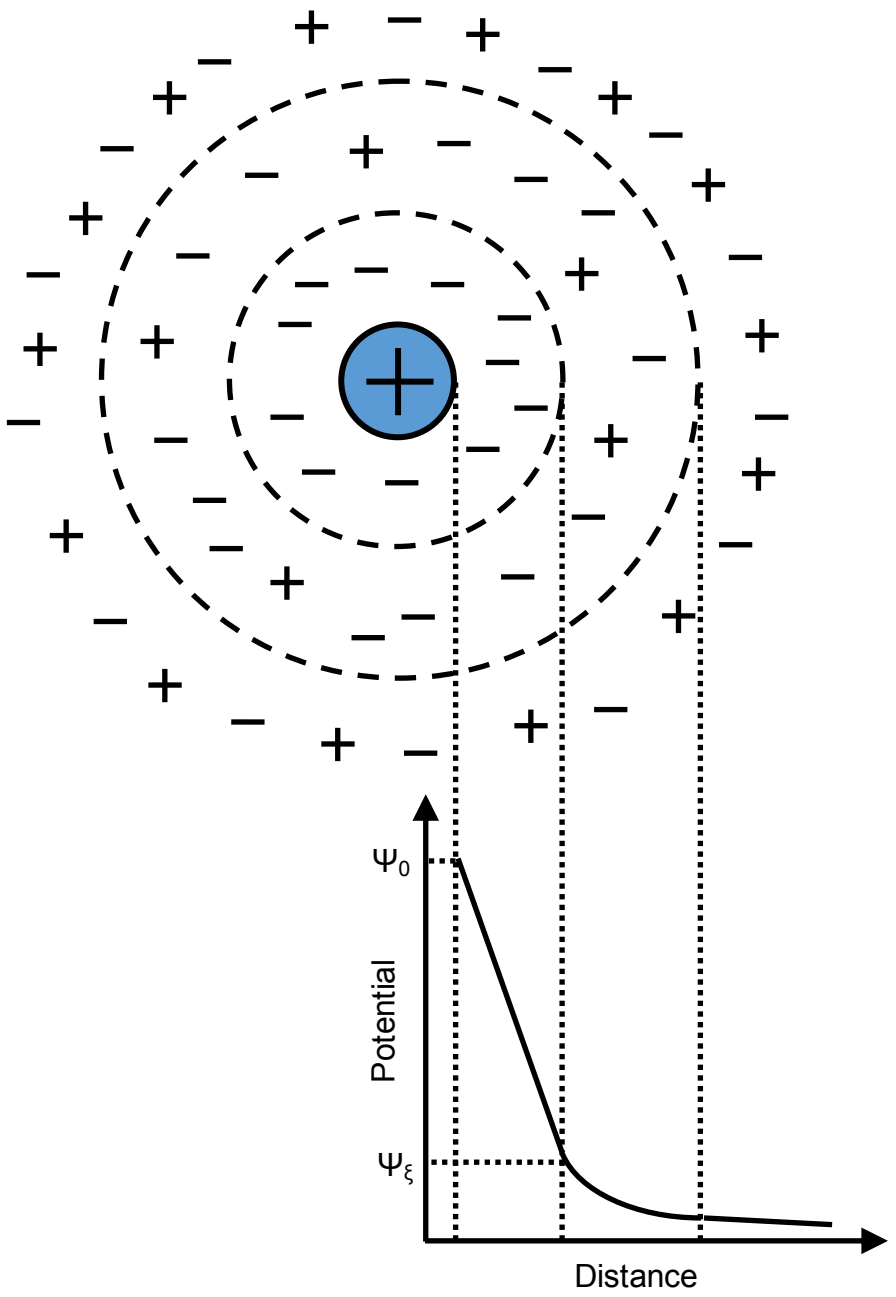

Figure 11. Schematic representation of the double layer on the surface of a particle and potential drop across the double layer[93-94]

As it is difficult to calculate and observe the movement of individual particles in an electric field, several models exist to equate the zeta potential to the electrophoretic mobility. These models depend strongly on the model used to define the double layer. The different models for the double layer are discussed earlier on in this thesis. The following equation combines some of these models to give an equation for electrophoretic mobility that takes into account the size of the double layer:

$$\mu_e = \frac{2\,\varepsilon\varepsilon_o\zeta}{3\,\eta_s} f(\kappa a)$$

Equation 24

Where:
ε = dielectric constant of the liquid
ε_o = permittivity of free space
ζ = zeta potential
f(κa) is Henry's function
η_s is the viscosity of the suspension[98]

Henry's function is a complex function that relates to the Debye length, κ which is the thickness of the double layer and the radius, a of the particle. Several attempts have been made to approximate Henry's function to ease the calculation of zeta potential. If κa is very small, i.e. there is a thin double layer f(κa) approaches 1 and the Hückel equation can be used:

$$\mu_e = \frac{2\,\varepsilon\varepsilon_o\zeta}{3\,\eta_s}$$

Equation 25

If the double layer is thicker so that κa is much greater than 1 the Smoluchowski approximation sets a value for f(ka) of 1.5. At this point the electrophoretic mobility, μ_e can be determined by the following equation:[98]

$$\mu_e = \frac{\varepsilon\varepsilon_o\zeta}{\eta_s}$$

Equation 26

As well as the radius of the particle and the suspension dielectric constant and viscosity, this means the electrophoretic mobility and ultimately the amount of material deposited is related to the electric double layer thickness. The thickness of the double layer is in itself affected by a range of properties of the suspension including ionic concentration and pH and surface conductivity of the particle.[98]

5.1.3 Deposition of the particle on a surface

Although the kinetics of the particle motion is relatively well understood, several theories exist that explain how the particles adhere to the electrode surface.

Hamaker and Verwey proposed a theory of flocculation by particle accumulation. In this they model electrophoretic deposition by considering the process as similar to the process of flocculation due to gravity in a colloidal suspension. They consider that the primary role of the electric field is to move the particles to the electrode surface where they can aggregate on the surface due to the force of that movement and not due to the electric field itself. This theory is also useful in explaining why membranes between electrodes can also be deposited on. However, this theory does not take into account the effect of polar and non-polar solvents at the surface of the electrode and how they interact with the charged electrode.[37]

Grillon proposed a theory based on particle charge neutralisation. This is based on that when a charged particle touches the electrode it is neutralised. The first layer of particles then acts as electric poles attracting the next layer of charged particles. This distorts the electric field at the new electrode surface which means the next layer of particles are deposited unevenly creating porosity within the EPD layer. The concept of charge neutralisation suggests particles will not move once they reach the surface and as such any porosity is locked onto the deposited surface. This mechanism could also explain the role of salt additives in the enhancement of deposition. The main disadvantage of this mechanism is that it fails to explain the mechanism at longer deposition times and is reliant on an inherent porosity that is not always seen in EPD samples. [99]

Koelmans et. al. proposed a theory based on the electrochemical coagulation of particles. When a potential is applied between the electrodes there is an increase in electrolyte concentration near the electrode surface. Koelmans et. al. calculated that the increase in electrolyte concentration is enough to destabilise the colloidal suspension by decreasing the repulsion between the particles. The main issue with this theory is that observations have shown that there is not always a change in electrolyte concentration near the electrodes and under these circumstances this mechanism is not valid.[100]

The final mechanism was proposed by Sarkar and Nicholson and suggests the application of the electric double layer to the mechanism for deposition. In this

theory they consider that the charged ions surrounding the particle, the double layer, will distort as the particle migrates between the electrodes forming a shape with a tail and a region at the front of the particle that is depleted of ions. When the particle reaches the electrode surface this distortion will lead to the particle approaching close enough for Van der Waals attractions between the particles to dominate. The tail on the now attached particle will then re-distribute itself to allow other particles to adhere to the surface.[94]

5.2 Factors affecting the amount of material deposited

In 1931 Hamaker related the electrophoretic mobility to the amount of material deposited during electrophoretic deposition using the following equation which combines aspects of the migration and deposition of a particle:[34]

$$m = C_s \mu_e S E_f t$$

Equation 27

Where:
m = mass of deposit
C_s = suspension concentration
μ_e = electrophoretic mobility
S = deposition area
E_f = electric field
t = deposition time.[101-102]

Although useful in giving an indication of the amount of material deposited, there are several limitations to the Hamaker equation. The first is the assumption that each particle that meets the deposited surface will attach to the surface. In a real system particle adhesion to the surface may not occur when every particle meets the surface. This has been accounted for by a “sticking factor” f which is between 0 and 1 and takes into account the ability of the deposit to adhere to the surface.[101, 103]

The Hamaker equation also does not take account of the variation of suspension concentration with time. Initially the suspension concentration can be considered constant but eventually the concentration may be reduced to an extent that the rate of deposition is affected. Material may be lost from the suspension through sedimentation which has an effect on concentration. Biesheuvel modified the Hamaker equation by replacing the term for

concentration of particles in the deposit, C_s with terms that take into account the particle concentration in the deposit and the change in the ratio of volumetric concentrations of particles in the suspension to the deposit over time.[94, 104-105] The effects of concentration over time can be mitigated through stirring the deposit suspension which moves particles from particle-rich areas of the suspension to depleted regions, for example next to the electrode.[103, 106]

Another factor not considered by this equation is the electric field variations during deposition. This is particularly important where the deposited material is a non-conducting coating as this could increase the resistance of the coated surface over time, affecting the ability of the electrodes to maintain the applied electric field.[103, 107] The variation of the suspension resistivity over time has also been considered in relation to the amount of material deposited.[108-109]

More recently applied electric field variations have been used in electrophoretic deposition. Pulsed fields where there is a short burst of applied potential have been primarily used to limit water splitting in aqueous electrophoretic deposition which can produce gas bubbles within the deposit. The short duration of the pulse does not allow enough time for the water to react and the time between the pulses allows for any gases formed to diffuse out of the deposit.[105] Symmetric and asymmetric alternating current fields have also been applied to electrophoretic deposition. In an alternating current electric field the particles can form a more ordered deposit as the reverse current enables particles to re-organise into a denser deposit.[105, 110-111]

5.3 Electrophoretic deposition for lithium ion batteries

The application of electrophoretic deposition in producing lithium ion batteries has been studied for some years. The advantage in the application of electrophoretic deposition for electrode materials is that the material is deposited as a particle instead of as ions. This enables nanostructured electrodes to be made using coated precursor nanoparticles deposited onto surfaces and structures. This is particularly important for LFP electrodes and other electrode materials which use a carbon coating to enhance conductivity.

In addition electrophoretic deposition is able to be used on a variety of substrate structures giving the potential for 3D batteries to be produced.[112]

Early studies focussed on placing electrodes in the conventional inks used for battery manufacture and developing electrophoretically deposited battery materials with carbon binder. Often a structured electrode was used as the deposition surface to enhance the stability of the deposition.[113-114] Later studies have focussed on the application of electrophoretic deposition to produce binder and carbon free electrodes and improve the active material content within a battery. A key advantage of the EPD system is that as it is conduction controlled it is thought to produce improved conductive pathways through the deposited particles of the electrode material.[54, 115-116]

Another advantage is that unlike other coating techniques electrophoretic deposition does not need to “see” the surface it is being deposited onto. This means that as with other electrodeposition techniques, electrophoretic deposition is capable of coating 3D surfaces and so research into electrophoretic deposition has focussed on the potential of the technique to deposit onto structures such as foams and porous media. Mazor et. al. used micro pores drilled into a silicon substrate to develop semi-3D electrodes with LFP electrophoretically deposited into the pores. Energy densities comparable with conventionally produced cells were achieved when the LFP was deposited with activated carbon and a PVDF binder from a suspension that also contained surfactant. They also found that a coating of CuS onto the electrode improved the power density of the cell.[116] Electrophoretic deposition has also been used to incorporate graphene and carbon nanotubes to improve conductivity and reduce the amount of active carbon in binder-free positive electrodes.[117-119]

Chapter 2: Experimental techniques

1 Electrochemical analysis techniques

1.1 Galvanostatic charging

Galvanostatic charging is also known as chrono-potentiometry. In this technique the current is initially stepped from zero to the value required and the voltage is measured over time. Although the results of this can be shown as a voltage-time graph, commonly the time axis is converted to capacity in mAh or as a percentage of initial capacity as shown in figure 12. A key advantage of this test method for measuring battery materials is that it enables the battery to be tested under more realistic conditions of charge or discharge. Another advantage is that because this technique applies a constant current, any effects of an ohmic drop in the electrode set up can be overcome.[4, 120]

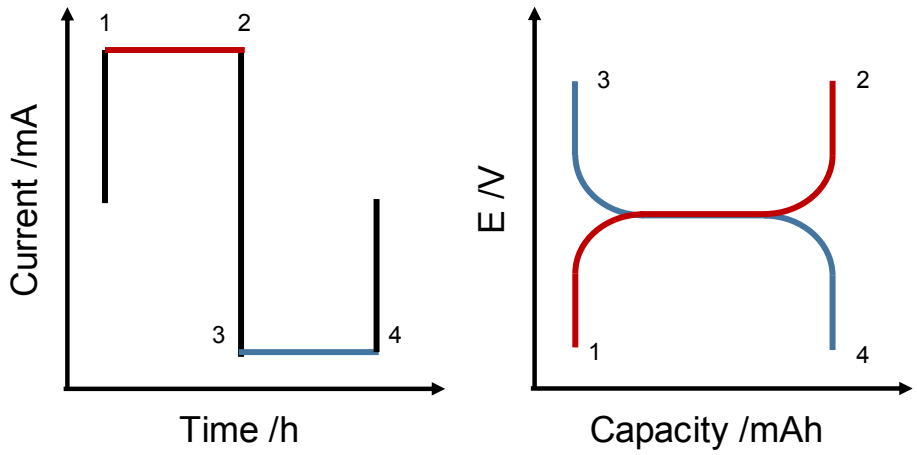

Figure 12. *Left* A typical current against time plot for a galvanostatic charging experiment. *Right* A typical galvanostatic charging experiment where the charge (*red*) and discharge (*blue*) profiles are plotted on the same diagram.

Batteries are often rated by their capacity in mAh, the amount of current flows during per hour of cell discharge. The C-rate is another way of expressing the applied current during galvanostatic charging. The C-rate expresses the current applied as a multiple of the theoretical capacity (in mAh) of the cell. For example, a battery rated at 300 mAh discharging with a C-rate of 1 would be the equivalent of testing the battery at a constant current of 300 mA for one hour. It is common to test a cell at different C rates to understand the rate performance of a cell.[120]

The initial change in the potential is due to the double layer charging of the cell. The potential then increases until it is at a point where the battery electrodes can react to maintain the constant current applied. The type of reaction will affect the profile of the next phase of the plot. As discussed earlier in this thesis, in a two phase system the potential will remain constant, in a single phase system the potential will slope downwards. A stepped pattern may be observed in cells where the charge or discharge moves through multiple chemical reactions.

As the cell reaches its maximum capacity, a peak in voltage is observed. This is due to surface concentration falling to zero. In batteries this is due to a depletion of lithium ions in the material which means there are not enough lithium ions at the surface to maintain the current and the potential rises to compensate for the drop in current. For safety, galvanostatic tests are undertaken between a set voltage range to stop over charge or discharge of the cell. Modern battery testing systems will move the test to open circuit voltage if the cell voltage goes beyond the values specified by the battery material manufacturer.[120-121]

1.2 Cyclic Voltammetry

Cyclic voltammetry is a potential sweep technique that has been used widely to study electrochemical systems. In cyclic voltammetry the potential is changed linearly between two values, E_1 and E_2 and the current is measured. The sweep rate, v can be varied to gain a greater understanding of the kinetics of electron transfer in the system. This applied potential is shown in figure 13.

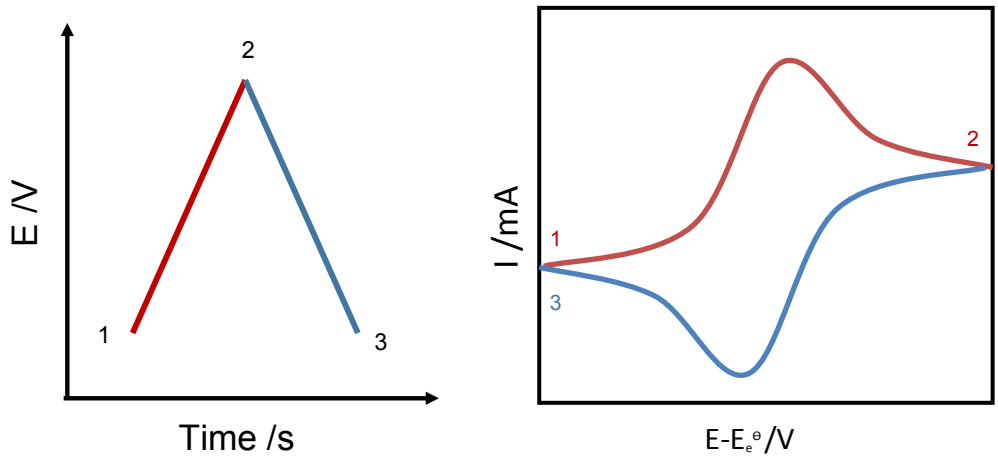

Figure 13. *Left* A typical potential against time plot for a cyclic voltammetry measurement. *Right* A typical cyclic voltammetry measurement.

By considering a reversible oxidation reaction, c_O/c_R can be determined from the Nernst equation at a distance from the electrode surface, x. As figure 14 shows, this means as the potential is made more negative the concentration gradient of the reactant is decreased. Since:

$$I = -nFAD\left(\frac{\partial c}{\partial x}\right)_{x=0}$$

Equation 28

Where:
I = current
n = number of electrons
F = Faraday constant
D = diffusion coefficient
c = concentration
x = distance from electrode

The current increases as the concentration gradient (δc/δx) increases. Eventually all of the reactant at the surface has been reduced. At slow sweep rates there is enough time for the surface concentration to equilibrate through diffusion so the peak in current density is small. At higher sweep rates there is not enough time for the reactant concentration at the surface to equilibrate. This leads to a peak in current density and beyond this point the reaction is controlled by the diffusion of the reactant to the surface.[2, 4]

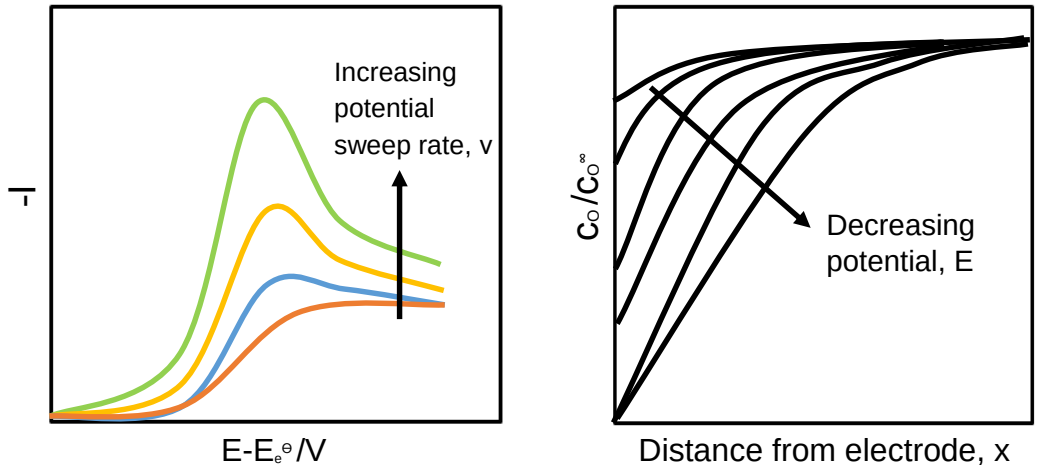

Figure 14. *Left* Plot to demonstrate the effect of increasing the potential sweep rate on measurements of cyclic voltammetry. *Right* Plot to demonstrate the effect of decreasing the potential on the concentration of oxidised species as a function of distance from the electrode.

When considering the reverse reaction, in this case an oxidation, we see a similar pattern but with reversed values. Initially there is a concentration of reactants at the electrode surface which are then oxidised during the reaction. In this case, as the potential becomes more positive the concentration of reactants also decreases to a point where the reaction is diffusion controlled giving the typical cyclic voltammogram shown in figure 13.

1.3 Impedance spectroscopy

Impedance spectroscopy is a technique used to understand the conductivity within a sample. Resistance is the ability of a circuit element to resist the flow of electrical current but is limited to an ideal resistor which has the following conditions:

- It follows Ohm's Law ($R = E/I$) at all current and voltage levels.
- Its resistance value is independent of frequency.
- AC current and voltage signals through a resistor are in phase with each other.

As these assumptions are not always valid for circuits, impedance is used and is defined as the ability of the whole circuit to resist the flow of electrons.

Impedance spectroscopy works by applying a small amplitude sinusoidal voltage to the sample and measuring the current response. At small amplitudes the current response is directly proportionate to the voltage change. If the applied potential follows the equation:

$$E = \Delta E \sin 2\pi f t$$

Equation 29

Where:
f =frequency
t = time

We can assume at small amplitudes that the current response will also be sinusoidal. The resistance of the sample means the current response may have a different amplitude and phase from the voltage:

$$I = \Delta I \sin (2\pi f t + \varphi)$$

Equation 30

This phase difference is demonstrated in figure 15.

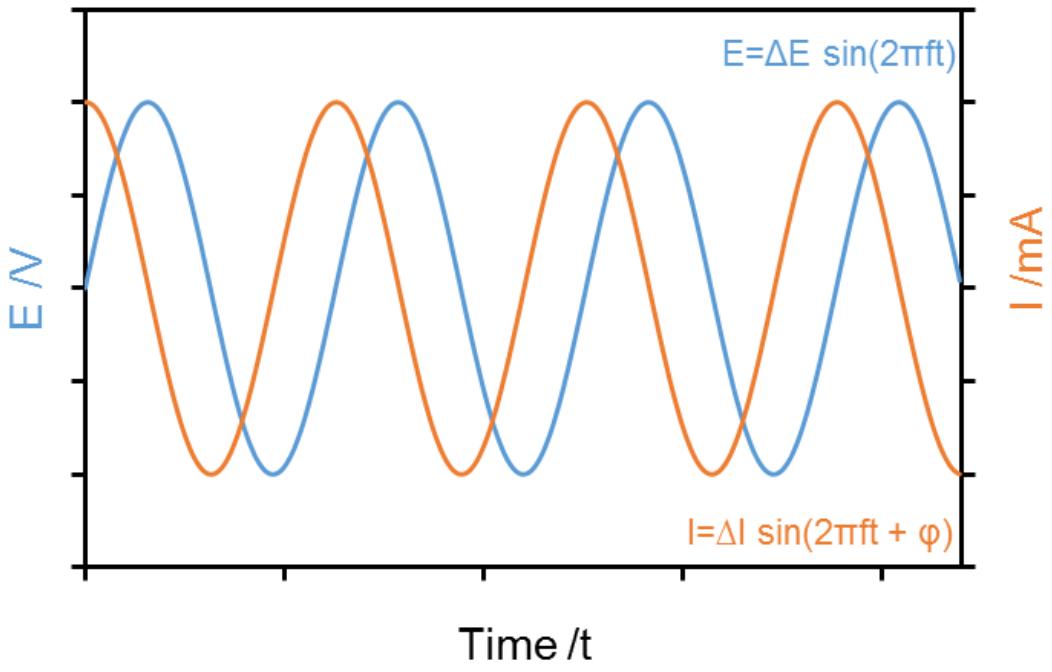

Figure 15. Graph to demonstrate the current response when a sinusoidal perturbation is performed.

This perturbation-response measurement is the basis of electrochemical impedance spectroscopy. Measurements are taken at different frequencies because the response of the system may be different at different frequencies.

The results of impedance spectroscopy are often difficult to interpret so the results are interpreted using complex notation. In this the sinusoidal perturbation is written as:

$$E = |E|(\cos(\omega t) + i\sin(\omega t))$$

Equation 31

Where:
$i = \sqrt{-1}$
$\omega = 2\pi f$

This means that instead of considering perturbation and response as a function of time we can consider them as a function of pulsation, ωt. The perturbation and response are now considered as angles on a circle giving each as a point on a circle that can be defined as Cartesian coordinates, (x,y). As Table 1 shows, the equations in complex notation are easier to perform arithmetic calculations on. Z can also be considered as a complex number where Z = Z' + i Z''. Impedance data is commonly shown using the Nyquist plot which plots -Z'' against Z'.

	Standard notation	Complex notation
Perturbation	$E = \|E\|\sin(\omega t)$	$E = \|E\|(\cos(\omega t) + i\sin(\omega t))$
Response	$I = C\frac{dE}{dt} = \omega C\|E\|\cos(\omega t)$ $= \omega C\|E\|\sin(\omega t + \frac{\pi}{2})$	$I = C\frac{dE}{dt} = \omega C\|E\|(-\sin(\omega t) + i\cos(\omega t))$
Impedance	$Z = \frac{\|E\|\sin(\omega t)}{\omega C\|E\|\cos(\omega t)}$	$Z = \frac{-i}{\omega C}$

Table 1 A summary of perturbation response and impedance in complex and standard notation for a capacitor.

1.3.1 Equivalent circuits

Most systems studied using impedance spectroscopy can be modelled using an equivalent circuit. Two components are key in the modelled equivalent circuits: the resistor and the capacitor.

Even with complex notation, the electrical environment of a practical electrochemical cell and its resulting impedance spectra are difficult to interpret. This means most interpretations consider an equivalent circuit which represents the electrode studied as a series of capacitors and resistors. In determining an electrode response to the perturbation, several components to the equivalent circuit must be considered.

As discussed previously, the electrode surface can be described as a double layer capacitor which will affect the response of the electrode (C_{dl}). Also affecting the response is the charge transfer resistance of the cell which will dominate the rate of response if the electrode reaction is slow (R_{ct}). As well as the electrode, the equivalent circuit also takes into account other aspects of the cell including the electrolyte-electrode resistance (R_u). Diffusion is represented in the equivalent circuit using the Warburg impedance (Z_w). The Randles circuit is used to model a typical shape for the Nyquist plot of battery materials under study:

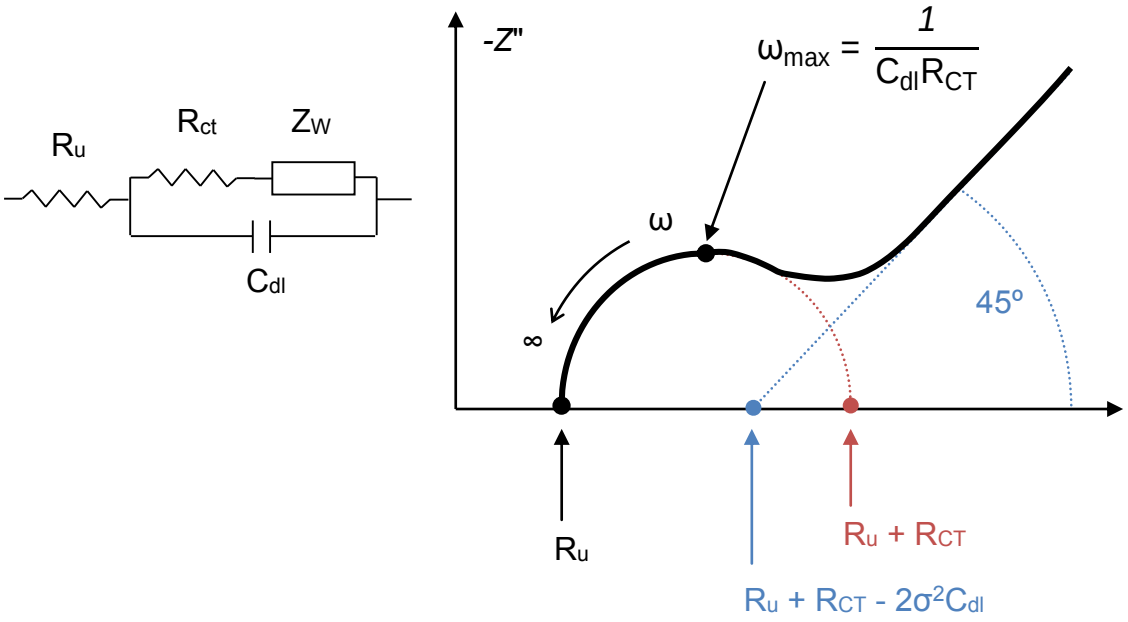

Figure 16. *Left* Diagram showing the equivalent circuit for the Randles circuit. *Right* A simulated Nyquist demonstrating the information available from impedance measurements.[122]

At low frequencies the current will pass preferentially through the top part of the Randles circuit shown in Figure 16, avoiding the capacitor. This means the electrode behaves as a resistor and the real and imaginary aspects of impedance change linearly, giving a straight line plot at high Z values due to the Warburg impedance. This usually has an angle of 45° but roughness of the electrode can affect this.[122] At high frequencies the capacitor can be considered as having a continuous flow of current through it so the current can flow through either part of the circuit. As the frequency tends to infinity the current will preferentially flow through the capacitor side of the circuit and at lower Z values capacitance will tend to zero. This means that from the Randles circuit the following data can be measured:

- R_u from the intercept on the real axis
- R_{CT} from the diameter of the semi-circle plotted. This can be used to find the exchange current, I_0 from $R_{CT} = RT/nFI_0$
- ω_{max} from the maximum radius of the circle. This can be used to determine the double layer capacitance from $\omega_{max} = (C_{dl}R_{CT})^{-1}$
- σ, the Warburg coefficient from the y intercept of the straight line due to the Warburg impedance. This gives values for diffusion, D_O and D_R since:

$$\sigma = \frac{RT}{2^{1/2} n^2 F^2 A}\left[\frac{1}{c_O D_O{}^{1/2}} + \frac{1}{c_R D_R{}^{1/2}}\right]$$

Equation 32

For more complex electrode systems the fit achieved using the Randles circuit is not good enough so other components are added to the equivalents circuit to improve the fit. Data from such circuits is often found using fitting software such as Zview where parameters can be determined based on an equivalent circuit.[123]

1.3.2 Constant phase element

The Randles circuit relies on the solid-electrolyte interface behaving as a perfect capacitor and although this is a good approximation it is not always valid. The semicircular representation of the capacitor can appear supressed. This suppression is due to frequency dispersion.[122, 124]

Where the semi-circle is surpressed, a constant phase element is used to account for the difference. For a constant phase element the phase angle is independent of frequency. Phase is found by multiplying -90 x α degrees. An ideal capacitor will have a value of $\alpha = 1$ and a phase angle of 90^o, an ideal resistor will have a phase angle of 0^o. The Warburg impedance is an example of a constant phase element used to describe diffusion. For the Warburg impedance $\alpha = 0.5$ so the phase angle is 45^o giving the distinctive linear relationship for the Warburg element. The constant phase element has an unclear physical meaning but is thought to be due to several factors affecting the non-ideal nature of the double layer capacitor. These include surface roughness and porosity, variation in composition and non-uniform potential and current distributions across the surface.[122]

1.3.3 Three electrode impedance

Electrochemical tests on materials for lithium ion batteries are usually performed using a two electrode set up where the counter electrode is also the reference electrode. This tests the batteries in similar conditions to their operation where connectors are placed at the positive and negative electrodes.

If we want to study only the positive electrode, for example, the reference and counter electrodes must be separated. This is done using a three electrode impedance test.

Three electrode impedance measurements can be performed in two main ways; using a T-cell arrangement or a ring electrode arrangement. The T-cell equipment uses a special Swagelok cell with three connecters, rather than the two described in section 3.1.3 of this chapter. It has been shown however that the separation between electrodes in the T-cells is large which can adversely affect the impedance results.

An alternative three electrode set up has been used in this project, using ring electrodes. In this, the standard Swagelok arrangement can be used with a positive electrode containing a ring of non-conductive polymer material. This creates a two electrode set up on the positive electrode as shown in figure 17. Although several options for a three electrode set up in this manner can be considered, Hseieh et. al. found that the impedance of the system with a small circular counter electrode and ring reference electrode was one of the best when compared to simulated measurements of the impedance in the Pt-PSZ system they studied.[125] The symmetry of the electrodes is also a benefit of this technique and enables the maximum surface area of the positive electrode to be studied.

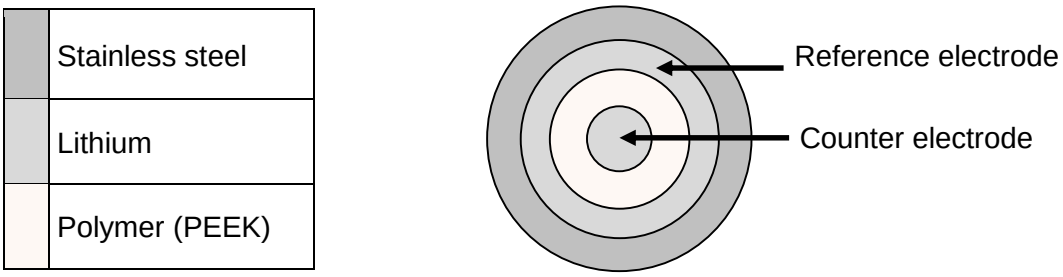

Figure 17. A diagram showing the ring electrode set up used for the 3 electrode impedance experiments.

2 Scanning electron microscopy

2.1 Basic principles

A scanning electron microscope functions in a similar way to a conventional microscope except instead of light it uses electrons. It is used to observe surfaces where conventional microscope magnifications (1000 x) are not enough to see the features required. By replacing the light with electrons up to 1000000 x magnification can be achieved, depending on the conditions. For scanning electron microscopy to function an electron gun produces a beam of electrons which are focussed to a small spot (1 nm) on the sample surface. When the electron beam reaches the sample surface the electrons back scatter towards a detector which is used to produce an image of the sample surface. The electrons from the beam will interact with the surface in different ways. Three key interactions are used by chemists and materials scientists to understand the nature of the surface studied: secondary electrons, backscattered electrons and X rays.[126-128]

2.2 Secondary electrons

Secondary electrons are the lowest energy backscattered electrons with energies of less than 50 eV, they are scattered back from the surface of the material and give high resolution information about the topography of the surface. Although mainly giving information about the topography of the surface, the secondary electron detector can also pick up some backscattered electrons which have interacted with the atoms on the surface of the sample. This gives the secondary-electron results some difference in contrast with elemental composition of the surface.[126]

2.3 Back scattered electrons

Back scattered electrons are electrons that have interacted with the nucleus of the sample and been scattered at a wide angle. As such they can be used to demonstrate information about the composition of the sample. Generally this is shown through contrast with higher atomic mass atoms showing as a brighter contrast on the image. The electrons can also interact with the crystallographic planes of the sample which affects how they back scatter. Electron back scatter

diffraction uses the difference in the backscattered electrons to determine crystallographic information and map the crystallographic planes of the sample.[126, 129]

2.4 X rays - Energy dispersive spectroscopy (EDS)

When a beam of electrons is fired at the surface, some electrons transfer their energy to the electrons in an atom creating an excited state. When the electron returns to the ground state it emits the extra energy as an X-ray beam. This X-ray beam can be detected. Different atoms will have a different X-ray response enabling the researcher to map the elemental composition of the sample.[126, 130]

3 Cell preparation

In the previous sections of this chapter we have discussed the theory behind experimental techniques used in this thesis. In this next section we will discuss the techniques typically used in cell preparation, outlining standard techniques for ink and EPD methods before discussing the typical test cell used.

3.1 Electrode preparations

3.1.1 Conventional ink technique

$LiFePO_4$ powder from Tatung Fine Chemicals was used for all LFP experiments with a quoted charge/discharge capacity of 152 ± 2 $mAhg^{-1}$ at a charge/discharge rate of 0.2C. In addition to $LiFePO_4$ material, the cathode powder had 1-3 weight % carbon. [131]

Inks were prepared by mixing 10% by weight carbon black with 10% by weight PVDF in NMP solvent. Further NMP solvent was added as required to decrease the viscosity of the ink and the mixture was stirred for 10 minutes. 80% by weight cathode material was added to the mixture and the mixture was macerated for 5 minutes using a fine blender.

The ink-like mixture was coated on an aluminium current collector using a doctor blade to provide an even coating. The plate was initially annealed on a hot plate at 70^{o}C to remove the solvent before being dried under vacuum at 120^{o}C for at least ten hours to ensure the sample had been thoroughly dried before being used to make a cell.

3.1.2 Electrophoretic deposition

Chapter three discusses the method development for EPD. This section will be used to outline the standard technique used to produce samples using EPD.

Firstly suspensions were prepared by dispersing LFP material from Tatung Fine Chemicals[131] in Iso Propyl Alcohol (IPA) (>99.9%) from Sigma Aldrich and ultrasonicated for 60 minutes. Next a small amount of LiCl was added and the suspension was stirred for a further 60 minutes. Electrodes were prepared by

sanding two aluminium plates to remove impurities and ultrasonicating them in IPA for 30 minutes.

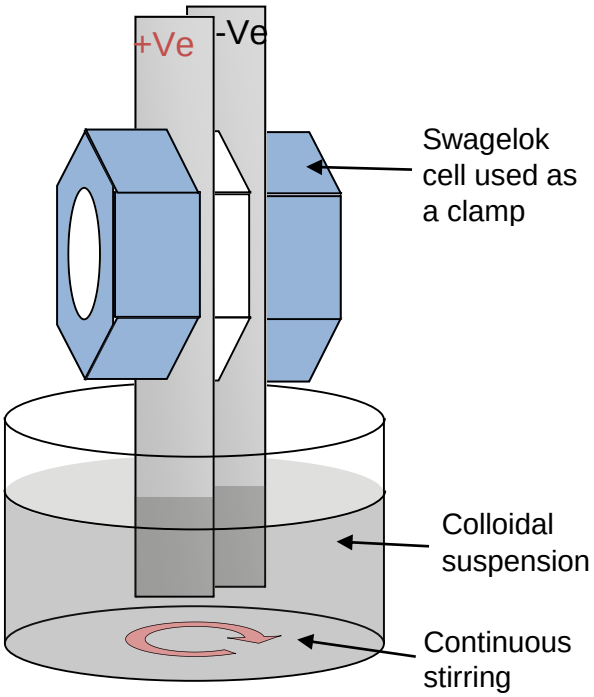

Figure 18. Diagram showing experimental set up for EPD experiments

As the diagram in figure 18 shows, the two electrodes were then placed in the centre of LFP suspension and held apart using a Swagelok cell to maintain a constant separation of 5 mm during the coating technique. The electrodes were connected to a power supply unit and a voltage of 35 V was applied across the gap for a period of 30 minutes. During the applied voltage the current was monitored and kept below 0.001 A to limit degradation of the electrode materials. To maintain a near constant concentration of particles near the electrode surface, the suspension was stirred during coating.

3.1.3 Pressing

To ensure that a good contact was made between the positive electrode material and the current collector, some of the samples were pressed. As not all samples were pressed, where the samples have been pressed it has been noted in the experimental description and on any plots. Pressing was performed using a pellet press. The sample was placed in the press and a 10 N force was applied to the sample for a period of 10 s.

3.2 Swagelok test cell

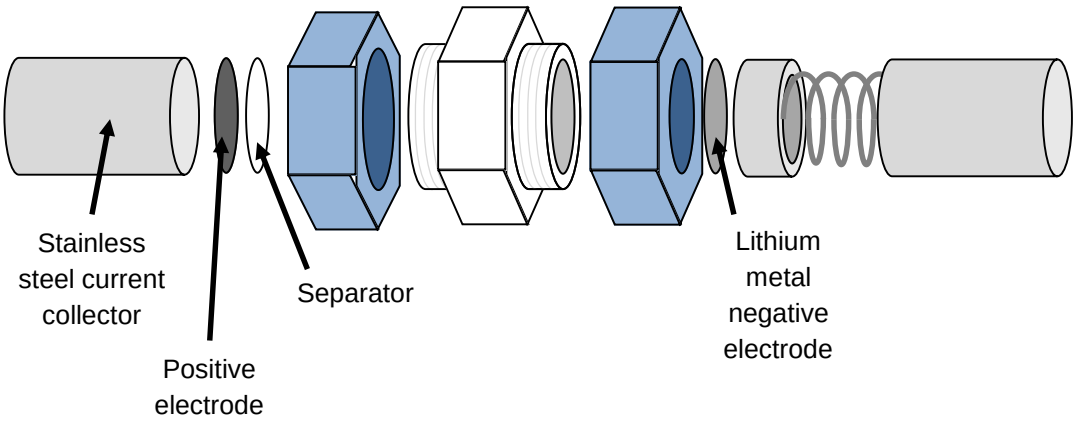

Figure 19. Expanded diagram to show construction of a typical “Swagelok cell”

Electrochemical tests were performed using a “Swagelok cell” shown in figure 19. The cell was assembled in a glove box to limit water ingress during assembly and testing. Ferules, not shown on the diagram, were included with the Swagelok valve to seal the cell. The cell was also wrapped in parafilm to further ensure water ingress was limited. The cell was constructed by pressing together both electrode ends and screwing the Swagelok elements together. The spring was used to maintain a constant pressure on the sample, minimising variability due to unexpected pressure changes during testing. This set up was used for all cells tested under each electrochemical test method. For the three electrode impedance a larger test cell was used with a specially modified electrode as discussed in section 1.3.3 of this chapter.

Chapter 3: Results and discussion

1 Introduction

In conventional manufacturing processes battery composite electrodes are produced by mixing the active material with activated carbon and a binder to form an ink-like material that is coated onto the current collector. The activated carbon increases conductivity between the particles of active material and the binder increases the mechanical stability of the cathode, enhancing rate cycling ability. In developing a novel battery it is a careful balancing act between incorporating as much active material as possible and ensuring the cathode is robust enough to withstand multiple cycles.

This thesis previously discussed methods of producing battery electrodes, focussing on 3D batteries which offer the advantages of a thicker electrode without losing conductivity. 3D batteries also offer greater flexibility in shapes and sizes, enabling battery materials to be optimised to fit within equipment constraints or for greater comfort when worn by dismounted soldiers. Electrophoretic deposition (EPD) has been identified as one such technique that could be used to develop 3D battery systems. Its use of an electric field and surface charge on particles make it compatible with carbon coated battery electrode materials such as LFP over other coating techniques and also offers the potential of creating a battery electrode without the addition of binder material or conducting additives.

This chapter will outline the research into the development of EPD techniques to produce LFP thin film cathodes that are binder-free. The first section will outline the steps in developing the coating process before using cyclic voltammetry and impedance spectroscopy to understand the electrochemistry of the binder-free electrodes in comparison to conventional composite electrodes.

2 A baseline of LFP composite electrodes

Initial investigations sought to understand the relationship between the LFP and the binder material in conventional cathode manufacturing processes. Two commercially available Polyvinylidene Fluoride (PVDF) binders; Solef 5130 and Solef 6020 were studied to understand their effect on the electrochemical performance of the LFP cathode. As table 2 demonstrates, the main difference between the two binders used is their different molecular weights but the two binders also differ slightly in their thermal and mechanical properties. The Solef 5130 has been modified to have a higher number of functional groups which the manufacturers claim will reinforce interactions between the polymer and any active material present, increasing adhesion.[132]

		PVDF Homopolymer	*Modified PVDF*
Properties	Units	Solef® 6020 2nd generation binder and porous separator	Solef® 5130 3rd generation binder for automotive application (or for high adhesion)
Molecular weight	Da	670,000 –700,000	1,000,000 –1,200,000
Melting point	°C	170 – 175	158 – 166
Heat of fusion (ΔHf)	J/g	55 – 65	40 – 48
Glass transition (Tg)	°C	-40	-40
Modulus	MPa	1,300 – 2,000	1,000 – 1,500
Volume resistivity	Ohm cm	≥ 1 x 10^{14}	≥ 1 x 10^{14}

Table 2 A summary of the properties of different PVDF binders * Molecular weight data were obtained by gel permeation chromatography in dimethylacetamide (DMAC), calibrated using a polystyrene standard. The results are useful for a relative comparison.[132]

Composite LFP electrodes were prepared using the two different binder materials and the standard ink technique as outlined in chapter 2, section 3.1. The same batch of LFP, manufactured by Tatung Fine Chemicals, was used

throughout the experiments outlined in this thesis to ensure repeatability when comparing between electrode preparation techniques.

Swagelok cells were constructed using solid lithium as the counter and reference electrode. A Whatman glass filter was used as a separator material and five droplets of 1.0M solution of $LiPF_6$ electrolyte in 1:1 EC:DMC were added to the separator as electrolyte.

Figure 20 shows a representative galvanostatic cycling test performed at a rate of C/10. Figure 20 demonstrates the performance of the LFP material to be used throughout the experiment when made into a cell using standard ink preparation techniques. The capacity at greater than 160 mAh/g is close to the theoretical capacity of LFP at 170 mAh/g. Figure 21 shows the capacity on charging of the two different binder materials and suggests they have similar performance when cycled at low rates.

Figures 22 and 23 demonstrate that at higher rates the lower molecular weight polymer 6020 performed much better. This would suggest that for these battery materials at higher cycle life the mechanical advantage in using the 6020 polymer outweighs the advantages of using the higher molecular weight 5130 polymer. However, these results can be used to highlight the delicate balance in developing coated battery materials with superior electrochemical and mechanical properties. Further tests using impedance spectroscopy would confirm the difference in these binder materials.

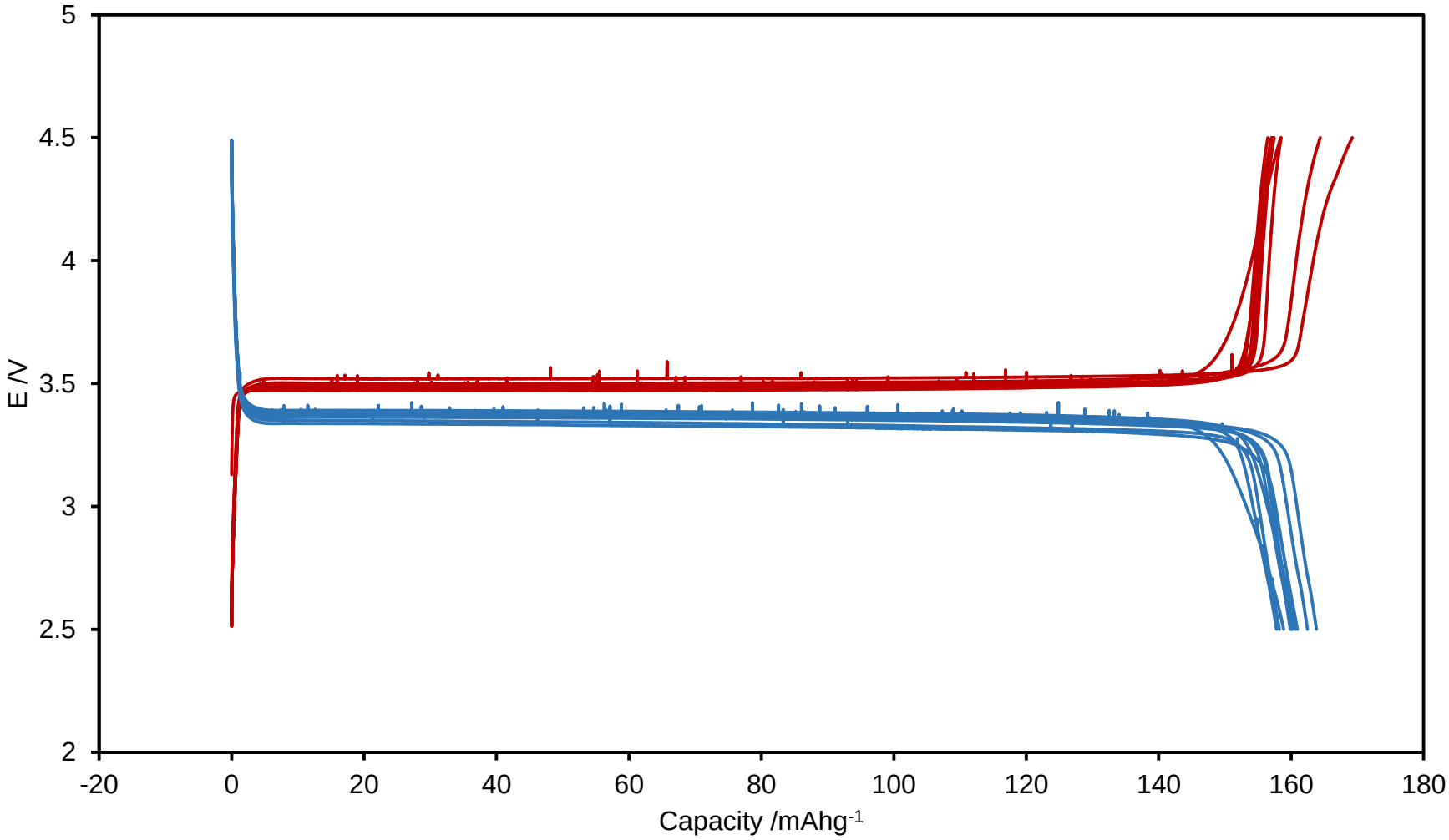

Figure 20. Galvanostatic charging of cell at C/10 rate, red and blue traces indicate the charge and discharge profiles respectively. The cell was produced using a solid lithium negative electrode and a LFP positive electrode using conventional ink methods and SOLEF 5130 binder material.

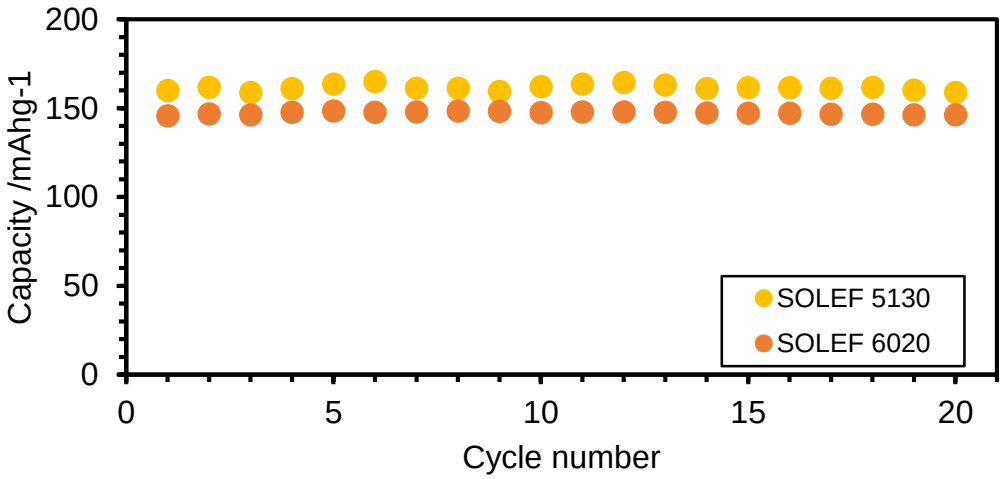

Figure 21. Chart showing the maximum capacity of LFP composite electrodes produced using SOLEF 5130 or SOLEF 6020 binders when cycled using galvanostatic cycling at C/10 rate.

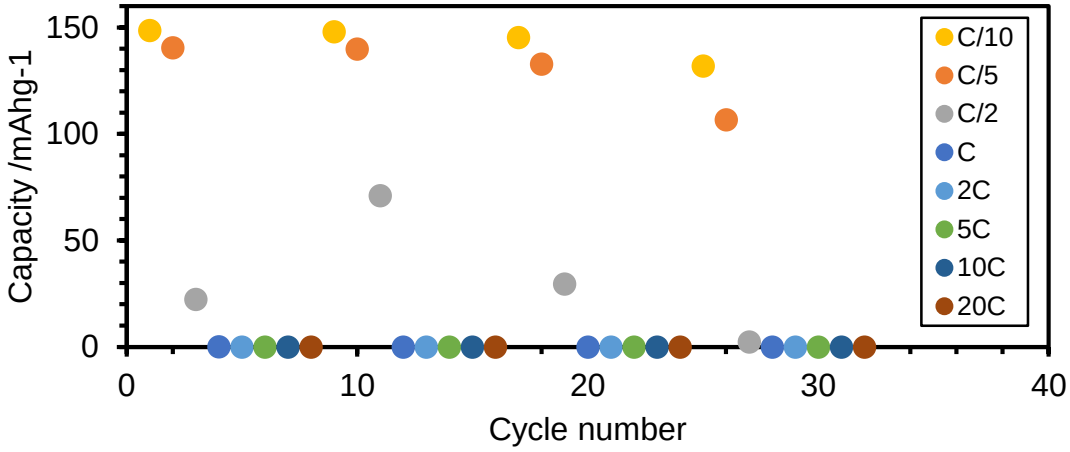

Figure 22. Chart showing the effect of C rate on the capacity with cycle number during galvanostatic charging of LFP composite electrodes produced using SOLEF 5130 binder material.

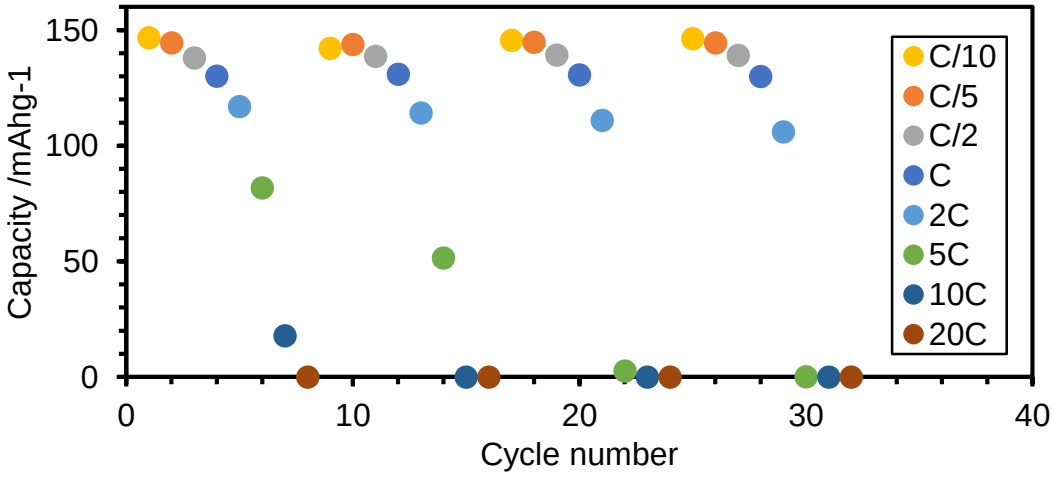

Figure 23. Chart showing the effect of C rate on the capacity with cycle number during galvanostatic charging of LFP composite electrodes produced using SOLEF 6020 binder material.

3 EPD and testing of LFP electrode materials

3.1 Suspension development

The initial step in developing a method to produce positive electrodes using EPD was to produce a suitable suspension. Three key aspects of developing a suspension for EPD were identified: the suspension medium, salt additives for the suspension and the level of mixing or ultra-sonicating to break up agglomerated particles.

Three solvent materials were initially identified as suspension media based on other EPD processes. NMP was also included because of its current application in preparing inks for electrode materials. Four samples were produced by mixing LFP with Ethanol, water or acetone and were stirred for a period of 2 weeks. After the stirring period the suspensions were left to settle. Three further samples were produced by mixing LFP with Ethanol, water or acetone, these samples were then sonicated.

				
Suspension medium	Water	Acetone	NMP	Ethanol

Table 3. A comparison of sonicated suspensions of LFP.

As table 3 demonstrates, water was the worst suspension media and the LFP was not miscible even after 2 weeks of stirring or sonication. From visual inspection the other suspensions appeared to have a similar stability and miscibility. Ethanol was selected based on other research of the EPD of nanotubes.[106] From observing the suspensions, there appeared to be no significant difference between those that had been sonicated or stirred so

sonication was selected due to the lower time required to disperse the suspension.

3.2 EPD – initial tests

An initial EPD experiment was performed by dispersing 0.49 g of LFP in 50 ml of ethanol and then sonicating the suspension. Based on the literature it was expected that the particles would deposit on the positive electrode so graphite was used as a negative electrode and aluminium was used as the positive electrode on which the deposit would form.[116] A Swagelok cell was modified to make an insulating holder for the electrodes that maintained a 5 mm separation between them, as shown in **Error! Reference source not found.**. A potential difference of 50 V was applied through the suspension. After 30 minutes the positive electrode surface was unchanged. Since electrodeposition had previously been undertaken with added water,[106] water was introduced to the suspension with the aim of improving it. Coating on the positive electrode still did not occur and the LFP particles began to agglomerate in the suspension. The failure of the material to deposit was thought to be due to insufficient charge on the surface of the LFP particles and their agglomeration.

Through reading the literature, it was identified that IPA had been successfully used as a suspension media for lithium ion battery materials with a metal salt additive to improve the surface charge on the samples[133]. 0.16 g of LFP was added to the IPA and ultra-sonicated for 30 minutes. 0.012 g of LiCl was added and the suspension was stirred for 15 minutes. As discussed in the introduction to this thesis it is thought that the ions in the suspension are adsorbed onto the particle, enhancing the surface charge and improving EPD.[118, 134]

Using the set up described previously the coating was again not successful so it was suggested that the coating could be occurring on the negative electrode rather than the positive electrode. The EPD experiment was then repeated using two aluminium plates rather than the graphite negative electrode to test this theory. In addition to this, the suspension was stirred and a larger vessel was used to perform the deposition to maintain a constant concentration of the LFP material near the surface.

3.3 SEM of EPD samples

From visual observation the plate was seen to darken, suggested the black LFP particles had deposited onto the surface. Scanning electron microscopy was used to confirm that the coating had occurred and to determine the nature of the coating. SEM was performed at 15 and 20 KeV to give 50 times and 500 times magnification respectively. As table 4 demonstrates, the SEM results confirm that the change in coating technique led to material being coated onto the surface of the aluminium plate. The higher magnification image suggests that the mechanical abrasion of the aluminium plate gave surface roughness to the plate which could aid in the adhesion of the LFP deposit.

The SEM images in table 4 however show that for each EPD experiment only a small amount of material has been coated onto the surface and that it has formed in patches or islands of material. The longer coating times produced an improved coating. In order to perform as a battery electrode a coated layer across the surface is desirable, so it was clear that the coating process needed further improvement. To verify this, the sample was weighed to determine the mass of material deposited. This was challenging since the small amount of material deposited meant that accurate measurements of the deposit weight were not possible.

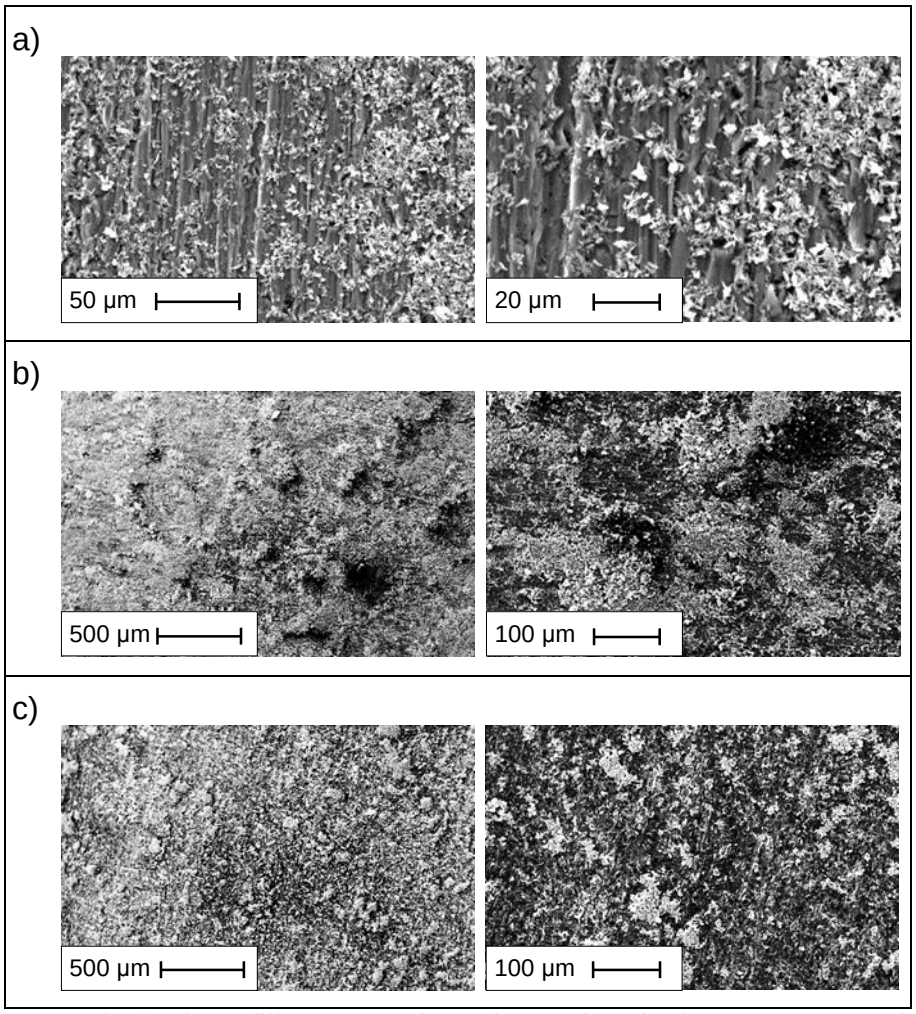

Table 4 SEM results for three different LFP electrodes produced using EPD onto an aluminium substrate with a 50.0 V applied potential, 0.1 A applied current. EPD experiments were run for a) 30 minutes and b) and c) 60 minutes.

3.4 Improving the deposit

After the initial success described in the previous section, several changes were made to the process to attempt to further improve the coating so it was thicker and more uniform. For the following coatings the voltage was reduced from 50 V to 35 V. This change was performed due to a lower voltage power supply being available. As discussed in the review section of this thesis, based on the Hamaker equation, a decrease in the applied voltage would mean a reduction in the electric field across the sample and so this was expected to lead to a reduction in the thickness of the coating.[101]

The aluminium plates were sanded for all EPD experiments which removed surface contaminants on the Al plate and also provided a roughened surface for the deposit to form on. In addition to sanding the plates, the aluminium plates were ultra-sonicated in the suspension media (Isopropyl Alcohol) for 60 minutes

prior to the deposition process to further remove contaminants. Minor changes were also made to the suspension preparation technique with both the stirring and sonicating times extended to ensure the suspension is homogeneous. To minimise contamination effects the suspension was prepared and the coating undertaken on the same day.

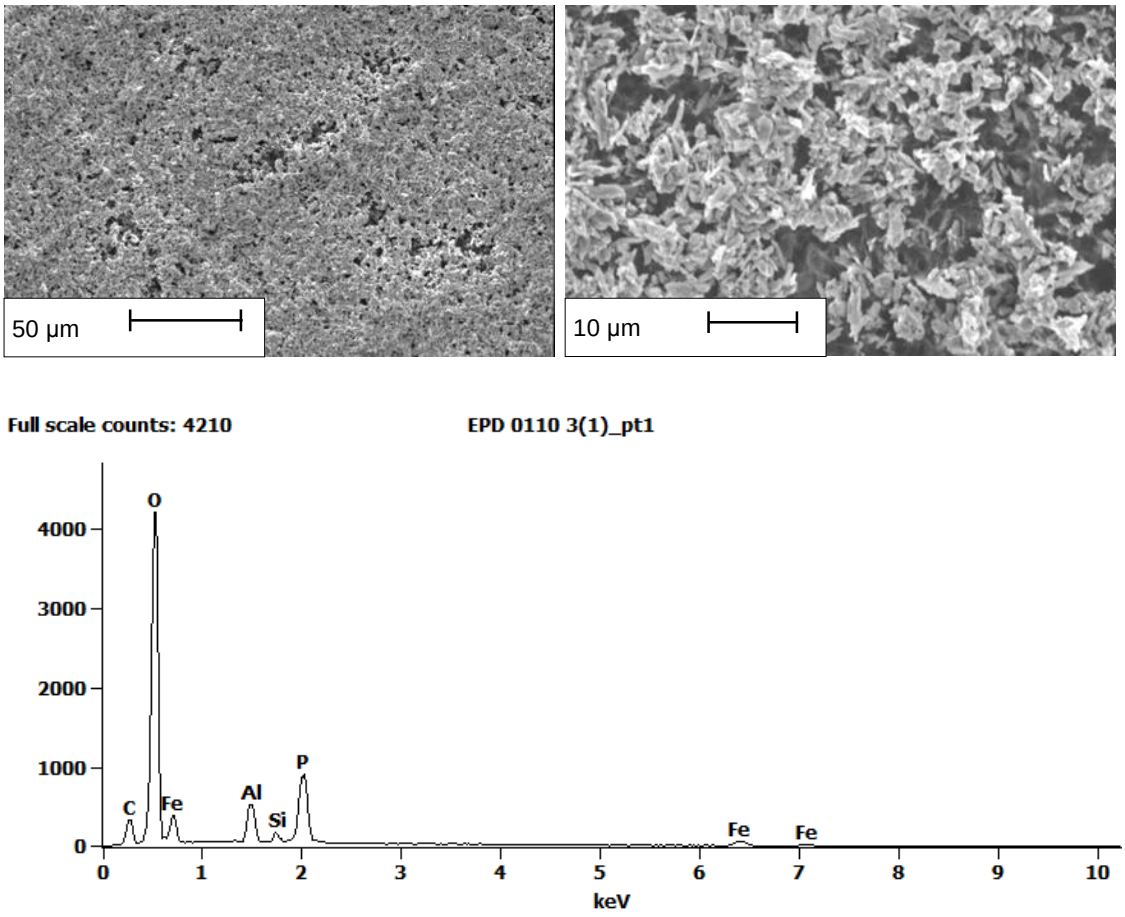

Figure 24. SEM results for LFP electrode produced using EPD onto an aluminium substrate with a 35.0 V applied potential, 0.1 A applied current *Top* SEM images of the sample at different magnifications. *Bottom* Energy dispersive spectroscopy (EDS) of the surface showing peaks that suggest the coating is carbon coated LFP

Scanning electron microscopy was used to confirm the quality of the coated material. As figure 24 shows, the minor changes to the experimental set up led to a much improved coating with a uniform covering on the aluminium. EDS analysis confirmed the coating was LFP with a carbon peak suggesting the carbon coating on the LFP had survived the coating process. The SEM images do suggest that the coating is of a relatively low density with dispersed particles adhered to the surface. Porosity in the coating could potentially affect the diffusion of lithium into the electrode as instead of following a path through the

conductive electrode material some of the lithium ions will diffuse across the pores, reducing their rate of movement through the electrode and reducing the rate capabilities of the electrode.

The improvement in the coating after a decreased voltage was not as expected and could be due to two main effects: the other subtle changes made may have led to a greater advantage than the disadvantages of a lower voltage coating. It could also be that there was a competing reaction occurring, potentially due to the aluminium electrodes that was lessened by decreasing the voltage. This could be studied further by replacing the aluminium electrodes with a less electrochemically active electrode material or through using coated electrodes.

In their paper, Bavykin et. al. discuss the effect of stirring rate on the deposition of titanate nanoparticles. In it they discuss the application of the stirring to clear the wrongly orientated nanotubes away from the larger titanate nanotubes.[135] Although this is different to the effect seen with the LFP particles, it is thought that the stirring acts in a similar way by ensuring that the LFP-depleted suspension is moved from between the electrodes, allowing LFP-rich suspension to be moved towards the electrode where the particles can be electrophoretically deposited. As with the research by Bavykin et. al. higher stirring rates were seen to destroy the deposit, leading to gaps in the centre of the deposit.

3.4.1 Particle size distribution

The original data supplied about the LFP material stated a median value of the diameter of the particles of 2-4 μm. This means that if the particles were ordered in terms of size, 50% of the particles would be larger than 2-4 μm and 50% would be smaller.[131] Through the SEM it can be seen that the particles maintained their size during the EPD process and were not broken up into smaller pieces. The effect on the distribution of the deposition process could be further confirmed by undertaking full particle size and morphology measurements on the dried powder from the suspension.

Using SEM it is also possible to confirm that a certain size was not preferentially deposited using EPD. A droplet of the EPD suspension was added to an

aluminium plate and left to dry. By comparing this with an EPD sample as shown in figure 25 it is possible to confirm that there has not been a significant effect of the EPD process on the particle size distribution. ImageJ image processing software[136] was used to measure the maximum lengths of 10 different particles from the SEM images of both EPD and droplet samples. The EPD and ink droplet particles had average diameters of 5.32 and 4.92 μm respectively. The median values were 4.93 and 4.61 μm respectively. This suggests that the EPD process is not preferentially depositing larger or smaller particles. However, particle size measurement was only possible on particles on the surface of the deposit so further analysis would be needed to confirm the distribution through the thickness of the deposit. This would be a complex measurement to perform as it would require removing the deposited material from the aluminium plate without breaking the particles in the process.

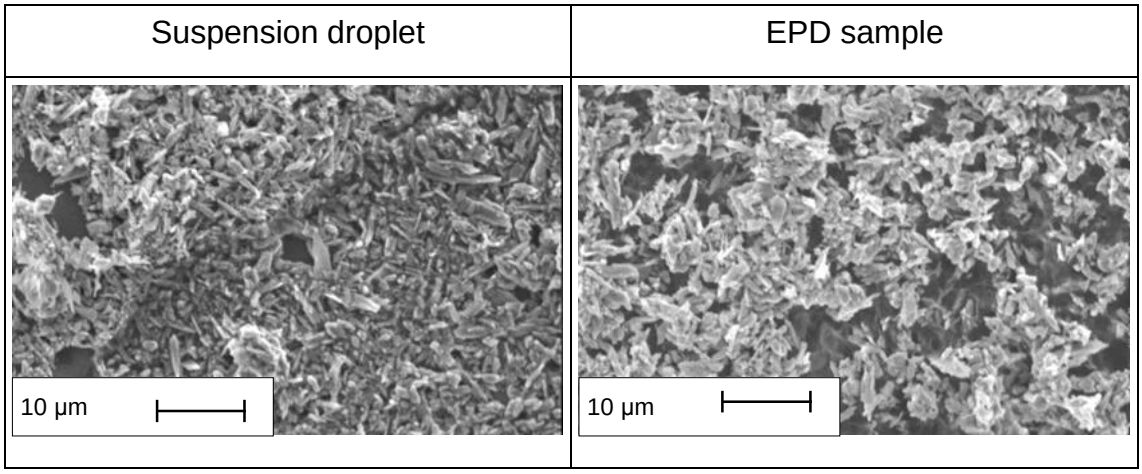

Figure 25. A comparison between a dried droplet of the LFP suspension in the suspension media and an EPD sample.

3.5 A comparison between the EPD sample and a conventional ink sample

Cyclic voltammetry measurements were taken to compare the electrochemical response of LFP composite electrodes with those produced through EPD. Figure 26 demonstrates the cyclic voltammetry measurement for a typical LFP electrode. If the battery system and measurement apparatus was ideal, the two phase behaviour of LFP would give a peak to infinity. In cyclic voltammetry of lithium ion batteries the peak is observed because when the experiment is run in the forwards direction (increasing voltage), the LFP is oxidised and loses

electrons. Once all the LFP has been oxidised there is no more to react at the electrode surface. In the standard electrode this leads to a peak in current density, beyond this point lithium ion diffusion affects the shape of the peak, giving the observed broadening. This is repeated when the voltage is then decreased.

By comparing the results in figures 26 and 27 we can see that the EPD samples are several orders of magnitude smaller than the material produced using the standard ink technique. This is in part due to much less material coated with the EPD technique than the ink method but could also be due to the lack of a binder or conductive carbon within the sample.

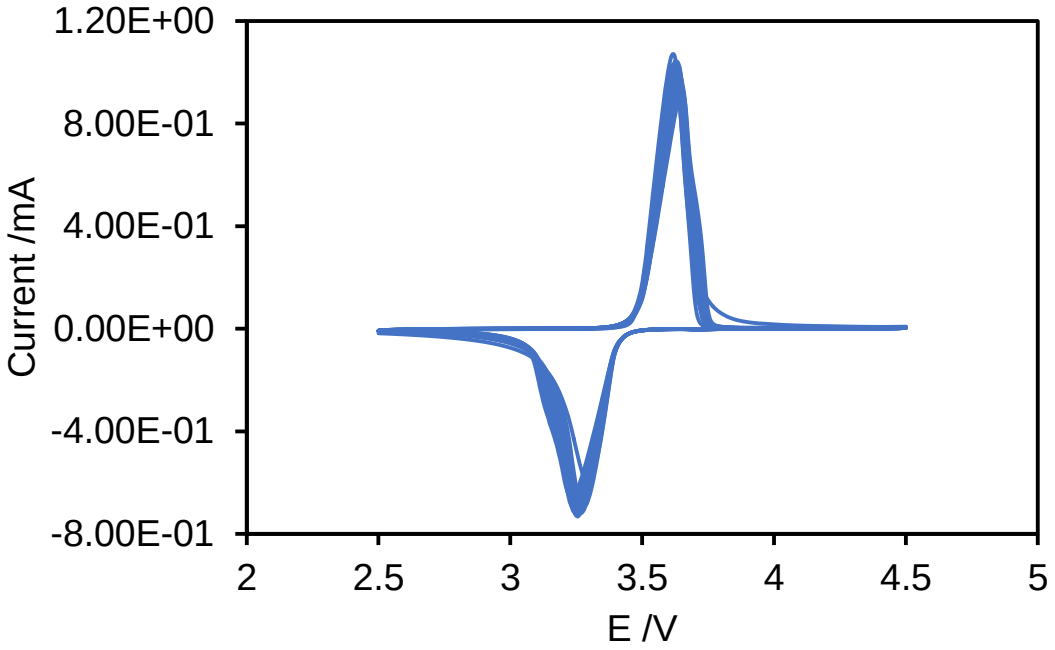

Figure 26. Cyclic voltammetry measurements of cells with solid lithium as negative electrode and LFP produced through conventional ink methods onto aluminium as positive electrode.

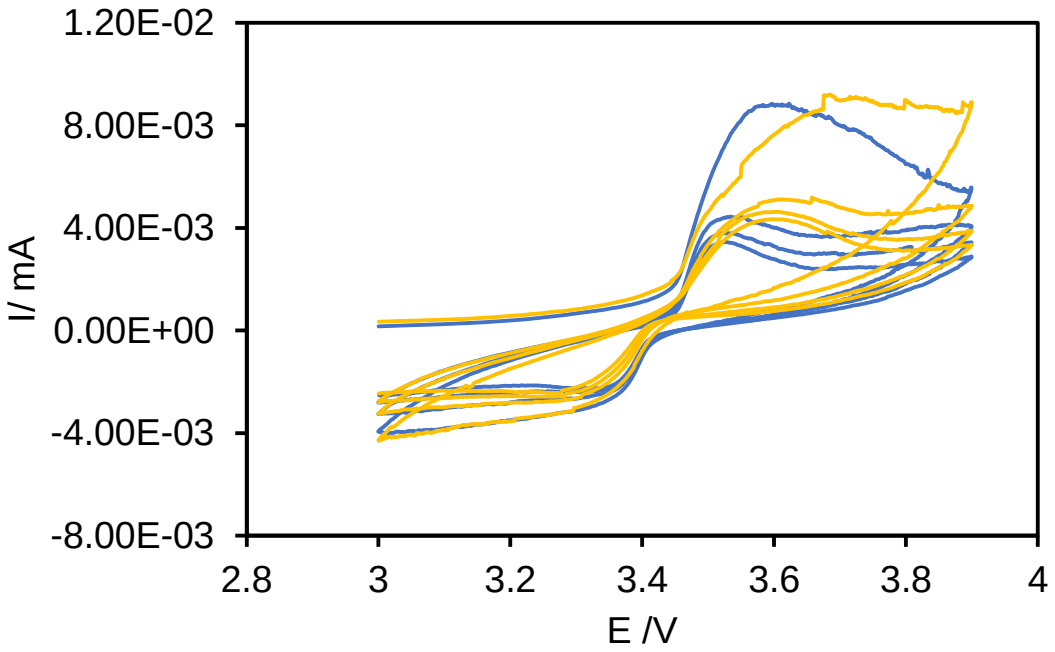

Figure 27. Two different cyclic voltammetry measurements of cells with solid lithium as negative electrode and using two different LFP positive electrodes produced during the same EPD coating of LFP onto aluminium.

Although in figures 26 and 27 the peaks of the two CVs are at a similar voltage, we see a distinct broadening of the peak in the EPD samples. This suggests that the kinetics in the EPD samples is much slower than in the standard composite electrodes. The poor kinetics of the reaction is due to lithium ion diffusion or electron transfer limiting the rate of reaction at high voltages. SEM confirmed the samples had quite high porosity. Although porosity is expected to improve lithium ion conductivity to the electrode it will worsen the electronic conductivity so electrodes are a careful balance of electronic and ionic conductivity. In addition to this, the lack of carbon additive or binder in the electrode is expected to have a detrimental effect on electronic conductivity through the sample. As figure 28 shows, the primary electron transfer path through the composite electrode is through the carbon additive and the LFP carbon coating. Without a carbon additive the electrons must conduct only through the carbon coating, reducing the conductivity of the material.[2, 137]

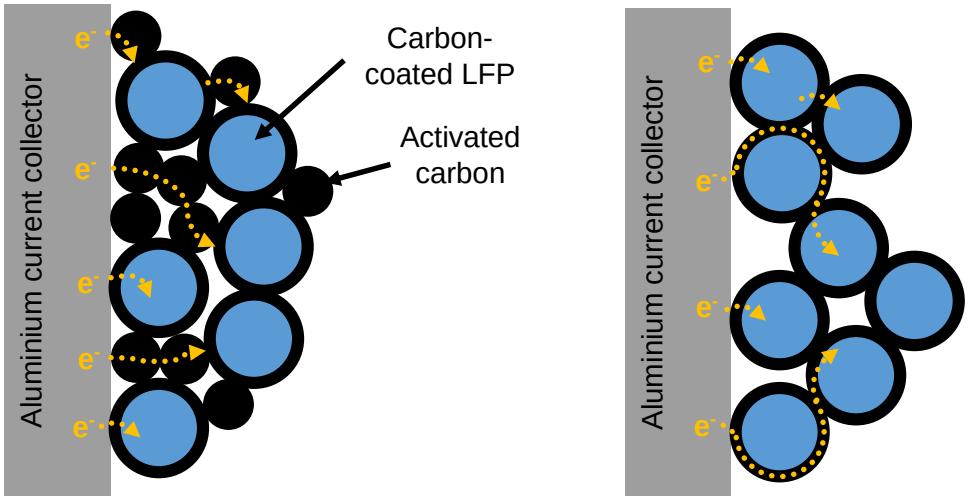

Figure 28. A diagram to demonstrate a comparison of electron transfer through *left* composite LFP electrodes and *right* EPD LFP electrodes.

The capacity of the electrodes can be determined from the cyclic voltammetry measurements since:

$$I = \frac{dQ}{dt}$$

Equation 33

Where:
I = current
Q = charge
t = time

$$Q = \int_{t_1}^{t_2} I \, dt$$

Equation 34

Therefore, by integrating a plot of current against time the total charge available can be determined. The mass of active material was measured for each electrode by measuring the mass of three aluminium discs of the same size as the electrode sample and from the same aluminium plate as the coated electrode. They were prepared at the same time as the coated electrode and using the same technique. The average of these values was then subtracted from the weight of the coated disc to give the electrode weight. As table 5 shows, the standard deviation of these disk weights for the composite sample was 3.34 % of the mass of active material which, although high, is acceptable when considering the performance of electrodes. For the EPD samples, which typically had a lower weight, the standard deviation is 24 % of the mass of active material which is too high to give an acceptable result from the samples, particularly when comparing coating weights. This technique also does not take into account any changes to the aluminium plate during the EPD process.

	Mass of pellet /g	*Average Mass of aluminium disc /g*	*Standard deviation in Al disc mass*	*Standard deviation in Al disc as a percentage of active material /%*	*Mass of active material*
EPD sample	3.43E-02	3.29E-02	3.30E-04	24.0	1.38E-03
Composite electrode	0.03663	3.35E-02	1.04E-04	3.34	2.50E-03

Table 5. The mass and standard deviation of the aluminium disc weights for representative composite and EPD electrodes

An alternate method of determining the sample weights is through using the total charge for the electrode. The Tatung data sheet quotes that the capacity of the material is 152 mAh g^{-1}. Using this value, the weight of material involved in the charge and discharge of the electrode can also be estimated. This is not a fully accurate measurement of the weight of material deposited as it assumes all material presented is involved in the electrochemical reaction which is unlikely. Resistive samples may also present a higher charge than those with lower resistance as the current is driven higher by the electrochemical equipment to maintain the voltage applied. This is, however, useful in giving the amount of material that has been deposited that could be used in future battery applications.

The cyclic voltammetry measurement of a weighed sample, such as in figure 26, can be used to verify the use of active mass to determine the weight of the sample. Using a given material capacity of 152 mAh g^{-1} at 0.2 C[131] this corresponds to a sample weight of 2.50 mg which is the same as the weighed sample mass shown in table 5. Although the results with ink samples suggest the accuracy of this approach, it is likely the lack of carbon additive and binder in the EPD samples may lead to lower conductivity between the current collector and the particles, leading to more particles that are not accessible for charge or discharge, reducing the active mass.

	Q_{charge}/mA.h	*Calculated mass /g*	*Maximum current /mA*
EPD, cell 1	0.00948	5.58E-05	8.85E-03
EPD, cell 2	0.0105	6.18E-05	9.20E-03
Composite electrode	0.380	2.50E-03	1.03E+00

Table 6 A comparison of the first cycle charging of two samples prepared using EPD with a sample prepared using the standard ink method

Table 6 shows the total charge, calculated from the CVs in figures 26 and 27 and the resulting active mass calculated based on the theoretical capacity of the LFP material. The table clearly shows the difference in charge between the two manufacturing techniques and this is reflected in the active mass calculation which is significantly lower than that achieved for the ink samples. This would suggest that the main reason the EPD coatings are performing poorer than the

ink samples is due to less material being deposited. However, the poorer performance could also be due to the lack of carbon or binder in the sample which could mean the conduction pathways are disrupted by gaps in the material, reducing the overall amount of material available to charge.

3.6 Repeatability of the performance across a sample

In order to understand the variability of the EPD coating across a sample, three samples were taken from the same EPD plate. Two samples were tested in the as-deposited condition; the third sample was pressed before testing as outlined in chapter 2, section 3.1.3. Figures 29 and 30 demonstrate the similarities between the three different samples.

It is clear from the graphs below that the pressed sample has a much better performance than the as-deposited samples. This is thought to be due to the effect of pressing the material, leading to a better contact between the electrode material and the aluminium current collector. It may also be that the porosity observed using SEM has been reduced, producing a better diffusion pathway through the material.

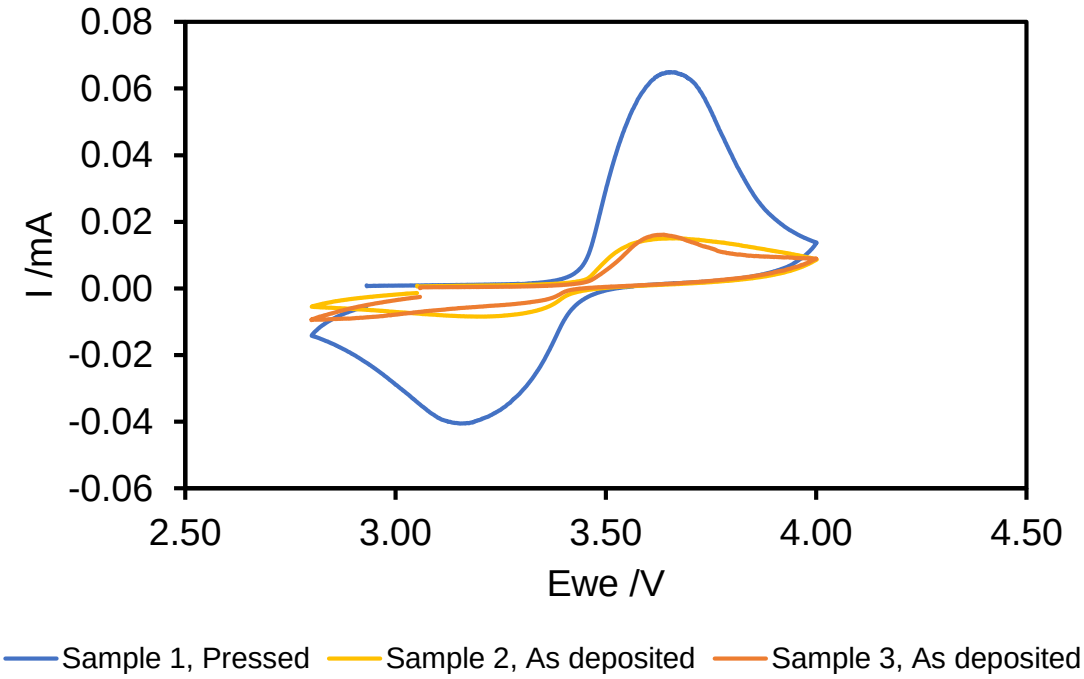

Figure 29. Cyclic voltammetry measurements of cells with solid lithium as negative electrode and LFP positive electrodes produced using EPD coating onto aluminium. Three different LFP EPD electrodes were tested and were taken from the same EPD coating. Sample 1 was pressed before testing and samples 2 and 3 were tested in the as-deposited state.

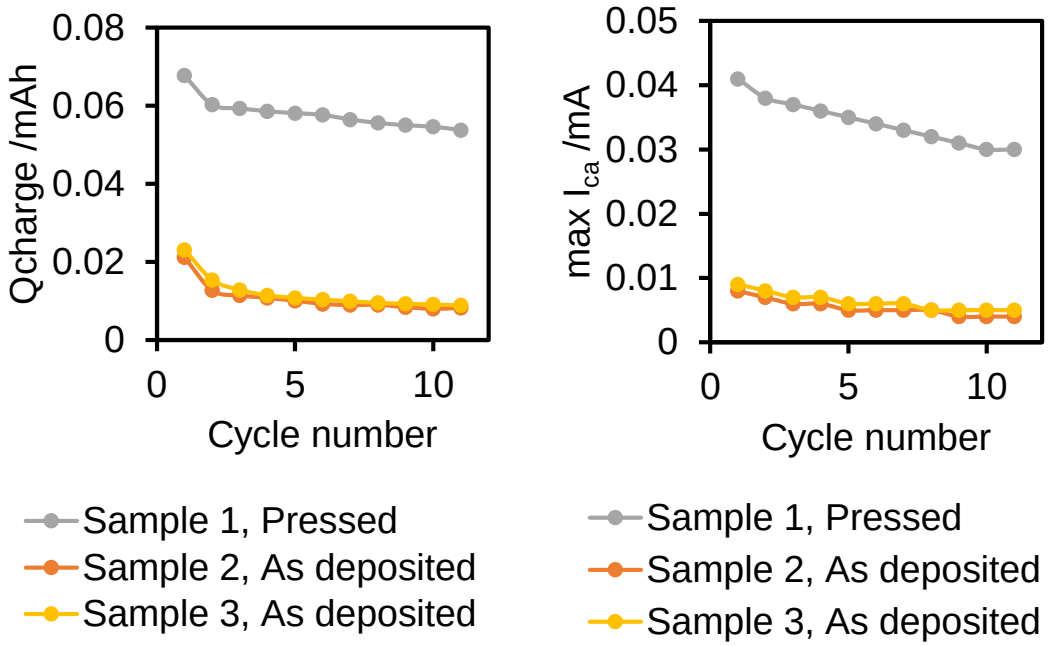

Figure 30. *Left* The total charge. *Right* Maximum current calculated based on three different cyclic voltammetry measurements of cells with solid lithium as negative electrode and LFP as positive electrode with the three electrode samples taken from the same EPD coating onto aluminium.

Although the pressed sample has a much higher maximum current, the peak in current occurs at a similar voltage for each sample, suggesting there is some uniformity in the electrochemical properties of the coating. However, figure 30 shows that there are some differences as well. The total charge observed for each of the samples is initially similar but sample 050516 has a much steeper decline in performance than 040516. This could indicate some difference in the adherence of the coating across the sample affecting the cycling performance of the cell at different locations but would need to be confirmed with further testing and SEM across the deposit.

3.7 Effect of salt additives during the EPD process on the electrochemistry of the electrode material

The role of salt additives in EPD is still not entirely understood. It is thought that the salt additive dissociates in the suspension and is then attracted to the particle where it bonds with the surface of the particle, enhancing the surface charge and improving the amount of material deposited.[93] In order to understand the effect of the charging agent on the deposited LFP, the mass of

LiCl was varied whilst maintaining the LFP concentration in the suspension. The EPD experiment was also attempted using the same conditions but without any LiCl additive. On visual inspection these coatings were unsuccessful, highlighting that some LiCl is important in the success of the coating.

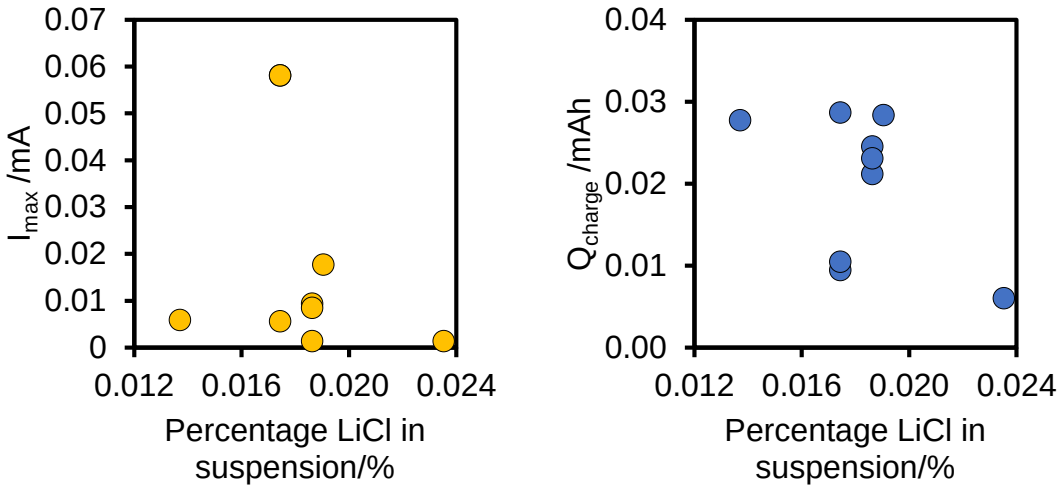

Figure 31. Graph to show the effect of the percentage of LiCl in the EPD suspension. *Left* The active mass and *Right* The maximum current of the materials when used as positive electrodes for lithium ion batteries with a solid lithium negative electrode.

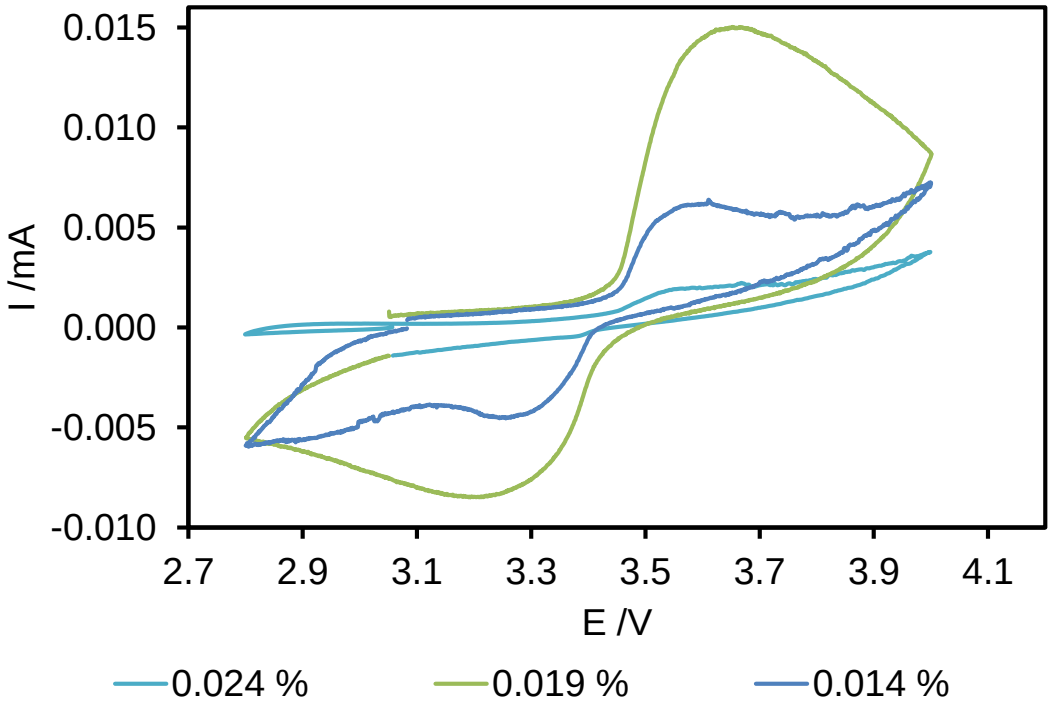

Figure 32. A comparison of the effect of LiCl percentage in the suspension on the cyclic voltammetry measurements at 0.1 mV/s were taken on cells with the EPD samples as positive electrode and a lithium negative electrode.

Electrodes were prepared using different concentrations of lithium chloride in the suspension. Cells were made using the Swagelok configuration described previously with lithium as negative electrode and the EPD samples as positive electrode.

Figures 31 and 32 show the results of cyclic voltammetry measurement of these cells. Figure 32 suggests that the EPD electrodes with a concentration of 0.019 % by weight performed better than those with higher or lower ratios. This suggests that there is a peak in the quality of the coatings at this amount of salt additive. This could be due to two effects: it is possible that at the higher concentrations of LiCl ions, the ions become conductive and adversely affect the EPD process. It may also be that the presence of LiCl could affect the performance of the electrode material when included in the suspension media at greater concentrations. The low concentrations of LiCl included in the suspension media would suggest that the effect is an EPD effect rather than electrochemical effects. This could be confirmed by taking zeta potential measurements of the suspension with different concentrations of LiCl salt present.

Although figure 31 demonstrates a peak in the maximum current achieved during cyclic voltammetry at 0.019 weight percent, the values are inconclusive and would need to be confirmed through further testing.

3.8 Effect of coating time on electrochemical properties

Using the Hamaker equation, one potential way to improve the mass of material deposited is to increase the length of time of the deposition. Although weight of material deposited is important, for an electrode material the quality of the deposit is also important as poor conductivity through the sample could lead to poor performance. To understand the impact of an extended deposition time on the electrochemical properties of the electrode, electrodes were prepared using different deposition times. One batch of suspension was prepared and the EPD coating was performed at 35 V using a half-size plate (3.5 cm x 2.5 cm) for coating times of 45 and 60 minutes. This was compared to a sample produced using the conventional EPD technique and coating time of 30 minutes.

To enhance the uniformity and conductivity in the samples, the three samples were pressed by applying a force of 10 N for 30 seconds as described in chapter 3, section 3.1.3. As the cyclic voltammetry measurements below show, the maximum current for the 30 minute samples showed the highest values but the total charge calculated for the 60 minute sample is higher. This can in part be attributed to the resistive behaviour of the 60 minute sample at high and low voltages causing the peak to broaden. The appearance of this effect suggests that the longer coating time, although potentially leading to a greater mass of deposit as discussed in the previous sections, does not lead to a greater quality of deposit.

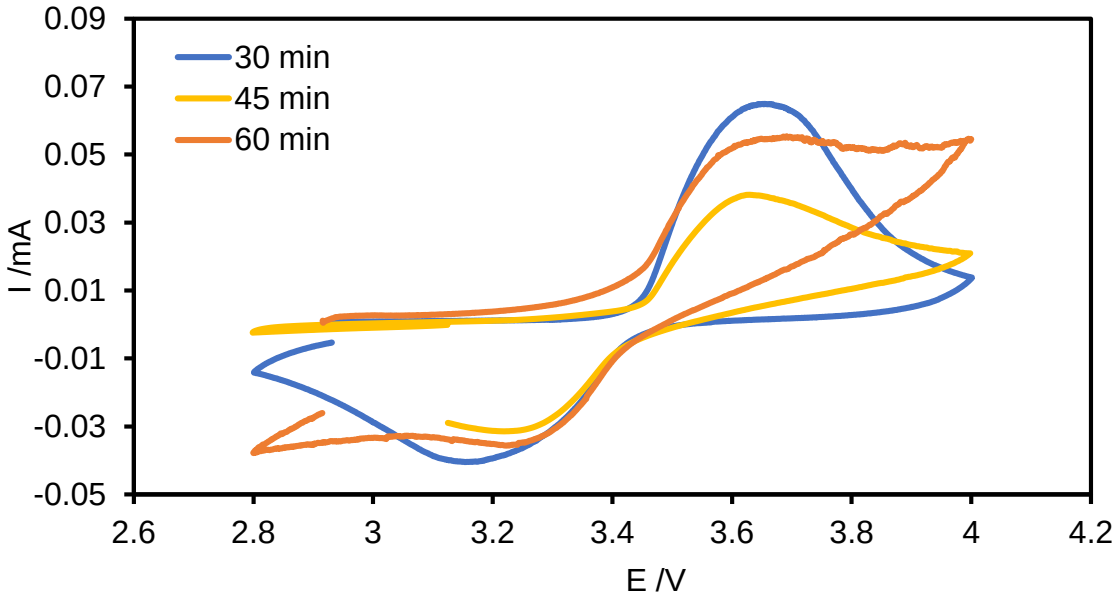

Figure 33. Graph to demonstrate the effect of coating time on the cyclic voltammetry measurement on cells with a lithium negative electrode and pressed EPD samples with different coating times.

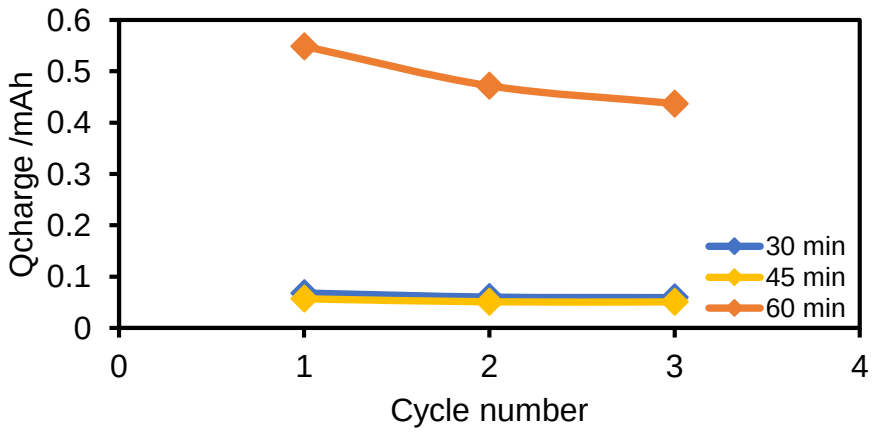

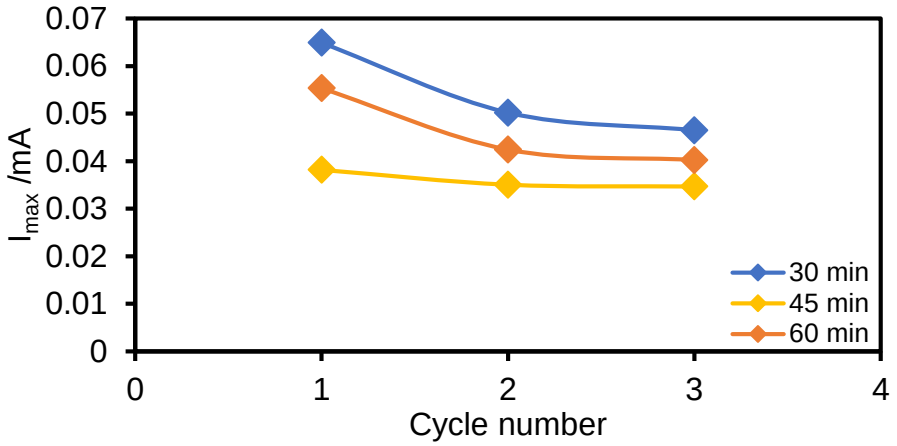

Figure 34. Graph to demonstrate the effect of coating time on *top* the charge and *bottom* the maximum current of cells with a lithium negative electrode and pressed EPD samples with different coating times.

There are several possible reasons for the potentially thicker coating to lead to a greater resistance in the sample. Firstly, as discussed previously, it could be due to poor conductivity of the sample due to porosity and the lack of active carbon to provide a route for conduction through the electrode. In the samples with thicker coatings the particles are further from the electrode and the effects of a longer coating could lead to a thicker deposit, so the electrons have further to diffuse to the aluminium current collector. The electrode quality may also be poorer at the longer coating times leading to a more porous electrode, further deteriorating the electronic conductivity.

The resistance at higher and lower voltages could be due to degradation of the sample due to strain as the particles expand and contract with lithium insertion and removal. In conventional manufactured samples the binder would aid with this strain and limit the effect on the particles of the coating. Without the binder this strain is loaded onto the particles which could potentially lead to them degrading during cycling. This would increase resistance and potentially reduce the number of particles available for charging. LFP has, however, been shown to have only a small change in lattice structure on charge/discharge so this is unlikely to be the observed effect.[51] This could be confirmed through in situ x ray diffraction studies of the strain in the coating during charging.

The large current at high and low voltages could also be due to contamination in the sample. It is possible that during the EPD process the different constituents of the suspension could dissociate or react and be included in the coating in

addition to the active material. Side reactions may have occurred with the following substances within the suspension:

- Lithium chloride
- Aluminium
- The solvent and any products of its oxidation

The longer coating times means the formation of more of these side reaction products which could have an adverse effect on the performance of the electrode material.

The resistance phenomena undergone within the sample could be confirmed by studying the samples further using AC impedance spectroscopy. This would enable an appropriate equivalent circuit to be identified to help determine the resistances present in the sample when compared to a conventionally made ink sample.

3.9 Conclusions

An EPD process has been developed that produces consistent thin films. SEM has been used to confirm that a uniform deposit has been produced and that the LFP material survived the deposition process without significant deterioration of particle size or chemistry.

Initial tests showed that the capacity and rate capability of the cells produced using the technique did not meet the requirements for a commercial battery system and performed particularly poorly in comparison to the conventionally produced ink cells. Pressing the samples significantly improved the capacity of the cells, suggesting that the poorer performance was due to a poor contact between the particles and the aluminium and that pressing improves the contact. Pressing the samples would not be possible when coating the material onto a 3D substrate so may not be a practical solution to improving the contact.

Attempts were made to quantify the effect of the EPD parameters on the electrochemical properties of the electrode. The concentration of salt additives and the deposition time were both separately varied. It was shown that there was a slight peak in performance for salt additive concentrations of 0.019% by

weight in the solution but the trend is not clear and further experiments would be required. Increasing the deposition time led to mixed results and the samples appeared more resistive, possibly due to competing side reactions damaging the coated material.

The next section of this thesis will seek to use impedance spectroscopy to understand and quantify the additional resistances in the binder-free electrode materials by comparing them with conventionally manufactured electrodes.

4 Impedance spectroscopy studies of electrophoretic deposited coatings.

Impedance tests were performed at open circuit voltage on EPD and composite electrode samples. As discussed in chapter 3, in three electrode impedance the charge transfer resistance is only due to the electrolyte and the positive electrode and not due to the negative electrode. As this research only sought to study the positive electrode, the impedance measurements were taken using a three electrode set up, as described in chapter 3, with a lithium ring as the reference electrode and a disk of lithium the same size as the electrode under study as counter electrode. The electrode to be studied was used as the working electrode.

4.1 Results of impedance tests

4.1.1 Nyquist plot

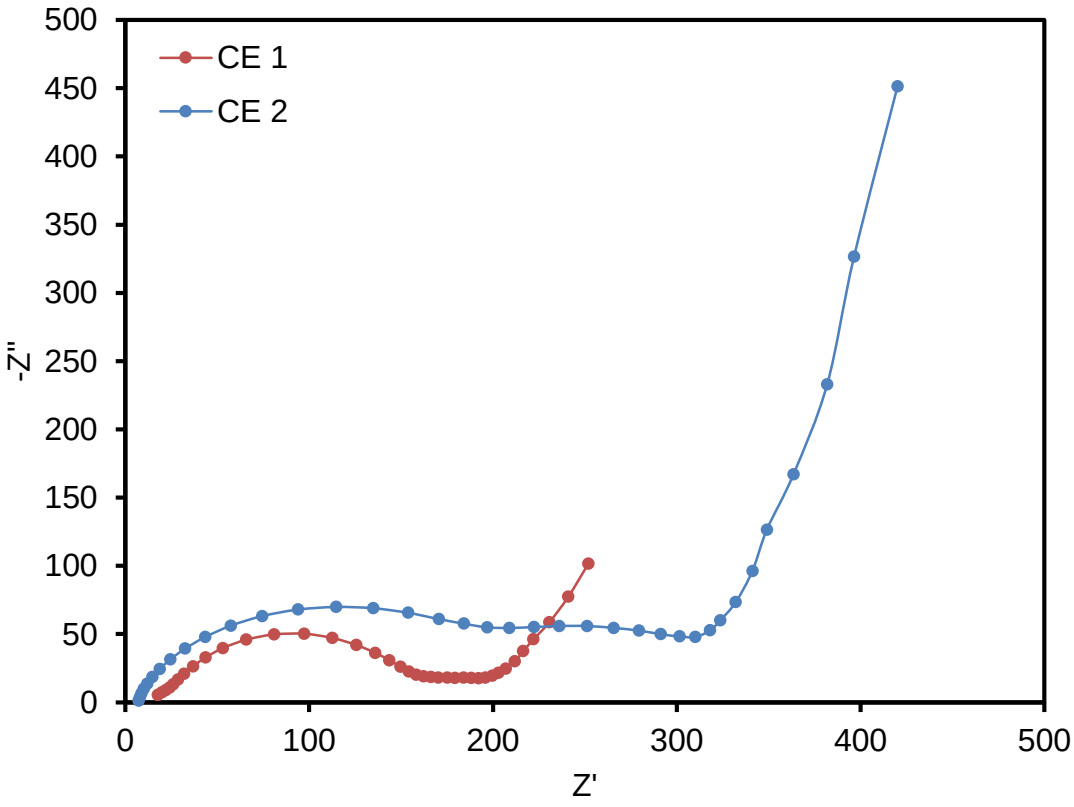

Figure 35. Nyquist plot of real versus imaginary components of impedance for three electrode impedance measurements of composite electrodes CE1 and CE2

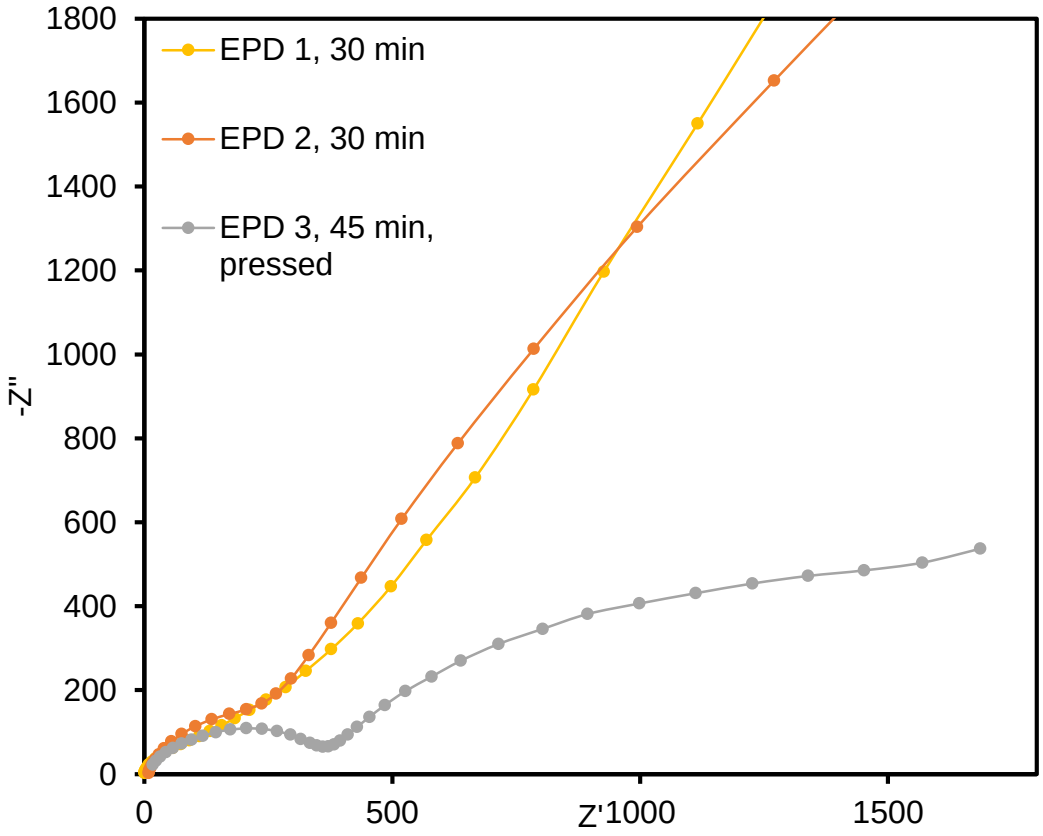

Figure 36. Nyquist plot of real versus imaginary components of impedance for three electrode impedance measurements of EPD electrodes

4.1.2 Bode plots

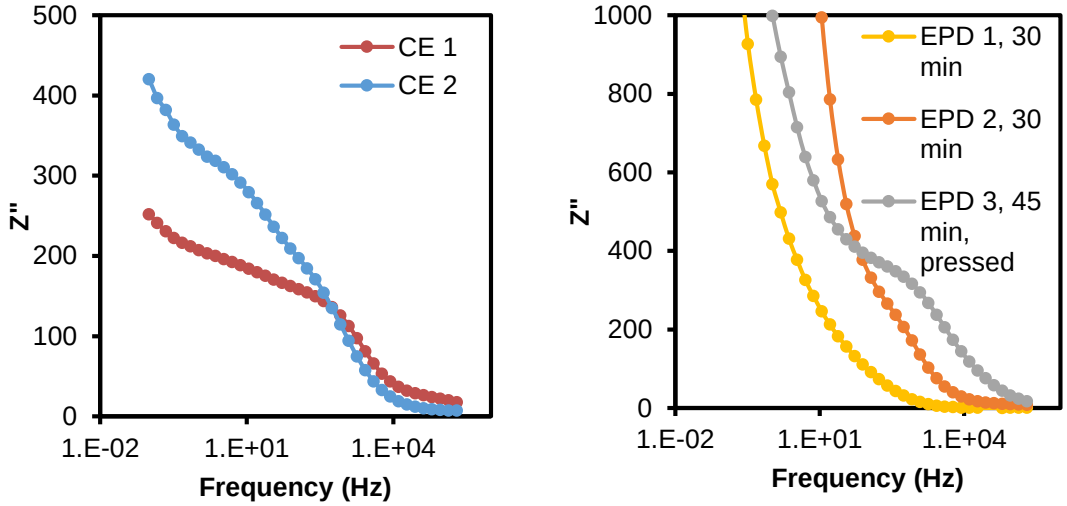

Figure 37. Real component, Z" of frequency response for three electrode impedance measurements of *Left* composite electrodes and *Right* EPD electrodes.

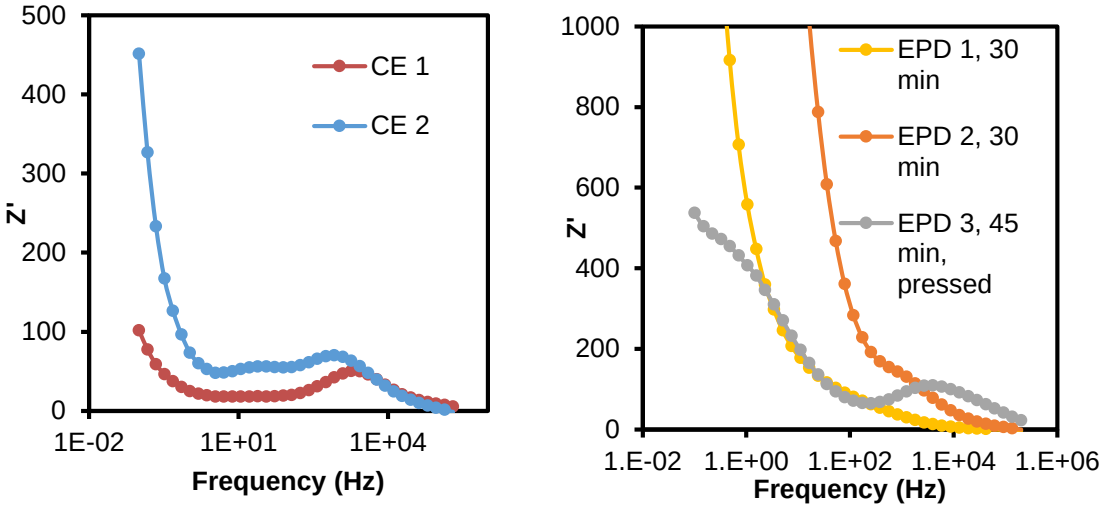

Figure 38. Imaginary component, Z' of frequency response for three electrode impedance measurements *Left* composite electrodes and *Right* EPD electrodes.

4.1.3 Equivalent circuit fitting

Equivalent circuit fitting was performed using the three impedance results; the pressed EPD sample and the two composite electrode samples which were not pressed. Impedance fitting was not possible on the un-pressed EPD samples due to the incomplete first arc.

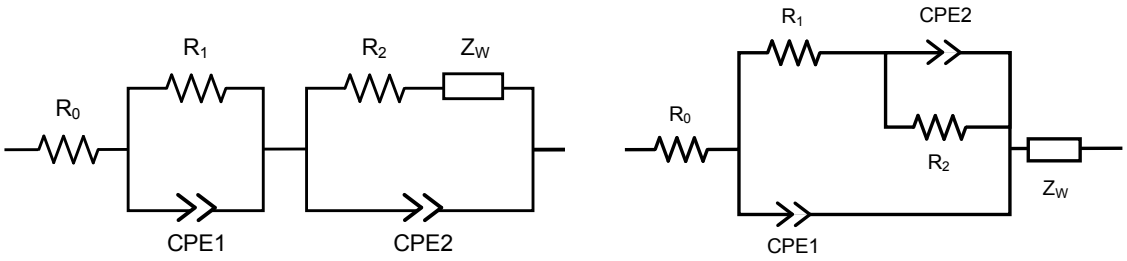

Figure 39. *Left* The modified Randles equivalent circuit. *Right* The modified Gaberscek circuit.

From a literature search, two potential equivalent circuits were identified to fit the remaining three impedance measurements as shown in Figure 39. The left hand circuit was a modified Randles circuit which had been shown by XiangFeng et.al. to achieve a good fit with LFP.[138] The right hand equivalent circuit is based on a model by Gaberscek et. al. when considering LFP particles on an electrode surface.[139] The data was fitted using the Zview application.[123] The results of fitting the two equivalent circuits shown in figure 39 are displayed in tables 7 and 8 below.

Sample	*R0 /Ω*	*R1 /Ω*	*T (CPE1) /µF*	*P (CPE1)*	*R2 /Ω*	*T (CPE2) /µF*	*P (CPE 2)*	*R (W) /Ω*	*T (W) /s*	*P (W)*
CE1	16.59 (1.8 %)	153.7 (1.2 %)	8.2 (7.9 %)	0.711 (1.1 %)	24.83 (10.7 %)	372.41 (19.9 %)	1.00[a]	308.6 (14.4 %)	7.94 (17.1 %)	0.61 (4 %)
CE2	6.6 (4.9 %)	190.4 (3.4 %)	4.3 (14.4 %)	0.803 (1.7 %)	108.7 (7 %)	51.19 (16.7 %)	1.00[a]	2683 (15.8 %)	14.61 (16.8 %)	0.79 (3.1 %)
EPD3 pressed	1.53 (61.1 %)[b]	356 (1.9 %)	2.6 (9.7 %)	0.67 (1.3 %)	1642 (5.1 %)	265.91 (6.1 %)	0.61 (3 %)	3139 (19.6 %)	12.75 (7.5 %)	0.93 (2.3 %)

Table 7 A comparison of the parameters for the three impedance tests based on the modified Randles equivalent circuit shown on the left in figure 39. The error of the fitting value is shown as a percentage in brackets. [a]For both of the composite electrodes CPE2 can be considered as a capacitor as this had an improved fit for the other parameters.

Sample	*R0 /Ω*	*R1 /Ω*	*T (CPE1) /µF*	*P (c1)*	*R2 /Ω*	*T (CPE2) /µF*	*P (CPE2)*	*R (W) /Ω*	*T (W) /s*	*P (W)*
CE1	17.54 (1.6 %)	151.2 (1 %)	7.3 (6.7 %)	0.724 (0.9 %)	20.52 (9.6 %)	479.58 (17.6 %)	1.00[a]	315.2 (11.9 %)	8.36 (14.7 %)	0.6 (3.3 %)
CE2	6.11 (5 %)	200.7 (2.4 %)	5.2 (11.2 %)	0.784 (1.3 %)	80 (6.9 %)	56.02 (15 %)	1.00[a]	1033 (6.9 %)	5.47 (6.4 %)	0.69 (2.0 %)
EPD3 calendared	1.58 (60.2 %)[b]	368.1 (1.8 %)	2.55 (10.1 %)	0.67 (1.3 %)	1433 (5.8 %)	257.90 (6.3 %)	0.619 (2.9 %)	2392 (18.8 %)	13.65 (8.7 %)	0.91 (2.6 %)

Table 8 A comparison of the parameters for the three impedance tests based on the equivalent circuit shown on the right in figure 39. The error

of the fitting value is shown as a percentage in brackets. [a]For both of the composite electrodes CPE2 can be considered as a capacitor as this had an improved fit for the other parameters.

4.2 Discussion of impedance results

Figures 35 to 38 show the results of the impedance spectra for EPD and composite electrode cells respectively. As observed in the cyclic voltammetry measurements, the two as-deposited EPD samples perform poorly and are difficult to resolve using the equation fitting commonly used to quantify the results of impedance measurements. The as-deposited EPD results can be used to help inform a physical description of the electrodes which will aid in identifying an appropriate equivalent circuit.

4.2.1 Resistance parameters

For all three EPD measurements we observe a similar initial arc suggesting that the pressed and un-pressed samples have a similar initial resistance value. For the pressed samples the arc is complete but for both the as-deposited samples the arc is incomplete. The initial arc is larger for the EPD samples than the composite electrode samples, suggesting this initial resistance term is larger for the EPD than the composite electrodes. This is confirmed by the results of circuit fitting shown in tables 7 and 8. This is also observed as a peak at high frequency in the frequency response plots in figures 37 and 38 with a more pronounced peak in the pressed composite electrodes than the EPD samples.

Next we can look at the second arc, where it is present. The pressed EPD sample and the two composite electrodes display a definite second arc which, as shown in tables 7 and 8, is significantly larger for the EPD sample. One of the as-deposited EPD samples also displays a second arc but this is difficult to distinguish from the slope since a low frequency diffusion slope dominates these plots. This could suggest that pressing has improved the low frequency diffusion response of the samples.

From these observations we can then determine two key conclusions. Firstly, the fact that the first arc is less affected by pressing than by method of manufacture. This suggests we are looking at a feature due to the performance of the material close to the current collector surface which is influenced by the presence of binder and carbon which would be observed at the electrode surface. This would suggest that it could potentially be due to the interface

between the particle and the aluminium current collector which we would expect to be similar for all samples and less affected by pressing.

Secondly, we observe that the second arc is affected by the presence of the binder and carbon and affected by pressing. This would suggest we are looking at the results of a phenomenon that is occurring further from the electrode surface where resistance would be reduced by both pressing in the EPD samples and the presence of the binder and added carbon in the composite samples.

4.2.2 Capacitance parameters

Unlike the EPD sample, for the composite electrodes, a better fit was achieved for the second arc without using a CPE. The CPE is used to account for non-ideal behaviour in double layer capacitors so its use in the composite electrode samples could suggest that the capacitance is behaving ideally at this point. In reality it is unlikely that the double layer capacitor is behaving ideally so it is more likely that using a CPE has a much greater negative effect on the fit of other parameters in the circuit than the fit of the second arc using a CPE.

The capacitances for each of the results are similar and we do not see a significant trend in capacitance with the different electrode preparation techniques. It is expected that the increase in mass and carbon content with the composite electrode preparation technique would lead to an increase in the observed capacitance. Further research would be required but the similarity could suggest that there is not a significant difference in surface effects on the electrode with the different production techniques.

4.2.3 Warburg impedance

As with the capacitance results, no significant trend is observed in the Warburg parameters R, T and P and the differences observed between the different cells are likely to be due to minor differences in cell construction and the electrolyte. The so-called short Warburg term was used and coincides with a finite diffusion length as opposed to an infinite diffusion length observed in the open Warburg.

4.3 Physical description of parameters

The previous sections give the numerical results of impedance and the two equivalent circuits that achieved the best fit. One of the first things to note is the similarity in the error of both of the equivalent circuits. This highlights an issue with the use of equivalent circuit modelling where subtle differences between equivalent circuits may not be observed as errors or significant alterations in the values. As discussed previously, the equivalent circuit must coincide with the physical interpretation of the electrode. This can be done by considering the three resistance terms observed R_0, R_1 and R_2. R_0 is generally considered to be the resistance of the electrolyte as there is no corresponding capacitive value.

R_1 is attributed to the first arc in the impedance spectra. Several studies have attributed this first arc in the Nyquist plot for a LFP electrode to the SEI layer as in other battery systems.[140] Gaberscek et. al. proposed that the first arc is instead due to the interaction of the coated electrode material with the aluminium current collector. They confirmed this by applying a conductive silver coating between the electrode and the aluminium plate. The first arc was significantly reduced.[139] This gives terms for the resistance of the contact and double layer capacitance of the aluminium surface. The impedance values, shown previously, in part confirm this since the change in preparation technique from composite electrodes to binder and carbon-free EPD electrodes has a lesser effect on the first arc. This would suggest that the particles near the electrode surface are similar in both preparation techniques.[139, 141]

The second arc, R_2, is typically attributed to the charge transfer resistance in the particles. As shown in Figure 28 in the previous section, the main electron transfer route through the EPD samples is through the carbon coating on the electrode whereas the composite electrodes can also undergo electron transfer through the carbon additive. The significant increase in the second resistance term with the change in electrode manufacture technique could suggest that this second resistance term is due to the resistance of the electrons as they travel to the particle, rather than the charge transfer resistance into the particle.

Gaberscek et. al. also propose that the second arc is due to the double layer capacitance of the interface between the particle and the electrolyte, c_1 and several resistances which account for:

- The resistance as an electron moves along the particle surface or surface film, r_1
- The resistance as lithium ions move across pores in the electrode material, r_4
- The resistance of charge insertion into the active particle, the charge transfer resistance, r_2
- The resistance due to the transfer of an electron between the particles, r_3

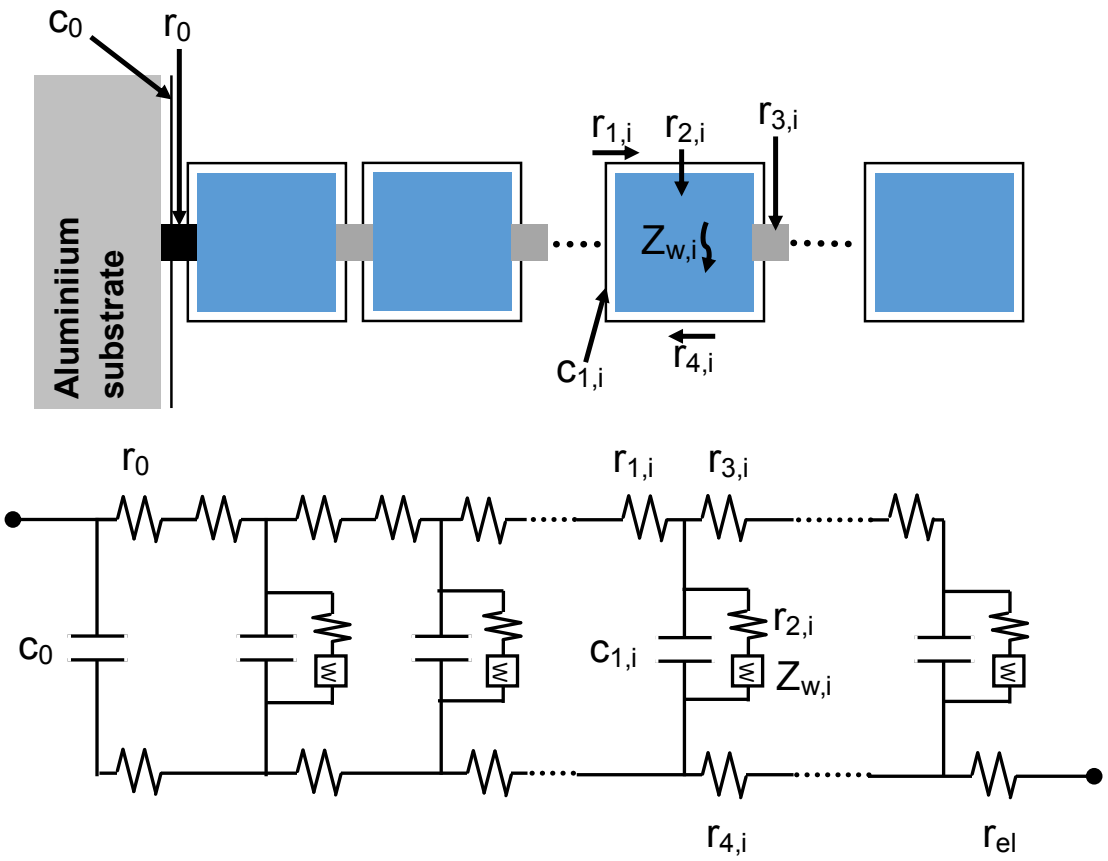

Figure 40. *Above* Schematics showing active particles and contacts in a composite insertion electrode. *Below* An equivalent circuit corresponding to situation under (a)[141]

As shown in figure 40 this generates a very complex equivalent circuit which cannot be resolved easily. For certain cases this circuit can, however, be resolved to an equation suitable for use in impedance fitting software such as Zview.[123] Figure 41 demonstrates two such applications where the charge transfer resistance (R_2) or the interparticle resistance (R_3) are significantly greater than the other resistances, simplifying to give the circuits shown.

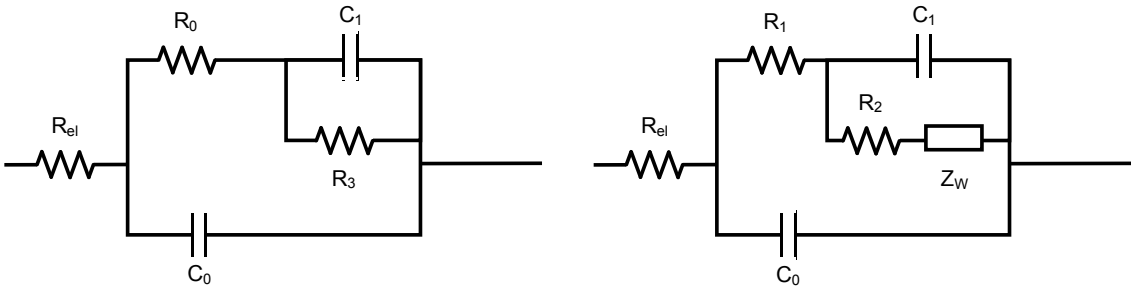

Figure 41. *Left* Equivalent circuit based on the circuit in figure 40 for circuits where $R_3 > R_1, R_2, R_4$. *Right* Equivalent circuit based on the circuit in figure 40 for circuits where $R_2 > R_1, R_3, R_4$

The circuit on the left where $R_3 > R_1, R_2, R_4$ is similar to the equivalent circuit fit achieved for the impedance data earlier on in this section but excludes the Warburg coefficient. For the carbon-free samples in particular this would coincide with a higher inter-particle resistance, r_3, than the other resistance parameters. For the composite electrodes the conductive carbon in particular should reduce the inter-particle resistance and may mean that the assumption is no longer valid. This could mean that the primary resistance term is due to the other resistances present and so would be much more complex to model using software such as Zview.

The parameters that could potentially relate to the interface between particles and the electrode are similar in value in the carbon-free EPD samples and the composite electrodes. Parameters that potentially relate to the inter-particle interactions vary more widely between the two manufacture techniques. This could suggest that the change in process is affecting these inter-particle parameters more than others. This also demonstrates that there may be merit in applying the Gaberscek model to this LFP battery system but further study would be needed to confirm this by, for example, altering layer thickness in the samples or slowly introducing conductive additives or binders to the material. The effect of pressing the samples on these results would also need to be further studied.

4.4 Conclusions

It is clear from the impedance data that the poorer performance of the EPD samples is due to a greater resistance in those samples than the composite electrodes. This is expected as the EPD samples lack the conductive carbon

additive which would increase resistance. The results do, however, demonstrate two arcs in the Nyquist plot of the impedance spectra. The second arc size and subsequently the resistance it represents is much more adversely affected by the method of manufacture, EPD or composite, than the first arc.

Two equivalent circuits are presented to which the impedance data achieved a good fit and they confirmed the much greater resistance in the EPD samples when compared to the composite electrode samples. A comparison of both capacitance and diffusion parameters for the composite and EPD did not show any trend in these values and further work would be required to understand the similarities in these parameters.

Two physical interpretations were presented for the two equivalent circuits. The first applies the more commonly held interpretation that the first arc in the Nyquist plot is due to the SEI layer and the second arc is due to charge transfer resistance. The second interpretation is that the first arc and coinciding resistance term are due to a phenomena near the surface of the current collector. This could be due to the behaviour of the particles near the electrode surface or the oxide layer on the aluminium current collector. The second arc is then considered as due to the particles further from the electrode surface. This explains the much greater value of the second term in EPD samples which SEM shows are low density and porous. This also agrees with the difference between the composite and EPD electrodes for electron transfer. Composite electrodes see additional electron conductivity through the carbon additive as well as through the LFP particle carbon coating. This second resistance term is improved by pressing the samples, further confirming this theory. It is possible we see this to a lesser extent in the ink samples.

It is not possible to conclude which interpretation is valid based on the results presented here and further testing would be required to confirm the theory. Further work could continue to use EPD as a technique to manufacture binder and carbon-free electrodes to alter the electrode construction and ultimately the resistances of the electrode. This could then be used with Gaberscek’s model of particles in a battery electrode to distinguish and quantify the different resistances present which will be greater or lesser in EPD samples.

Chapter 4: Conclusions and recommendations

1 Conclusions

EPD has been successfully used to generate binder-free electrodes from commercially available LFP battery materials. The materials, which were coated without binders or carbon additives, displayed a consistent but slightly porous coating with some mechanical stability observed during handling and sampling. By changing the experimental parameters such as coating time and the amount of LiCl additive the coating was improved. Mechanically roughening the material to be coated through sanding improved the ability of the coating to adhere to the surface.

The cyclic voltammetry measurements of the EPD electrodes gave results that were not as good as using conventional composite electrodes. This is thought to be due to a combination of factors but primarily is due to the lack of conductive carbon and binder increasing resistance in the sample, particularly at distances further from the electrode where the EPD samples are more porous and where carbon additives provide an additional pathway for electrons to conduct to the sample. Electrode performance was improved by pressing, suggesting this could improve electron conductivity through the samples.

Three electrode impedance measurements were performed on the EPD and composite electrode samples. All the impedance results showed two arcs in the Nyquist plot. This suggests that, in addition to the electrolyte resistance, two resistance terms coupled to capacitance elements describe the impedance behaviour of the electrodes. Both resistance terms were larger for the EPD electrodes than the composite electrodes but the different manufacturing techniques for the electrodes appeared to affect the second term more than the first term. This suggests that the primary increase in resistance was observed at a distance from the aluminium plate where particles had poorer conduction paths to the current collector. This suggests that Gaberscek's model of particles in a battery electrode may be valid for this system and that EPD samples could be used to confirm and quantify some of the resistance terms present in the model.[139]

2 Recommendations

There are two approaches to furthering the research initiated as part of this thesis. The first would be to continue to improve the EPD coating and consider its use in 3D batteries. The second approach would be to continue to use the binder and carbon additive-free EPD samples to understand the electrochemistry of carbon coated particles and how this is influenced by the addition of carbon and binder. This section will outline these approaches but it is likely that any future work will look at both, using the greater understanding of the electrochemical system to improve the 3D batteries in development and using the improved EPD process to produce more representative samples for electrochemical testing.

2.1 Further improvements to the EPD process

Although this project has gone some distance to develop the EPD coatings of LFP, there are still further improvements required of the EPD process before it can be used in commercial battery systems.

Initially, further research should investigate improving the quality of the films produced through EPD. Further experiments should be performed to optimise the coating so it is thicker which could improve its electrochemical performance. Zeta potential measurements of the suspension medium would aid in understanding the electrophoretic deposition and quickly quantify the effect on the deposit of incremental changes to the suspension media or experimental conditions.

It may be necessary to introduce conductive additives to the battery material and some success has been seen in EPD of lithium ion battery electrodes with graphene or carbon nanotube additives.[119] By including these materials in the suspension, a co-deposit could be generated with an improved electrochemical performance.

Once the positive electrode coating has been optimised, it will be necessary to focus on EPD of other aspects of the battery through coating materials for negative electrodes and electrolytes. These could then be used to develop a complete battery system using EPD.

The research into the other aspects of the battery could also focus on identifying suitable 3D substrates that could be used to develop the system into a full 3D battery. Replacing the aluminium plate with an aluminium foam material would enable the battery materials to be coated onto a 3D substrate to generate a 3D battery with the potential to offer the advantages of a thin film battery in a thick film format. Another, more optimised approach to producing the substrate would be to use additive manufacturing or 3D printing in metal to produce the substrate material. This could then be optimised for the EPD process to gain the best possible packing of the battery system for the space required. This could also enable the battery to be fitted into a required shape or space for application in military systems.

2.2 Additional electrochemical studies based on binder and carbon-free samples

It would be necessary to expand the impedance spectroscopy studies to confirm whether the results presented here are representative. The next stage would be to alter the amount of pressing applied to the EPD samples and investigate the effect this has on the parameters involved. It would also be useful to use the EPD parameters to change the coating thickness. It is expected that as the thickness is increased and the proportion of bulk particles is increased in comparison to the near electrode particles this would affect the balances of resistances in the cell.

The addition of known quantities of carbon and binder may also enable the identification and quantification of resistances due to these additives and the effect on the overall sample. It may also be possible through the application of additional techniques to understand how the impedance alters as the battery charges and discharges. Techniques such as GITT and impedance at voltages greater or less than the OCV could enable the study of the cell in different charging states.

Chapter 5: References

1 References

1. Vincent, C.; Scrosati, B., *Modern Batteries 2nd Edition*. Elsevier: 1997.
2. Pletcher, D., *A first course in electrode processes*. Royal Society of Chemistry: 2009.
3. Nernst, W., *Ber. Deutsche. Chem. Ges.* **1897**.
4. Pletcher, D.; Greff, R.; Peat, R.; Peter, L.; Robinson, J., *Instrumental methods in electrochemistry*. Elsevier: 2001.
5. Zhou, H., Two-phase transition of Li-intercalation compounds in Li-ion batteries. *Materials Today* **2014,** *17* (9), 451-463.
6. Liu, C.; Neale, Z. G.; Cao, G., Understanding electrochemical potentials of cathode materials in rechargeable batteries. *Materials Today* **2016,** *19* (2), 109-123.
7. Nazri, G.-A.; Pistoia, G., *Lithium batteries: science and technology*. Springer Science & Business Media: 2008.
8. Palacin, M. R., Recent advances in rechargeable battery materials: a chemist's perspective. *Chemical Society Reviews* **2009,** *38* (9), 2565-2575.
9. Levi, M. D.; Aurbach, D., Frumkin intercalation isotherm — a tool for the description of lithium insertion into host materials: a review. *Electrochimica Acta* **1999,** *45* (1–2), 167-185.
10. Helmholtz, H., Ueber einige Gesetze der Vertheilung elektrischer Ströme in körperlichen Leitern mit Anwendung auf die thierisch-elektrischen Versuche. *Annalen der Physik* **1853,** *165* (6), 211-233.
11. Chapman, D. L., LI. A contribution to the theory of electrocapillarity. *The London, Edinburgh, and Dublin Philosophical Magazine and Journal of Science* **1913,** *25* (148), 475-481.
12. Gouy, G., *Compt. Rendus Geosci.* **1910,** *149*, 654.
13. Namisnyk, A.; Zhu, J. In *A survey of electrochemical super-capacitor technology*, Australian Universities Power Engineering Conference, University of Canterbury, New Zealand: 2003.
14. Stern, O., Electrochem. 30, 508 (1924). *Google Scholar*.
15. Grahame, D. C., The electrical double layer and the theory of electrocapillarity. *Chemical reviews* **1947,** *41* (3), 441-501.
16. Manthiram, A., Materials challenges and opportunities of lithium ion batteries. *The Journal of Physical Chemistry Letters* **2011,** *2* (3), 176-184.
17. Mizushima, K.; Jones, P.; Wiseman, P.; Goodenough, J., LixCoO2 (0< x<-1): A new cathode material for batteries of high energy density. *Materials Research Bulletin* **1980,** *15* (6), 783-789.
18. Nitta, N.; Wu, F.; Lee, J. T.; Yushin, G., Li-ion battery materials: present and future. *Materials Today* **2015,** *18* (5), 252-264.
19. Whittingham, M. S., Lithium batteries and cathode materials. *Chemical reviews* **2004,** *104* (10), 4271-4302.
20. Thackeray, M., Lithium-ion batteries: An unexpected conductor. *Nat Mater* **2002,** *1* (2), 81-82.
21. Imanishi, N.; Fujiyoshi, M.; Takeda, Y.; Yamamoto, O.; Tabuchi, M., Preparation and 7Li-NMR study of chemically delithiated Li1−xCoO2 (0<x<0.5). *Solid State Ionics* **1999,** *118* (1–2), 121-128.
22. He, P.; Yu, H.; Li, D.; Zhou, H., Layered lithium transition metal oxide cathodes towards high energy lithium-ion batteries. *Journal of Materials Chemistry* **2012,** *22* (9), 3680-3695.
23. Choi, N. S.; Chen, Z.; Freunberger, S. A.; Ji, X.; Sun, Y. K.; Amine, K.; Yushin, G.; Nazar, L. F.; Cho, J.; Bruce, P. G., Challenges facing lithium batteries and electrical double-layer capacitors. *Angew Chem Int Ed Engl* **2012,** *51* (40), 9994-10024.
24. Yamada, S.; Fujiwara, M.; Kanda, M., Synthesis and properties of LiNiO2 as cathode material for secondary batteries. *Journal of Power Sources* **1995,** *54* (2), 209-213.
25. Ohzuku, T.; Ueda, A.; Nagayama, M., Electrochemistry and structural chemistry of LiNiO2 (R3m) for 4 volt secondary lithium cells. *Journal of The Electrochemical Society* **1993,** *140* (7), 1862-1870.
26. Palacin, M.; Larcher, D.; Audemer, A.; Sac-Épée, N.; Amatucci, G.; Tarascon, J. M., Low-Temperature Synthesis of LiNiO2 Reaction Mechanism, Stability, and Electrochemical Properties. *Journal of The Electrochemical Society* **1997,** *144* (12), 4226-4236.
27. Armstrong, A. R.; Dupre, N.; Paterson, A. J.; Grey, C. P.; Bruce, P. G., Combined Neutron Diffraction, NMR, and Electrochemical Investigation of the Layered-to-Spinel Transformation in LiMnO2. *Chemistry of Materials* **2004,** *16* (16), 3106-3118.

28. Armstrong, A. R.; Paterson, A. J.; Dupré, N.; Grey, C. P.; Bruce, P. G., Structural Evolution of Layered LixMnyO2: Combined Neutron, NMR, and Electrochemical Study. *Chemistry of Materials* **2007,** *19* (5), 1016-1023.
29. Shaju, K. M.; Bruce, P. G., Macroporous Li(Ni1/3Co1/3Mn1/3)O2: A High-Power and High-Energy Cathode for Rechargeable Lithium Batteries. *Advanced Materials* **2006,** *18* (17), 2330-2334.
30. Yabuuchi, N.; Ohzuku, T., Novel lithium insertion material of LiCo 1/3 Ni 1/3 Mn 1/3 O 2 for advanced lithium-ion batteries. *Journal of Power Sources* **2003,** *119*, 171-174.
31. Itou, Y.; Ukyo, Y., Performance of LiNiCoO2 materials for advanced lithium-ion batteries. *Journal of Power Sources* **2005,** *146* (1–2), 39-44.
32. Bloom, I.; Jones, S. A.; Battaglia, V. S.; Henriksen, G. L.; Christophersen, J. P.; Wright, R. B.; Ho, C. D.; Belt, J. R.; Motloch, C. G., Effect of cathode composition on capacity fade, impedance rise and power fade in high-power, lithium-ion cells. *Journal of Power Sources* **2003,** *124* (2), 538-550.
33. Liu, W.; Kowal, K.; Farrington, G., Mechanism of the Electrochemical Insertion of Lithium into LiMn2 O 4 Spinels. *Journal of The Electrochemical Society* **1998,** *145* (2), 459-465.
34. Thackeray, M. M., Manganese oxides for lithium batteries. *Progress in Solid State Chemistry* **1997,** *25* (1), 1-71.
35. Bhaskar, A.; Mikhailova, D.; Kiziltas-Yavuz, N.; Nikolowski, K.; Oswald, S.; Bramnik, N. N.; Ehrenberg, H., 3d-Transition metal doped spinels as high-voltage cathode materials for rechargeable lithium-ion batteries. *Progress in Solid State Chemistry* **2014,** *42* (4), 128-148.
36. Aurbach, D.; Markovsky, B.; Talyossef, Y.; Salitra, G.; Kim, H.-J.; Choi, S., Studies of cycling behavior, ageing, and interfacial reactions of LiNi0.5Mn1.5O4 and carbon electrodes for lithium-ion 5-V cells. *Journal of Power Sources* **2006,** *162* (2), 780-789.
37. Yamada, A.; Chung, S.-C.; Hinokuma, K., Optimized LiFePO4 for lithium battery cathodes. *Journal of the electrochemical society* **2001,** *148* (3), A224-A229.
38. Takeda, Y.; Nakahara, K.; Nishijima, M.; Imanishi, N.; Yamamoto, O.; Takano, M.; Kanno, R., Sodium deintercalation from sodium iron oxide. *Materials Research Bulletin* **1994,** *29* (6), 659-666.
39. Eyob, P.; Andersson, A. S.; Thomas, J. O., A neutron powder diffraction study of electrochemically lithiated R-Li3+xFe2(PO4)3 for x = 1.8. *Journal of Materials Chemistry* **2002,** *12* (8), 2343-2347.
40. Padhi, A. K.; Nanjundaswamy, K.; Goodenough, J., Phospho-olivines as positive-electrode materials for rechargeable lithium batteries. *Journal of the electrochemical society* **1997,** *144* (4), 1188-1194.
41. Yamada, A.; Hosoya, M.; Chung, S.-C.; Kudo, Y.; Hinokuma, K.; Liu, K.-Y.; Nishi, Y., Olivine-type cathodes: Achievements and problems. *Journal of Power Sources* **2003,** *119–121*, 232-238.
42. Jung, S.; Jung, H.-Y., Charge/discharge characteristics of Li-ion batteries with two-phase active materials: a comparative study of LiFePO4 and LiCoO2 cells. *International Journal of Energy Research* **2016,** *40* (11), 1541-1555.
43. Sides, C. R.; Croce, F.; Young, V. Y.; Martin, C. R.; Scrosati, B., A High-Rate, Nanocomposite LiFePO4/Carbon Cathode. *Electrochemical and Solid-State Letters* **2005,** *8* (9), A484-A487.
44. Xia, Y.; Yoshio, M.; Noguchi, H., Improved electrochemical performance of LiFePO 4 by increasing its specific surface area. *Electrochimica acta* **2006,** *52* (1), 240-245.
45. Prosini, P. P.; Zane, D.; Pasquali, M., Improved electrochemical performance of a LiFePO4-based composite cathode. *Electrochimica Acta* **2001,** *46* (23), 3517-3523.
46. Yang, S.; Song, Y.; Ngala, K.; Zavalij, P. Y.; Stanley Whittingham, M., Performance of LiFePO4 as lithium battery cathode and comparison with manganese and vanadium oxides. *Journal of Power Sources* **2003,** *119–121*, 239-246.
47. Park, K. S.; Son, J. T.; Chung, H. T.; Kim, S. J.; Lee, C. H.; Kang, K. T.; Kim, H. G., Surface modification by silver coating for improving electrochemical properties of LiFePO4. *Solid State Communications* **2004,** *129* (5), 311-314.
48. Chung, S. Y.; Bloking, J. T.; Chiang, Y. M., Electronically conductive phospho-olivines as lithium storage electrodes. *Nat Mater* **2002,** *1* (2), 123-8.
49. Kang, B.; Ceder, G., Battery materials for ultrafast charging and discharging. *Nature* **2009,** *458* (7235), 190-193.
50. Meethong, N.; Huang, H. Y. S.; Speakman, S. A.; Carter, W. C.; Chiang, Y. M., Strain Accommodation during Phase Transformations in Olivine-Based Cathodes as a Materials Selection Criterion for High-Power Rechargeable Batteries. *Advanced Functional Materials* **2007,** *17* (7), 1115-1123.

51. Srinivasan, V.; Newman, J., Discharge Model for the Lithium Iron-Phosphate Electrode. *Journal of The Electrochemical Society* **2004,** *151* (10), A1517-A1529.
52. Reddy, T. B.; Linden, D., *Linden's Handbook of batteries. [electronic resource]*. New York : McGraw-Hill, c2011.
4th ed.: 2011.
53. Goriparti, S.; Miele, E.; De Angelis, F.; Di Fabrizio, E.; Proietti Zaccaria, R.; Capiglia, C., Review on recent progress of nanostructured anode materials for Li-ion batteries. *Journal of Power Sources* **2014,** *257*, 421-443.
54. Ha, D. H.; Islam, M. A.; Robinson, R. D., Binder-free and carbon-free nanoparticle batteries: a method for nanoparticle electrodes without polymeric binders or carbon black. *Nano Lett* **2012,** *12* (10), 5122-30.
55. Kaskhedikar, N. A.; Maier, J., Lithium Storage in Carbon Nanostructures. *Advanced Materials* **2009,** *21* (25-26), 2664-2680.
56. Schauerman, C. M.; Ganter, M. J.; Gaustad, G.; Babbitt, C. W.; Raffaelle, R. P.; Landi, B. J., Recycling single-wall carbon nanotube anodes from lithium ion batteries. *Journal of Materials Chemistry* **2012,** *22* (24), 12008-12015.
57. Zhao, J.; Buldum, A.; Han, J.; Ping Lu, J., First-Principles Study of Li-Intercalated Carbon Nanotube Ropes. *Physical Review Letters* **2000,** *85* (8), 1706-1709.
58. Jung, H.-G.; Jang, M. W.; Hassoun, J.; Sun, Y.-K.; Scrosati, B., A high-rate long-life Li4Ti5O12/Li [Ni0. 45Co0. 1Mn1. 45] O4 lithium-ion battery. *Nature communications* **2011,** *2*, 516.
59. Hertzberg, B.; Alexeev, A.; Yushin, G., Deformations in Si−Li Anodes Upon Electrochemical Alloying in Nano-Confined Space. *Journal of the American Chemical Society* **2010,** *132* (25), 8548-8549.
60. Aurbach, D.; Talyosef, Y.; Markovsky, B.; Markevich, E.; Zinigrad, E.; Asraf, L.; Gnanaraj, J. S.; Kim, H.-J., Design of electrolyte solutions for Li and Li-ion batteries: a review. *Electrochimica Acta* **2004,** *50* (2-3), 247-254.
61. Aurbach, D., Review of selected electrode–solution interactions which determine the performance of Li and Li ion batteries. *Journal of Power Sources* **2000,** *89* (2), 206-218.
62. Aurbach, D.; Gamolsky, K.; Markovsky, B.; Salitra, G.; Gofer, Y.; Heider, U.; Oesten, R.; Schmidt, M., The Study of Surface Phenomena Related to Electrochemical Lithium Intercalation into Li x MO y Host Materials (M = Ni, Mn). *Journal of The Electrochemical Society* **2000,** *147* (4), 1322-1331.
63. Pistoia, G., *Lithium-ion batteries: advances and applications*. Newnes: 2013.
64. Song, J. Y.; Wang, Y. Y.; Wan, C. C., Review of gel-type polymer electrolytes for lithium-ion batteries. *Journal of Power Sources* **1999,** *77* (2), 183-197.
65. Bachman, J. C.; Muy, S.; Grimaud, A.; Chang, H.-H.; Pour, N.; Lux, S. F.; Paschos, O.; Maglia, F.; Lupart, S.; Lamp, P.; Giordano, L.; Shao-Horn, Y., Inorganic Solid-State Electrolytes for Lithium Batteries: Mechanisms and Properties Governing Ion Conduction. *Chemical Reviews* **2016,** *116* (1), 140-162.
66. Storage battery. https://www.britannica.com/technology/storage-battery (accessed 09/12/2017).
67. Roberts, M.; Johns, P.; Owen, J.; Brandell, D.; Edstrom, K.; El Enany, G.; Guery, C.; Golodnitsky, D.; Lacey, M.; Lecoeur, C., 3D lithium ion batteries—from fundamentals to fabrication. *Journal of Materials Chemistry* **2011,** *21* (27), 9876-9890.
68. Yoshio, M.; Brodd, R. J.; Kozawa, A., *Lithium-Ion Batteries*. Springer: 2009; Vol. 1.
69. Yang, H.; Jiang, P., Large-Scale Colloidal Self-Assembly by Doctor Blade Coating. *Langmuir* **2010,** *26* (16), 13173-13182.
70. Hu, L.; Wu, H.; La Mantia, F.; Yang, Y.; Cui, Y., Thin, Flexible Secondary Li-Ion Paper Batteries. *ACS Nano* **2010,** *4* (10), 5843-5848.
71. Schmitt, M.; Baunach, M.; Wengeler, L.; Peters, K.; Junges, P.; Scharfer, P.; Schabel, W., Slot-die processing of lithium-ion battery electrodes—Coating window characterization. *Chemical Engineering and Processing: Process Intensification* **2013,** *68*, 32-37.
72. Gaikwad, A. M.; Whiting, G. L.; Steingart, D. A.; Arias, A. C., Highly Flexible, Printed Alkaline Batteries Based on Mesh-Embedded Electrodes. *Advanced Materials* **2011,** *23* (29), 3251-3255.
73. Gaikwad, A. M.; Steingart, D. A.; Ng, T. N.; Schwartz, D. E.; Whiting, G. L., A flexible high potential printed battery for powering printed electronics. *Applied Physics Letters* **2013,** *102* (23), 233302.
74. Kang, K.-Y.; Lee, Y.-G.; Shin, D. O.; Kim, J.-C.; Kim, K. M., Performance improvements of pouch-type flexible thin-film lithium-ion batteries by modifying sequential screen-printing process. *Electrochimica Acta* **2014,** *138*, 294-301.

75. Park, M. S.; Hyun, S. H.; Nam, S. C., Characterization of a LiCoO2 thick film by screen-printing for a lithium ion micro-battery. *Journal of Power Sources* **2006,** *159* (2), 1416-1421.
76. Park, M.-S.; Hyun, S.-H.; Nam, S.-C., Mechanical and electrical properties of a LiCoO2 cathode prepared by screen-printing for a lithium-ion micro-battery. *Electrochimica Acta* **2007,** *52* (28), 7895-7902.
77. Wang, Z.; Winslow, R.; Madan, D.; Wright, P. K.; Evans, J. W.; Keif, M.; Rong, X., Development of MnO2 cathode inks for flexographically printed rechargeable zinc-based battery. *Journal of Power Sources* **2014,** *268*, 246-254.
78. Singh, N.; Galande, C.; Miranda, A.; Mathkar, A.; Gao, W.; Reddy, A. L. M.; Vlad, A.; Ajayan, P. M., Paintable Battery. *Scientific Reports* **2012,** *2*, 481.
79. Ho, C. C.; Evans, J. W.; Wright, P. K., Direct write dispenser printing of a zinc microbattery with an ionic liquid gel electrolyte. *Journal of Micromechanics and Microengineering* **2010,** *20* (10), 104009.
80. Wang, Z.; Chen, A.; Winslow, R.; Madan, D.; Juang, R.; Nill, M.; Evans, J.; Wright, P., Integration of dispenser-printed ultra-low-voltage thermoelectric and energy storage devices. *Journal of Micromechanics and Microengineering* **2012,** *22* (9), 094001.
81. Sun, K.; Wei, T.-S.; Ahn, B. Y.; Seo, J. Y.; Dillon, S. J.; Lewis, J. A., 3D Printing of Interdigitated Li-Ion Microbattery Architectures. *Advanced Materials* **2013,** *25* (33), 4539-4543.
82. Gu, Y.; Wu, A.; Sohn, H.; Nicoletti, C.; Iqbal, Z.; Federici, J. F., Fabrication of rechargeable lithium ion batteries using water-based inkjet printed cathodes. *Journal of Manufacturing Processes* **2015,** *20, Part 1*, 198-205.
83. Ho, C. C.; Murata, K.; Steingart, D. A.; Evans, J. W.; Wright, P. K., A super ink jet printed zinc–silver 3D microbattery. *Journal of Micromechanics and Microengineering* **2009,** *19* (9), 094013.
84. Potiron, E.; Le Gal La Salle, A.; Verbaere, A.; Piffard, Y.; Guyomard, D., Electrochemically synthesized vanadium oxides as lithium insertion hosts. *Electrochimica Acta* **1999,** *45* (1–2), 197-214.
85. Sarciaux, S.; Le Gal La Salle, A.; Verbaere, A.; Piffard, Y.; Guyomard, D., γ-MnO2 for Li batteries: Part I. γ-MnO2: Relationships between synthesis conditions, material characteristics and performances in lithium batteries. *Journal of Power Sources* **1999,** *81–82*, 656-660.
86. Nathan, M.; Golodnitsky, D.; Yufit, V.; Strauss, E.; Ripenbein, T.; Shechtman, I.; Menkin, S.; Peled, E., Three-dimensional thin-film Li-ion microbatteries for autonomous MEMS. *Journal of Microelectromechanical Systems* **2005,** *14* (5), 879-885.
87. Mosby, J. M.; Prieto, A. L., Direct Electrodeposition of Cu2Sb for Lithium-Ion Battery Anodes. *Journal of the American Chemical Society* **2008,** *130* (32), 10656-10661.
88. Oudenhoven, J. F.; Baggetto, L.; Notten, P. H., All-Solid-State Lithium-Ion Microbatteries: A Review of Various Three-Dimensional Concepts. *Advanced Energy Materials* **2011,** *1* (1), 10-33.
89. Archer, N. J., Chemical vapour deposition. *Physics in Technology* **1979,** *10* (4), 152.
90. Wang, X.; Yushin, G., Chemical vapor deposition and atomic layer deposition for advanced lithium ion batteries and supercapacitors. *Energy & Environmental Science* **2015,** *8* (7), 1889-1904.
91. Delgado, A.; González-Caballero, F.; Hunter, R.; Koopal, L.; Lyklema, J., Measurement and interpretation of electrokinetic phenomena (IUPAC technical report). *Pure and Applied Chemistry* **2005,** *77* (10), 1753-1805.
92. Corni, I.; Ryan, M. P.; Boccaccini, A. R., Electrophoretic deposition: From traditional ceramics to nanotechnology. *Journal of the European Ceramic Society* **2008,** *28* (7), 1353-1367.
93. Van der Biest, O. O.; Vandeperre, L. J., Electrophoretic deposition of materials. *Annual Review of Materials Science* **1999,** *29* (1), 327-352.
94. Besra, L.; Liu, M., A review on fundamentals and applications of electrophoretic deposition (EPD). *Progress in Materials Science* **2007,** *52* (1), 1-61.
95. Hanaor, D.; Michelazzi, M.; Leonelli, C.; Sorrell, C. C., The effects of carboxylic acids on the aqueous dispersion and electrophoretic deposition of ZrO2. *Journal of the European Ceramic Society* **2012,** *32* (1), 235-244.
96. Ata, M. S.; Liu, Y.; Zhitomirsky, I., A review of new methods of surface chemical modification, dispersion and electrophoretic deposition of metal oxide particles. *RSC Advances* **2014,** *4* (43), 22716-22732.
97. Popa, A. M.; Vleugels, J.; Vermant, J.; Van der Biest, O., Influence of surfactant addition sequence on the suspension properties and electrophoretic deposition behaviour of alumina and zirconia. *Journal of the European Ceramic Society* **2006,** *26* (6), 933-939.

98. Swan, J. W.; Furst, E. M., A simpler expression for Henry's function describing the electrophoretic mobility of spherical colloids. *Journal of Colloid and Interface Science* **2012,** *388* (1), 92-94.
99. Grillon, F.; Fayeulle, D.; Jeandin, M., QUANTITATIVE IMAGE-ANALYSIS OF ELECTROPHORETIC COATINGS. *Journal of Materials Science Letters* **1992,** *11* (5), 272-275.
100. Koelmans, H.; Overbeek, J. T. G., Stability and electrophoretic deposition of suspensions in non-aqueous media. *Discussions of the Faraday Society* **1954,** *18* (0), 52-63.
101. Ferrari, B.; Moreno, R., EPD kinetics: A review. *Journal of the European Ceramic Society* **2010,** *30* (5), 1069-1078.
102. Hamaker, H. C., Formation of a deposit by electrophoresis. *Transactions of the Faraday Society* **1940,** *35* (0), 279-287.
103. Sarkar, P.; Nicholson, P. S., Electrophoretic deposition (EPD): mechanisms, kinetics, and application to ceramics. *Journal of the American Ceramic Society* **1996,** *79* (8), 1987-2002.
104. Biesheuvel, P. M.; Verweij, H., Theory of Cast Formation in Electrophoretic Deposition. *Journal of the American Ceramic Society* **1999,** *82* (6), 1451-1455.
105. Neirinck, B.; Van der Biest, O.; Vleugels, J., A Current Opinion on Electrophoretic Deposition in Pulsed and Alternating Fields. *J. Phys. Chem. B* **2013,** *117* (6), 1516-1526.
106. Bavykin, D. V.; Passoni, L.; Walsh, F. C., Hierarchical tube-in-tube structures prepared by electrophoretic deposition of nanostructured titanates into a TiO2 nanotube array. *Chem Commun (Camb)* **2013,** *49* (62), 7007-9.
107. Ma, J.; Cheng, W., Electrophoretic deposition of lead zirconate titanate ceramics. *Journal of the American Ceramic Society* **2002,** *85* (7), 1735-1737.
108. Anne, G.; Vanmeensel, K.; Vleugels, J.; Van der Biest, O., A Mathematical Description of the Kinetics of the Electrophoretic Deposition Process for Al2O3-Based Suspensions. *Journal of the American Ceramic Society* **2005,** *88* (8), 2036-2039.
109. Ferrari, B.; Moreno, R.; Cuesta, J. A. In *A resistivity model for electrophoretic deposition*, Key Engineering Materials, Trans Tech Publ: 2006; pp 175-180.
110. Neirinck, B.; Fransaer, J.; Biest, O. V. d.; Vleugels, J., Aqueous electrophoretic deposition in asymmetric AC electric fields (AC–EPD). *Electrochemistry Communications* **2009,** *11* (1), 57-60.
111. Solomentsev, Y.; Böhmer, M.; Anderson, J. L., Particle Clustering and Pattern Formation during Electrophoretic Deposition: A Hydrodynamic Model. *Langmuir* **1997,** *13* (23), 6058-6068.
112. Franger, S.; Le Cras, F.; Bourbon, C.; Rouault, H., LiFePO4 synthesis routes for enhanced electrochemical performance. *Electrochemical and Solid State Letters* **2002,** *5* (10), A231-A233.
113. Ferrari, B.; Moreno, R.; Hernán, L.; Melero, M.; Morales, J.; Caballero, A., EPD of thick films for their application in lithium batteries. *Journal of the European Ceramic Society* **2007,** *27* (13–15), 3823-3827.
114. Caballero, A.; Hernán, L.; Melero, M.; Morales, J.; Moreno, R.; Ferrari, B., LiNi0.5Mn1.5O4 thick-film electrodes prepared by electrophoretic deposition for use in high voltage lithium-ion batteries. *Journal of Power Sources* **2006,** *158* (1), 583-590.
115. Koichi, U.; Funo, S.-y.; Nagase, H.; Idemoto, Y.; Koura, N., Fabrication of binder-free positive electrode for Li-ion secondary batteries by electrophoretic deposition method. *Electrochemistry* **2006,** *74* (6), 474-478.
116. Mazor, H.; Golodnitsky, D.; Burstein, L.; Gladkich, A.; Peled, E., Electrophoretic deposition of lithium iron phosphate cathode for thin-film 3D-microbatteries. *Journal of Power Sources* **2012,** *198*, 264-272.
117. Xiao, W.; Xia, H.; Fuh, J. Y.; Lu, L., Electrophoretic-deposited CNT/MnO2 composites for high-power electrochemical energy storage/conversion applications. *Physica Scripta* **2010,** *2010* (T139), 014008.
118. Diba, M.; Fam, D. W. H.; Boccaccini, A. R.; Shaffer, M. S. P., Electrophoretic deposition of graphene-related materials: A review of the fundamentals. *Progress in Materials Science* **2016,** *82*, 83-117.
119. Huang, Y.; Liu, H.; Lu, Y.-C.; Hou, Y.; Li, Q., Electrophoretic lithium iron phosphate/reduced graphene oxide composite for lithium ion battery cathode application. *Journal of Power Sources* **2015,** *284*, 236-244.
120. EC-Lab Software: Techniques and Applications. 10.34 ed.; Biologic scientific instruments: 2013.
121. Linden, D. In *Handbook of batteries*, Fuel and Energy Abstracts, 1995; p 265.
122. Denault, G. CHEM 8002 Advanced Impedance lecture course.

123. Johnson, D., ZView: a Software Program for IES Analysis, Version 2.8, Scribner Associates. *Inc., Southern Pines, NC* **2002,** *200*.
124. Córdoba-Torres, P.; Mesquita, T. J.; Nogueira, R. P., Relationship between the Origin of Constant-Phase Element Behavior in Electrochemical Impedance Spectroscopy and Electrode Surface Structure. *The Journal of Physical Chemistry C* **2015,** *119* (8), 4136-4147.
125. Hsieh, G.; Mason, T. O.; Garboczi, E.; Pederson, L., Experimental limitations in impedance spectroscopy: Part III. Effect of reference electrode geometry/position. *Solid State Ionics* **1997,** *96* (3), 153-172.
126. Vernon-Parry, K. D., Scanning electron microscopy: an introduction. *III-Vs Review* **2000,** *13* (4), 40-44.
127. Dehm, G.; Howe, J. M.; Zweck, J., *In-situ electron microscopy: applications in physics, chemistry and materials science*. John Wiley & Sons: 2012.
128. Ohring, M., *Materials science of thin films*. Academic press: 2001.
129. Venables, J.; Harland, C., Electron back-scattering patterns—A new technique for obtaining crystallographic information in the scanning electron microscope. *Philosophical Magazine* **1973,** *27* (5), 1193-1200.
130. Ebnesajjad, S., *Handbook of adhesives and surface preparation: technology, applications and manufacturing*. William Andrew: 2010.
131. *Certificate of Analysis of LiFePO4*; Tatung fine chemicals: 29/02/2012, 2012.
132. Solvay speciality polymers. *Solef PVDF for Batteries* **2014**.
133. Priya Nair, S.; Jyothsna, U.; Praveen, P.; Balakrishnan, A.; Subramanian, K. R. V.; Nair, S. V.; Sivakumar, N., Synthesis and Characterization of Electrophoretically Deposited Nanostructured LiCoPO 4 for Rechargeable Lithium Ion Batteries. *ISRN Nanotechnology* **2013**, 653237 (5 pp.)-653237 (5 pp.).
134. Wu, M. S.; Chan, D. S.; Lin, K. H.; Jow, J. J., A simple route to electrophoretic deposition of transition metal-coated nickel oxide films for electrochemical capacitors. *Materials Chemistry and Physics* **2011,** *130* (3), 1239-1245.
135. Bavykin, D. V.; Passoni, L.; Walsh, F. C., Hierarchical tube-in-tube structures prepared by electrophoretic deposition of nanostructured titanates into a TiO 2 nanotube array. *Chemical Communications* **2013,** *49* (62), 7007-7009.
136. Schneider, C. A.; Rasband, W. S.; Eliceiri, K. W., NIH Image to ImageJ: 25 years of image analysis. *Nature methods* **2012,** *9* (7), 671-675.
137. Orikasa, Y.; Gogyo, Y.; Yamashige, H.; Katayama, M.; Chen, K.; Mori, T.; Yamamoto, K.; Masese, T.; Inada, Y.; Ohta, T., Ionic conduction in lithium ion battery composite electrode governs cross-sectional reaction distribution. *Scientific reports* **2016,** *6*.
138. Li, X.; Luo, D.; Zhang, X.; Zhang, Z., Enhancement of electrochemical performances for LiFePO4/C with 3D-grape-bunch structure and selection of suitable equivalent circuit for fitting EIS results. *Journal of Power Sources* **2015,** *291*, 75-84.
139. Gaberscek, M.; Moskon, J.; Erjavec, B.; Dominko, R.; Jamnik, J., The Importance of Interphase Contacts in Li Ion Electrodes: The Meaning of the High-Frequency Impedance Arc. *Electrochemical and Solid-State Letters* **2008,** *11* (10), A170-A174.
140. Shin, H. C.; Cho, W. I.; Jang, H., Electrochemical properties of carbon-coated LiFePO4 cathode using graphite, carbon black, and acetylene black. *Electrochimica Acta* **2006,** *52* (4), 1472-1476.
141. Atebamba, J.-M.; Moskon, J.; Pejovnik, S.; Gaberscek, M., On the Interpretation of Measured Impedance Spectra of Insertion Cathodes for Lithium-Ion Batteries. *Journal of The Electrochemical Society* **2010,** *157* (11), A1218-A1228.